Rapid Fabrication of Miniaturized Electric Double-Layer Capacitors Based on Laser Patterned Graphene oxide-Poly (Furfuryl Alcohol) Nanocomposites

by

Dilara Yilman

A thesis

presented to the University of Waterloo

in fulfillment of the

thesis requirement for the degree of

Master of Applied Science

in

Chemical Engineering

Waterloo, Ontario, Canada, 2018

Author's Declaration

I hereby declare that I am the sole author of this thesis. This is a true copy of the thesis, including any required final revisions, as accepted by my examiners.

I understand that my thesis may be made electronically available to the public.

Abstract

Miniaturization of various technologies has accelerated and drives new requirements for energy harvesting and storage solutions to power such devices. Reduction in size and designs requiring mechanical flexibility fuel the development of new materials and fabrication processes. The most advanced solutions to date have been to engineer thinner, more flexible rechargeable batteries. However, their short cycle-lifetime due to the intrinsic chemical nature of their energy storage mechanism, their low power density, high cost and safety concerns limit their application in variety of areas. For long-term electronic use in health-monitoring, smart-implants and the internet of things, a new form of power source which no longer requires replacement and offers consistent performance is needed. These concerns can be addressed if another energy storage technology is considered – the electrochemical supercapacitor. Such devices are generally reliable, offer long lifetimes, are safer and can be operated efficiently at high power. However, they typically store less energy per unit mass or volume than batteries.

This thesis focuses on the development of miniaturized supercapacitors with improved performance as an energy storage solution for self-sufficient, micro-scale, and flexible electronics. Specifically, a type of supercapacitor called an electrical double-layer capacitor (EDLCs) is well known for high-power capabilities and a long-lasting cycle-life, typically above 100,000 charge and discharge cycles. The approach adopted in this study aims to improve the energy density using sustainable materials through a scalable and cost-effective fabrication technique. We will demonstrate that a polymer resin formed from an inexpensive monomer derived from waste biomass such as corn husks can be carbonized into a high surface area, electronically conductive material using a commercial CO_2 laser. High resolution laser patterning of electrodes onto this material results in a micro-supercapacitor with much improved performance compared to state-of-the-art flexible and miniaturized supercapacitors.

This thesis work initially focused on the understanding and development of laser irradiation as a fabrication technique using commercially available carbonaceous materials such as commercial Kapton® polyimide films as well as lab-made graphene oxide. A complete understanding of the variables involved in the fabrication process helped to optimize the laser irradiation technique. This achieved the highest reported micro-supercapacitor energy density compared to published research on similar materials. The main focus of this work was to develop an improved electrode

material in terms of both cost and performance that could be laser activated in a similar way. To this end, we hypothesized that poly (furfuryl alcohol) (pFA), which is known to form a dense, microporous glassy carbon upon conventional heat treatment, might be a good candidate material for more effective laser activation. Several methods of polymer synthesis from the low cost, abundant, biomass waste derived monomer of pFA were explored to create a laser-inducible substrate including acid-catalyzed emulsion polymerization and bulk resinification. Surprisingly, despite a high yield conversion to carbon using conventional heating, the neat material could not be carbonized with the laser system. However, the addition of a small amount of graphene oxide was found to catalyze the formation of the carbonized structure which ultimately led to an improved supercapacitor. The optimum pFA synthesis conditions and the effect of graphene oxide incorporation were explored to maximize device performance. In each case, evolution of the carbonized structure was investigated by Raman and X-ray photoelectron spectroscopy. The resulting micro-supercapacitors boast a simple, inexpensive and rapid fabrication technique that are promising for future device applications. Notably, optimized electrodes achieved the highest specific areal capacitance presented in literature compared to other laser irradiated carbon precursors. The specific capacitance has been improved four times (4x) from literature's highest measurement at 31 mF/cm^2 to 147 mF/cm^2 during this thesis work. pFA is heralded as a new renewable and environmental friendly energy storage source; recycled from common biomass waste into the solution to today's most pressing micro-electronics need - power.

Acknowledgements

I would like to thank God for giving me the ability to learn and understand nature, and all the wonderful blessings that he has provided throughout my time doing research.

It is with great pleasure that I acknowledge my mentor, Prof. Michael Pope, for suggesting this topic of research, supervising the work and his involvement in the lab. It has been an honour to work under his thoughtful supervision.

I would also like to express my deepest thanks and sincere appreciation to Prof. Chris Backhouse, who provided additional supervision in the joint project with Colin Tittle, and Prof. Alexander Penlidis, who guided and motivated me throughout my research at the University of Waterloo.

My sincere gratitude is extended to my office and lab mates, Irene Lau, Mursal Ashrafi and Luzhu (Amanda) Xu. Their laughter, concern, tears, joy and hard work throughout the many terms will be cherished for all time. I would also like to thank the co-op students which I supervised in this project, both Nathan Chan and Joanna Liu, for their hard work in the synthesis and analysis at various points throughout my research.

Finally, I would like to acknowledge my family for convincing me and supporting my degree here in Canada.

Dedication

This thesis work is dedicated to my love of my life, Jared Lenos who has showed unending patience, love and support for all time.

Table of Contents

List of Figures

List of Tables

Chapter 1. Introduction

1.1. Overview

The recent explosion of public interest and investment in microelectronic devices for medical, telecommunication, environmental sensing, and microelectromechanical systems (MEMS) has driven the desire for inventions to be self-powered. Small devices which generate power can be integrated into clothing, remote or portable electronics and preferably function long-term without the need for external power circuitry or sources[1,2]. This power is discontinuously harvested from sources like electromagnetic radiation such as solar cells, kinetic energy conversion from piezoelectric transducers or thermal energy conversion concerning the area of the device used. Needless to say, this harvested power needs to be stored or buffered for later use by the device. Therefore, integration of energy storage devices into microelectronics is a crucial need for microelectronic technology. Currently, self-powered microelectronic devices rely on the use of rechargeable batteries. Although a few miniaturized batteries and thin film batteries are accessible in the market as an energy storage provider, their limited cycle life and low power density are major disadvantages for their integration into microelectronics. The replacement of batteries in health care electronic monitoring devices is critical element their widespread use, especially in implant or direct-contact monitoring using inert and flexible electronics. Supercapacitors are an alternative energy storage solution for these applications that use physical charge separation rather than a chemical reaction to store energy. This allows supercapacitors to provide a high power density and rapid discharge/charge characteristics combined with a long cycle life typically reaching over 100,000 cycles[3,4]. Consequently, miniaturized supercapacitors could provide low maintenance costs, decrease the complexity and possible health risks associated with batteries while enhancing the performance and longevity of microelectronic devices[1].

Over the past decade, the miniaturization of supercapacitors has been studied intensively including the development of techniques to fabricate microscopic supercapacitors. The bulk of these studies can be categorized as lithographic techniques[5,6,7], chemical vapour deposition[5], layer-by-layer deposition combined with photo-lithographic techniques[8], ink-jet printing[9], and direct laser writing techniques[10–14]. Most of these techniques require expensive, specialized equipment which has slowed progress towards commercialization. More recently, the exploration of direct laser writing as a fabrication technique has generated a new opportunity for micro-supercapacitors. Particularly, the demonstration of laser-patterning of electrodes using inexpensive, medium throughput industrial laser cutting machines has provided various advantages including accessibility and low manufacturing costs. Simple low-cost systems are even available to hobbyists. These key market ingredients indicate that achieving sufficient energy density in devices fabricated in such a way would be a significant step towards large-scale adoption.

The specialty polyimide, Kapton™, and graphene oxide have been the two primary substrate materials used for laser conversion to graphene-like carbon derivatives which have been to pattern electrodes for supercapacitors. While promising results have been demonstrated, laser-induced electrodes made from these substrates have achieved only low capacitance compared to large format devices and the materials used are relatively expensive. The study is motivated to combine the advantages of laser irradiation on polymer materials using inexpensive and green alternatives to the commercial imide derived polymer in prior works. Poly (furfuryl alcohol) (pFA) is derived from saccharidic biomass waste and serves as non-graphitizable, dense carbon structure as an alternative carbon precursor. It has been studied in literature as an electrode material for batteries and supercapacitors, as a catalyst support, as a membrane for separation and after carbonization of

the polymer and its polymeric composites[15–17]. The studies intensively focus on creating microporous domains using the unique nature of pFA and its carbonization at high temperature.

In this thesis work, we have investigated the use of laser irradiation on this inexpensive, green polymer material in order to build a miniaturized energy storage solution. The study focuses on the understanding and improvement of the fabrication technique and observation of its application on polymer and polymer composite materials. Using this technique, a common product of biomass waste has been recycled through its polymerization and carbonization for energy storage purposes. The combination of graphene oxide (GO) and pFA helps us to investigate further and improve micro-supercapacitor fabrication and to achieve high energy storage performance for miniaturized electronic applications.

1.2. Research Objectives

The primary purpose of this research is to develop an improved micro-supercapacitor through an inexpensive and rapid fabrication route while achieving high energy and power density. A secondary goal is to develop a system which is mechanically flexible and could be implemented in future wearable technologies. The fabrication technique should be versatile yet simple to operate despite micro-fabrication. Laser irradiation through the use of CO_2 laser cutting technology is selected as a suitable approach to generate micro-patterned polymer and polymeric nanocomposites. These polymer and composite substrates must convert into an electronically conductive pattern with high energy storage capacity when irradiated. One such possibility is the generation of porous but interconnected carbon structures from a polymeric base when exposed to localized thermal and photo-excitation. This research focuses on the synthesis of polymer nanocomposites that, upon strong irradiation, develop into interdigitated electrodes onto a flexible substrate. A prototype is designed and optimized based on its electrochemical performance and

proved competitive compared to leading-edge literature in this field. Electrode design and the selection of electrolyte are also investigated as essential variables to increase the capacitance and stability upon cycling.

The specific objectives of this thesis project include:

1. Investigation and development of a laser irradiation technique to pattern electrodes into commercial polymers which exhibit maximum specific capacitance
    - Optimize laser treatment parameters for effective laser-induced carbonization of carbonizable precursors; Kapton™ polyimide film and graphene oxide films
    - Analysis of electrode morphology and material limitations
2. Development of alternative polymer systems that more effectively carbonize into high surface area structures upon laser irradiation
    - Development and testing of various synthesis and casting methods to create electrode precursor films from poly (furfuryl alcohol)
    - Exploring the effect of graphene oxide as an additive to enhance carbonization
    - Electrochemical testing and optimization of materials and test cell

Thesis Outline

This thesis consists of five chapter in total. Chapter one gives insight to an overview of the thesis, an outline of the research carried out with specific objectives of the project. Chapter two provides a summary of the background behind supercapacitors, specifically electrochemical double layer capacitors, electrode materials, a literature review of miniaturized supercapacitors and their fabrication methods. This chapter is oriented towards understanding supercapacitors and their performance criteria, pointing out fabrication methods to create desired electrode materials and

integration of electrodes into full device configurations. The chapter concludes with current challenges and applications of supercapacitors with a focus on micro-supercapacitors.

Chapter three analyzes laser irradiation on insulating materials towards successful micro-patterning of interdigitated planar-supercapacitors. By controlling laser parameters and electrode design, the performance of micro-supercapacitors can be increased with a deeper understanding. This chapter systematically studies the effects of infrared laser parameters on a commercial Kapton™ films as well as graphene oxide as a starting point for our studies in order to understand the current limitations of using these materials.

Chapter four investigates the use of poly (furfuryl alcohol) as a carbonizable precursor which can be laser-induced, and explores the effect of various synthesis methods to maximize the areal specific capacitance in the micro-supercapacitor application. This chapter is divided into two main section; polymer synthesis and laser irradiation of polymeric nanocomposites. The first section focuses on understanding the parameters that affect the synthesis of poly (furfuryl alcohol). The second section of the chapter focuses on applying these parameters and other fabrication parameter for successful laser irradiation of pFA. At the end of this chapter, a summary and comparison between the carbon precursors for laser irradiation in this study and those in literature studies is presented regarding their structural differences and electrochemical performances.

Finally, chapter five summarizes and states conclusive results from the work done in this thesis study.

Chapter 2. Research Background and Literature Review

2.1. Supercapacitors

2.1.1. Overview

There are two main categories of supercapacitors: electrical double layer capacitors (EDLCs) and pseudocapacitors. EDLCs are the most commonly used and store energy in the capacitor formed between an electrically charged electrode surface and the oppositely charged ions in the electrolyte that populate the layer adjacent the electrical charge. The two oppositely charged layers at this interface are separated by only a few solvent layers, which act as a dielectric. In the simplest approximation, the interface can be modelled as a parallel plate capacitor and thus the capacitance per area can be approximated by $C_{DL} = k \cdot (\varepsilon/\delta)$. Since δ is small (~ O(Å)) the C_{DL} can be very large (~5-40 $\mu F/cm^2$)[18]. Since the specific surface area (SSA) or interfacial area for double-layer charging of some carbonaceous materials and metal oxides can be as high as 100-2000 m^2/g, very high gravimetric (~100 F/g) and volumetric capacitance (~100 F/cm^3) result for a single electrode which are many orders of magnitude larger than dielectric capacitors. To fabricate an EDLC, a voltage must be applied between two such high surface area electrodes (one negatively polarized and one positively) which are separated by an electrically insulating but ionically conducting separator immersed in an electrolyte. The double-layer formed at each electrode act as capacitors in series. Two capacitors in series cause the total device capacitance to be half that of the single-electrode capacitance with twice the mass, leading to ~25 F/g of active material.

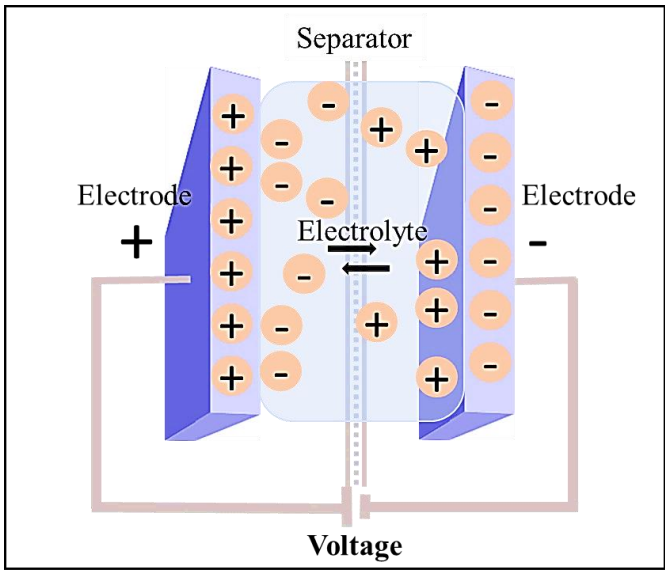

Figure 1. Schematic of a supercapacitor assembly

The energy storage mechanism for EDLCs does not depend on reduction-oxidation (redox) reactions like that of batteries. Since they are not dependent on chemical reaction kinetics, EDLC-based supercapacitors have fast charge and discharge capabilities and can exhibit almost limitless cycle-life, typically above 100,000 cycles. The coulumbic efficiency is maintained at 100% due to the reversible physical nature of this simple charge rearrangement energy storage. Fast charging and discharging indicate that EDLCs can be operated safely at high-power density. Figure 2.2 compares the energy and power capabilities of EDLC supercapacitors compared to other energy storage technologies. They occupy the significant gap between the traditional dielectric and electrolytic capacitors and batteries, demonstrating improved power density compared to batteries and much higher energy density (energy per mass or volume) than traditional capacitors.

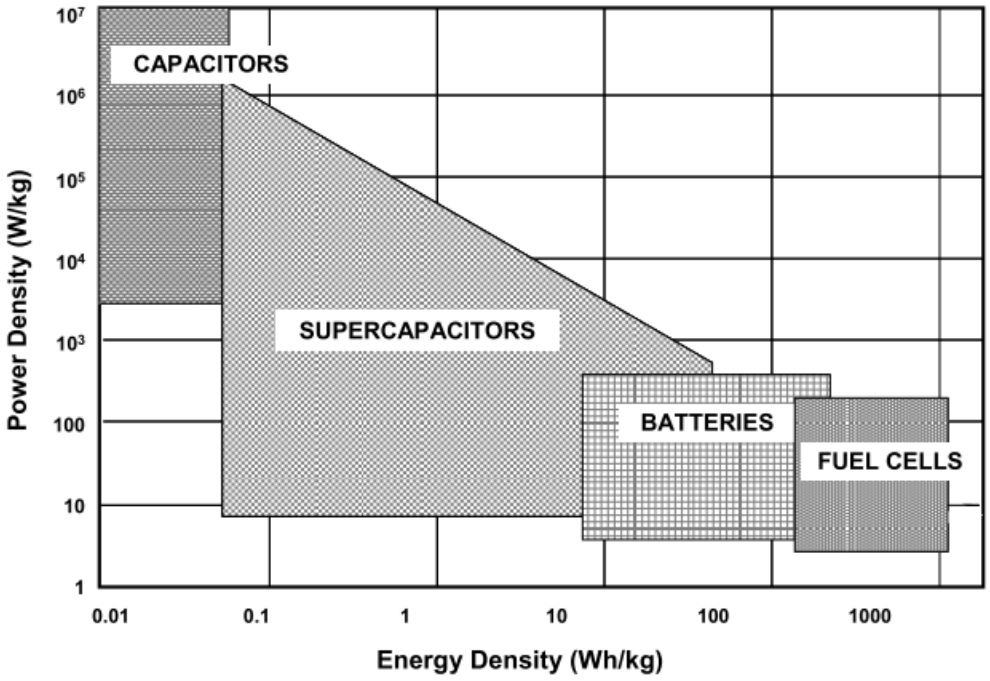

Figure 2. Ragone plot comparing the energy and power density of various energy storage technologies[3]

The second major category of the supercapacitor is the pseudo-capacitor. Such devices exhibit so-called pseudo-capacitance, which is the additional capacitance associated with redox reactions, partial chemisorption or intercalation which act in parallel to the conventional EDLC charging mechanism. These electron transfer reactions (known broadly as Faradaic processes) can significantly enhance the total capacitance. An example pseudocapacitive material is hydrous ruthenium oxide which is capable of a series of proton transfer reactions when oxidation state changes occur in ruthenium over a broad voltage range. This distributed pseudocapacitance resembles EDLC charging. The drawback to this type of supercapacitor is poorer cycle-life and rate capabilities due to the only quasi-reversible nature associated with the redox processes and slower chemical kinetic phenomena (typical first order chemical rate constants are much less than 1 s^{-1}). While pseudo-capacitors based on ruthenium dioxide have been commercialized for military

applications, their high cost has limited widespread use. Other materials such as redox active polymers and other metal oxide systems are an active area of research and hold significant promise if problems with stability, a low voltage window and poor kinetics can be overcome.

2.1.2. Double-layer charging mechanism

When a power source is used to apply a voltage across two electrically insulated and non-reactive metallic electrodes, excess electrons are pumped into one electrode while the holes (i.e., the absence of electrons) accumulate within the other electrode. For a metal with a high density of electronic states, this electronic charge builds up at the electrode/electrolyte interface. Due to an applied voltage to the system, charges accumulate at the electrodes and cause ions within the electrolyte to migrate through the separator towards the interface between the electrolyte and its oppositely charged electrode. Thus, negatively charged ions will move towards the positively polarized electrode while positively charged ions will migrate towards the negatively polarized electrode. This phenomenon was described by Helmholtz in 1853 while studying a large parallel plate capacitor. Based on his model, the excess electric charge will concentrate at the surface of the metallic electrode. In response, the oppositely charged ions in the electrolyte will migrate as near as possible to the surface of the metallic electrode. In the absence of a solvation shell, the distance between the charges is approximately the ionic radius. The name "double-layer" comes from this dual layer of polarized charges[18]. Therefore, capacitance (C_H) in the system is dependent on the specific surface area (A) of the electrode, dielectric constants (ε and ε_0) and the effective thickness of the double-layer (d) based on Helmholtz's model as shown in Equation 1.

$$C_H = \frac{\varepsilon \varepsilon_0 A}{d} \qquad (1)$$

According to this theory, the capacitance is a constant value that only depends on the distance of closest approach of the ion to the electrode surface. However, in this model, the effect of thermal motion, ion diffusion, and adsorption onto the surface is not considered as parameters that affect the capacitance. Hence, the model fails to explain the change in the capacitance with potential and ion concentration in the bulk electrolyte[18]. Later studies done by both Gouy and Chapman, independently from each other, built on this description by incorporating the effect of thermal motion which acts to retard ions from all lining up at the interface in response to the electric field. Thermal fluctuations cause there to be a broader distribution of ionic charge at the interface called a diffuse layer that extends a further distance into the electrolyte from the surface. This distribution of ionic species in an electric field and considering thermal motion can be described using the Boltzmann equation (Equation 2):

$$n_i = n_i^0 \, exp^{\left(\frac{-z\,e\phi}{\kappa T}\right)} \qquad (2)$$

where n_i represents the concentration of ion species at layer *i*, and n_i^0 is the bulk concentration of the ion. The other parameters represent the charge of the ion, z, the Boltzmann constant, κ, the temperature, *T*, the charge on the electron, e, and the potential with regards to the bulk solution, ϕ.

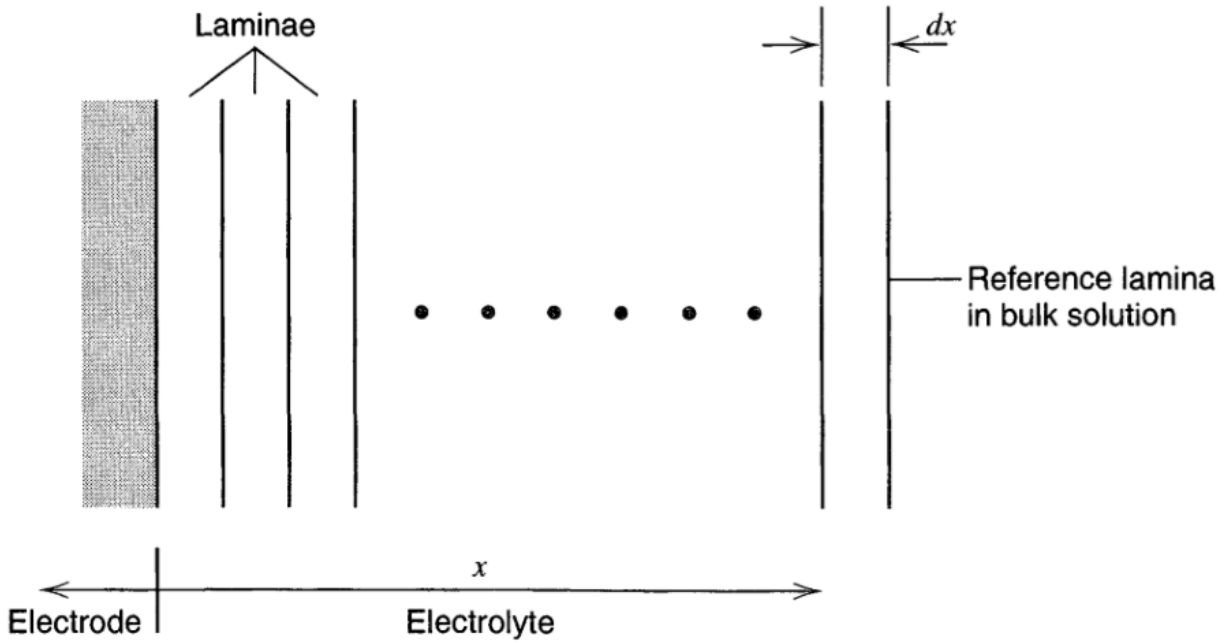

Figure 3. Schematic view of the electrolyte solution at the electrode-electrolyte interface as a series of laminae[18]

The solution phase can be imagined to be a series of vertical laminae as depicted in **Figure 3**. All laminae are assumed to be in thermal equilibrium with each other. The effect of the electrostatic potential on any ionic species is explained in Boltzmann equation (Equation 2), therefore summation of the all ionic species at any lamina will give the charge density $\rho\ (x)$ described in Equation 3. From electrostatics the relationship between the electric potential at distance x and the charge density is given by Poisson's equation (Equation 4). Combining (3) and (4) leads to the Poisson-Boltzmann equation (Equation 5) which can be solved to describe the concentration and potential profiles in the diffuse layer.

$$\rho\ (x) = \sum n\,{}_i^0 ze\ exp^{\left(\frac{-z\,e\phi}{\kappa T}\right)} \qquad (3)$$

$$\rho\ (x) = -\varepsilon\varepsilon_0 \frac{d^2\phi}{dx^2} \qquad (4)$$

$$\frac{d^2\phi}{dx^2} = -\frac{e}{\varepsilon\varepsilon_0}\sum_i n_i^0 z\, exp^{\left(\frac{-z\,e\phi}{\kappa T}\right)} \qquad (5)$$

The integration of Equation 5 gives;

$$\left(\frac{d\phi}{dx}\right)^2 = \frac{2\kappa T}{\varepsilon\varepsilon_0}\sum_i n_i^0 exp^{\left(\frac{-z\,e\phi}{\kappa T}\right)} + constant \qquad (6)$$

If the distance is far from the electrode, then the potential will be equal to zero and $\left(\frac{d\phi}{dx}\right) = 0$. The constant is evaluated based on this relationship, and is described in Equation (7) below.

$$\left(\frac{d\phi}{dx}\right)^2 = \frac{2\kappa T}{\varepsilon\varepsilon_0}\sum_i n_i^0 \left[exp^{\left(\frac{-z\,e\phi}{\kappa T}\right)} - 1\right] \qquad (7)$$

For 1:1 symmetrical electrolyte solution:

$$\left(\frac{d\phi}{dx}\right)^2 = -\left(\frac{8\kappa T n^0}{\varepsilon\varepsilon_0}\right)^{1/2} \sinh\frac{z\,e\phi}{2\kappa T} \qquad (8)$$

At metallic side, $\phi = \phi_0$; the potential drop across the diffuse layer:

$$\left(\frac{d\phi}{dx}\right)^2 = -\left(\frac{8\kappa T n^0}{\varepsilon\varepsilon_0}\right)^{\frac{1}{2}} \sinh\frac{z\,e\phi_0}{2\kappa T} \qquad (9)$$

The charge at the metallic side: $q = \varepsilon\varepsilon_0 A \left(\frac{d\phi}{dx}\right)_{\phi=\phi_0}$ (10)

The excess charge density of the metallic side:

$$\sigma^M = (8\kappa T\varepsilon\varepsilon_0 n^0)^{1/2} \sinh\frac{z\,e\phi_0}{2\kappa T} \qquad (11)$$

The capacitance of the diffuse layer:

$$C_{diffuse} = \frac{d\sigma^M}{d\phi_0} = \left(\frac{8\kappa T n^0}{\varepsilon\varepsilon_0}\right)^{1/2} \cosh\frac{z\,e\phi_0}{2\kappa T} \qquad (12)$$

Stern explained this extended model of double-layer charging in 1924. His approach to double-layer charging consisted of the combination of Gouy-Chapman's and Helmholtz's models. Consequently, the double-layer capacitance can be expressed for these two models by considering them as two capacitors in series as seen in Equation 13.[18,19]

$$C_{double-layer} = \frac{1}{C_H} + \frac{1}{C_{diffuse}} \qquad (13)$$

Based on Gouy-Chapman theory, ions act like point charges and are expected to approach to the electrode surface arbitrarily closely. Realistically ions have a finite size. Therefore their approach to the electrode surface is limited by their radius and depends on their solvation degree. If they are solvated ions, the distance between the centre of the ion and the electrode surface will become larger. At low concentration of the electrolyte solution, the impact of this layer is negligible due to the dominant effect of the diffuse layer at the interface. On the other hand, the capacitance approaches the Helmholtz model due to compressed, tightly packed ions closer to the electrode and electrolyte boundary while the electrolyte concentration increases in the system as can be seen in **Figure 4**. In Equation 13, C_H is defined by the capacitance of the Stern layer, and $C_{diffuse}$ corresponds to the capacitance between the charge at the surface and the charge in the diffuse layer or bulk solution. Therefore, $C_{diffuse}$ is a function of voltage and directly affected by the concentration of the electrolyte as can be seen in **Figure 4**, whereas C_H is independent of potential. Consequently, Stern's modification to Gouy-Chapman's work helps to develop a model that explains charging in high and low electrolyte concentrations by taking into account the finite size of ions and their approach to the electrode surface.

\

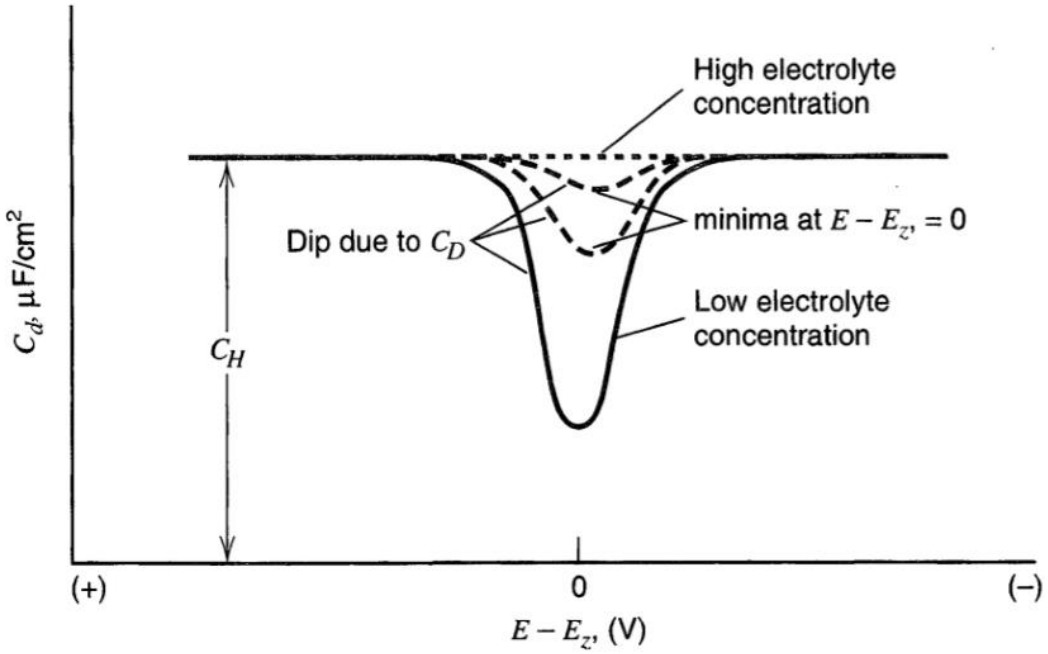

Figure 4. Expected behaviour of double-layer capacitance concerning the electrolyte concentration based on the Gouy-Chapman model[18].

2.1.3. Energy and Power Density

This stored energy is calculated using Equation 14 as shown below. *Q* is defined as the accumulated charge under a specific voltage (*V*) difference.

$$E = \frac{1}{2}QV \qquad (14)$$

The capacitance (*C*) of the capacitor is expressed by equation 8. The effect of the diffuse layer and the area of the electrode surface are the main contributors to the change in the absolute amount of charge by the potential difference. Therefore, the energy density of the device measured is directly related to the specific capacitance and the applied voltage of the cell as shown in Equation 16 below.

$$C = \frac{Q}{V} \qquad (15)$$

$$E = \frac{1}{2}CV^2 \qquad (16)$$

The power density in energy storage devices is a measure of energy delivery, and it is a function of the applied voltage and the equivalent series resistance (ESR) of the device. ESR is defined as the effective resistance of the entire system including ionic, electronic and contact resistance. Moreover, the current response of the device competes with the internal resistance while voltage is applied to the system. Internal resistance changes as a function of time in the system, therefore it is complicated to calculate the exact value of the power density. However, it is possible to estimate maximum power by the use of internal resistance (R_s) and the applied voltage to the system based on a series RC circuit model. The voltage drop can be calculated according to Ohm's law as shown in Equation 16. The maximum power density (P_{max}) is expressed using the derivative of power density (P). Current and voltage at maximum power can be found by solving the derivative of Equation 18 equal to zero, as shown in Equation 19.

$$V = V_0 - iR_s \qquad (17)$$

$$P = iV = i\,(V_0 - iR_s) \qquad (18)$$

$$P_{max} = \frac{V_{max}^2}{4R_s} \qquad (19)$$

Internal resistance (R_s) plays an essential role in the power density of the device and is constructed by the electric resistance, ionic conductivity and resistance due to the separator layer. Electronic conductance is dependent on the electrode material's conductivity and the thickness of the electrode. A thick electrode is preferred to ensure that the active material is a significant fraction of the total device weight which includes packaging, current collectors and the separator layer. However, increased electrode thickness causes a voltage drop as electrons travel through the low

conductive carbon electrodes. Therefore, thin film electrodes achieve better high rate performance due to less resistance. The second significant factor in internal resistance is the ionic conductivity which is dictated by ionic charge carriers and their mobility due to an electric field. A high electrolyte concentration (many ionic species and therefore more charge carriers) and a small solvated ionic radius (smaller ions are more mobile) are the two main ways to decrease the ionic conductivity. Moreover, electrolyte resistance is also dictated by the distance that ions have to travel between two electrodes. Therefore, the ionic path length is another significant parameter that will affect the internal resistance (R_s) in the cell.

The maximum power density can be increased by decreasing the internal resistance and increasing the cell voltage which is typically dictated by the voltage stability window of the electrolyte. As described above, the electrode and the electrolyte both dominate the internal resistance of the device. Therefore, optimization of the electrode and the electrolyte play a vital role in both the energy and power density of the device.

2.1.4. Specific Capacitance

The ultimate aim of the study of EDLCs is to achieve high energy density while maintaining high power capabilities and good cycle-life. As indicated by the double-layer charging mechanism, the capacitance is a function of both the electrode and the electrolyte. Hence, a higher surface area electrode/electrolyte interface will directly increase the capacitance. Carbon materials are considered to be the best candidate due to their ability to tailor both surface area and conductivity. Moreover, the microstructure of the electrode material plays a crucial role in the energy storage mechanism due to ion accessibility in the porous structure. Without a porous structure, the interaction between the ions in solution and the charged electrode interface would be minimal, but if the pores impose on ion transport, great amounts of surface area will become inaccessible. In

the case of high surface area carbon electrodes, the geometric surface area is different from the real surface area of the electrodes where the ions can migrate into the porous structure of the material. Typically, pores smaller than the solvated ion radius cannot participate in double-layer charging because they simply cannot fit. Therefore, the expression for the Helmholtz capacitance (C_H) can be modified based on the pores structures of the electrode surface as shown in equation 19.[20]

$$\frac{C}{SSA} = \frac{\varepsilon\varepsilon_0}{d}\left(\frac{R_{pore}-d}{R_{pore}}\right) \qquad (19)$$

This equation takes into account the three-dimensional (3D) structure of the pores and assumes the shape of the pores are spherical. The specific capacitance of the EDLC is typically reported in gravimetric units in order to quantify the performance of the device. Gravimetric specific capacitance is a very easy way to evaluate performance. It is practically simplistic to measure the mass of the active electrode and calculate the specific capacitance. Considering the density of the thick, high surface area carbon materials, evaluating the performance of the EDLC in the gravimetric unit is not fair for loosely packed electrode materials. In this case, the volumetric specific capacitance is an alternative unit which includes the density of the electrode and the volume of the electrolyte in the calculation. On the other hand, it is also important to report the areal specific surface for miniaturized, flexible thin EDLCs towards integration into micro-structured electronic devices.

In the light of the information above, the specific surface area of the electrode material is one of the most important parameters in EDLC devices as it directly affects the energy density of the EDLC. It is an important tool in order to use in an evaluation of the performance of peer devices.

2.2. Porous Carbonaceous Electrodes

2.2.1. High Surface Area Carbons

As discussed above, the double-layer charging mechanism requires large ion-accessible specific surface area to improve specific capacitance and thus provide high energy density. Carbonaceous materials are typically chosen as the base material due to their relatively low cost, electrochemically stability, and high surface area[21]. A wide variety of carbonaceous materials have been reported with suitable porosity and pore size distribution for use in applications ranging from EDLCs to conductive additives for lithium-ion batteries. Simply measuring specific surface area, depending on the measurement method, does not always indicate performance as ion accessibility at the interface of the electrode and the electrode will be limited if the pore size is too small. Thus, high surface area, pore size distribution, the pore shape and structure, and electrical conductivity are important parameters which affect performance due to the electrode-electrolyte or two-phase interface.

Activated carbons - One of the most common materials used are activated carbons (ACs)[21]. These are synthesized via the partial graphitization of carbon precursors through a thermal treatment followed by an activation process which etches away amorphous carbon from the structure, leaving behind a porous material. The activation is usually carried out by thermal treatment using steam, CO_2, and/or potassium hydroxide. The specific precursor, thermal treatment and activation recipe dictates the final surface area, pore-size distribution and electrical conductivity. The surface area of ACs can reach as high as 1000-3000 m^2/g (as determined by gas adsorption analysis). Practically, all of this surface area cannot be accessed by the electrolyte and results in limited specific capacitance when assembled as an EDLCs[22]. Furthermore, ACs engineered with high surface area typically have a low electric conductivity which limits the power density in the EDLC[23,22]. Despite these limitations, ACs are used in most commercial supercapacitors today[24].

Carbon nanomaterials - Other common, well-studied carbon structures include carbon nanotubes, graphene and its derivatives such as functionalized graphene oxide (GO). Carbon nanotubes (CNTs) have demonstrated excellent characteristics such as electrochemical, chemical, and mechanical stability as well as high electrical conductivity. As such, CNTs have been proposed as a candidate in the fabrication of electrodes for energy storage. CNTs are divided into two main groups; single wall carbon nanotubes (SWCNTs) and multi-wall carbon nanotubes (MWCNTs)[25]. Both types of CNTs have demonstrated promising performance as electrode materials for EDLCs. However, while the theoretically achievable specific surface area of a single-walled CNT at 1320 m^2/g is relatively high, the surface area drops significantly with multi-walled CNTs since ions cannot penetrate the space between them. Furthermore, due to strong van der Waals forces between adjacent tubes during fabrication, CNTs have an innate tendency to bundle together, resulting in the restricted surface area as overlapping cylinders do not touch at a point but bend into contact, preventing ions from accessing this surface area. Thus, the ions in the electrolyte are not able to access the full surface area of CNTs[26, 27]. Synthesis of SWCNTs has been very well studied in the last decade, and many studies focus on inexpensive and practical technique to achieve SWCNTs with a controlled diameter using chemical vapour deposition[28], laser ablation[29], etc.

Graphene is a more recent arrival to the list of carbonaceous materials. It was discovered in 2004 by two researchers from University of Manchester, Prof. Andre Geim and Prof. Kostya Novoselov who received the Nobel Prize in physics based on their discovery. They demonstrated, for the first time, that mechanically exfoliating graphite could isolate a single layer of graphite (called graphene) with tape. Theoretically, the surface area of an isolated graphene sheet is twice that of a single-walled CNT – reaching 2630 m^2/g.

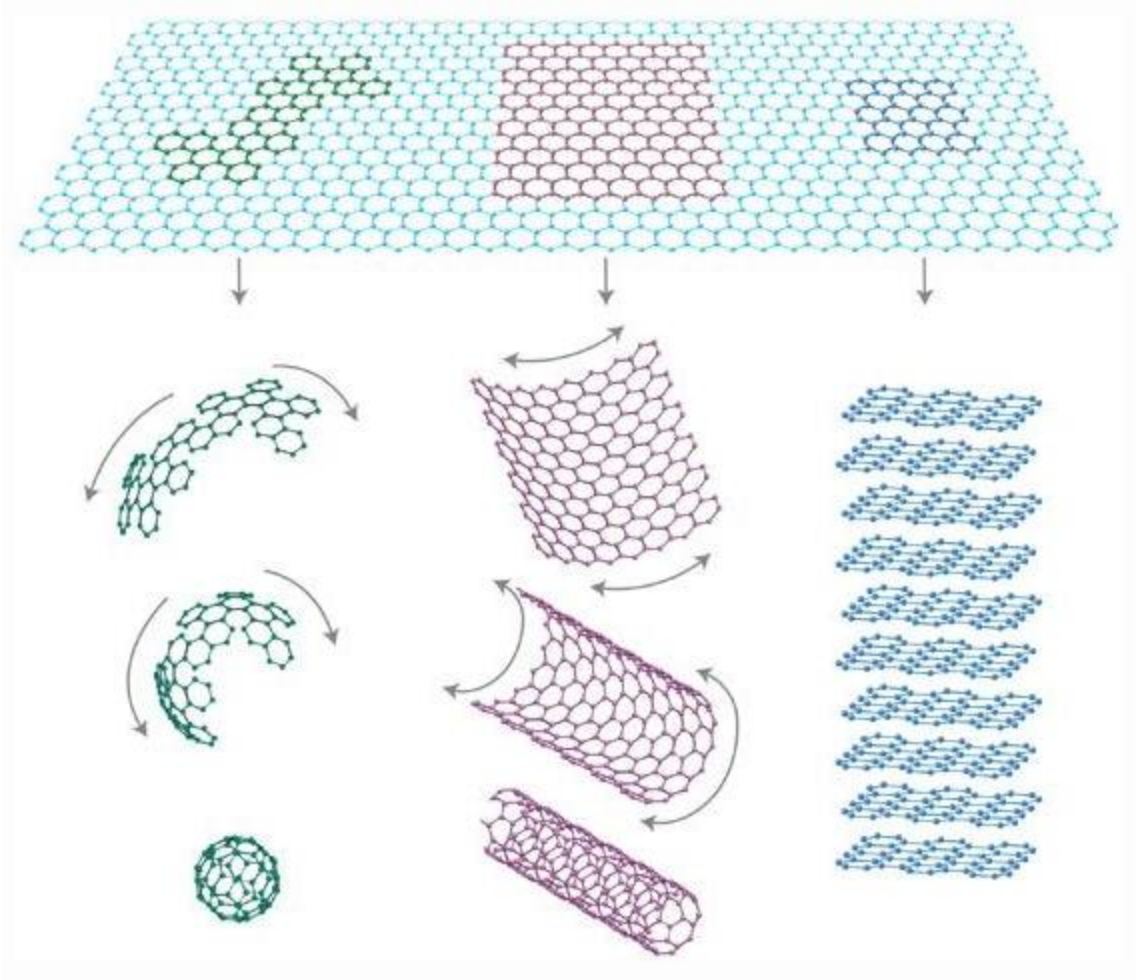

Figure 5. Illustration of SWCNT, MWCNT and graphene[30]

Besides using tape to exfoliate graphite, there have been many other methods used to produce graphene-based materials in larger scale and which could be used as electrode materials for supercapacitors. This family of materials results from the chemical or solvent exfoliation of graphite. For example, milling of graphite in different solvents can be used to reduce the thickness of the graphite to the single-sheet level. However, typically this results in stacks of few-layer graphene which significantly lowers the specific surface area of the material. On the other hand, chemical oxidation of graphite can be used to convert graphite into graphite oxide which is a 2D material easily exfoliated into single sheets in water and other polar solvents. A common technique

to synthesize graphite oxide is using the technique developed by Marcano et al. in 2010 which is referred to as the modified Hummers method. This method relies on the intercalation of oxidizer species between graphite sheets using $KMnO_4$ and strong acids like sulfuric acid (H_2SO_4) and phosphoric acid (H_3PO_4)[31]. Compared to other chemical oxidation of graphite (Hummer Method), this modified method increased the yield of the reaction, and increased the degree of oxidation, resulting in heavily oxidized graphene flakes. Graphene oxide (GO) is an electrical insulator and can be exfoliated into single sheets by ultrasonication in polar solvents. GO is reduced to rGO by removing oxygen-rich functional groups such as epoxy groups, carboxyl groups, and hydroxyl groups through thermal, chemical or electrochemical treatments. rGO is considered to be a form of graphene. However it has defects due to the removal of functional groups from lattice structure[32]. The number of defects and the ratio of carbon to oxygen are dependent parameters to the type of reduction procedure applied. Thus, this material offers the ability to retain the high specific surface area, single sheet nature of the graphene while the defects and residual functional groups can yield additional functionality. Preventing restacking of graphene sheets through functionalization leads to increased double-layer capacitance due to increasing accessible surface area of the electrode. Additionally, the introduction of defects and functional groups boosts the density of electronic states and enhances the capacitance as pristine graphene is limited in this respect due to electronic effects associated with its low density of electronic states near the Fermi level. Furthermore, the functional groups remaining on the rGO can lead to pseudo-capacitance which contributes to higher capacitive performance of aqueous-based EDLC[33].

2.2.2. Carbon Precursors

Carbon precursors provide an environmentally friendly, inexpensive, and scalable solution to manufacture ion-accessible high surface area carbonaceous materials such as graphene, CNTs, activated carbon and so forth for energy storage applications.

Utilization of biomass waste to create a green alternative in energy storage, and the ability to process these renewable sources into various microstructured carbon materials are the primary motivations for carbon precursors in industry. There is a significant payoff for the re-use rather than consumption of natural resources, fueling the move forward in utilizing natural hydrocarbons such as waste materials and food products to supply cheap, green raw materials from nature in industrial production. As shown in **Figure 6**, there are many such materials for carbon precursors that are capable of being converted into high surface area carbonaceous materials. Examples include aromatic polyimides, saccharidic biomass waste, petroleum organic waste compounds, and natural fibres such as wood, fibre-rich plants, etc[34].

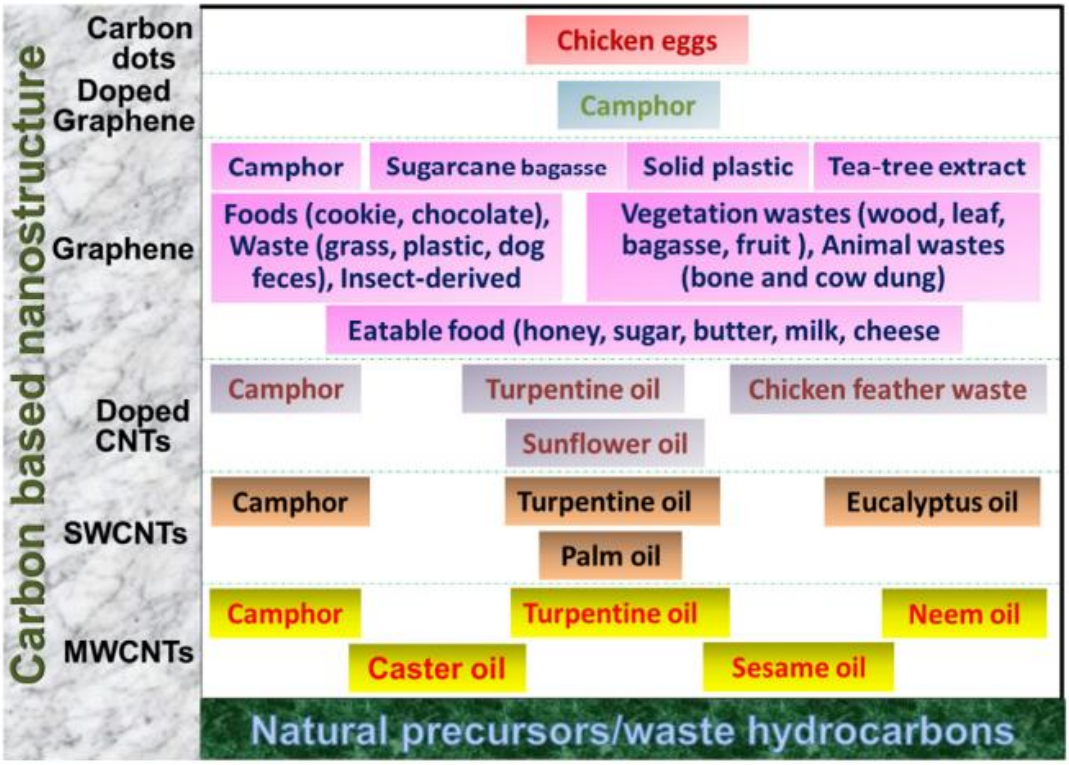

Figure 6. Natural carbon precursor and their use in manufacturing various carbon materials[34]

To fabricate high-surface area carbons from pre-cursors, established methods include chemical vapour deposition (CVD), thermal pyrolysis, arc discharge and recently laser irradiation. The laser irradiation technique has been established and used widely in ablation of polymer materials. In 2014, Lin et al. demonstrated use of a carbon dioxide laser on an aromatic polyimide precursor[35]. For the first-time, laser irradiation of carbon precursors was employed to carbonize rather than ablate the material. Further, they demonstrated the ability of carbonized polyimide as a graphene-like, high surface area electrode and used this technique to build EDLCs. Due to the patterning capabilities of the laser source, they were able to build micro-supercapacitors with the specific capacitance over 4 mF/cm^2. This was approximately an order of magnitude higher than the micro-supercapacitors fabricated via laser irradiation of graphene oxide[4]. They studied the effect of the

laser power on carbonization of polyimide, and even at low laser power (approximately 4 W), they were able to graphitize aromatic polyimide into stacked few-layer graphene as suggested by the similar Raman spectrum. Furthermore, the same research group showed the carbonization of a lignocellulose structure in wood into graphitized carbon structure through laser irradiation in 2017[36]. Based on this recent study, they discussed the effect of the different magnitude of laser power (between 7.5 to 32.5 W power) which can tailor the microstructure between meso- and micro-porous, while even higher laser power (above 33 W) demonstrated a graphene dominated carbon structures as shown in TEM images. These two studies demonstrated successful carbonization of carbon precursors via laser irradiation in a rapid manufacturing process. However both polyimide and wood with high lignin content are expensive raw materials to produce electrode materials and are not as attractive as waste-biomass sources. Therefore, there is still demand for the rapid production of high surface area, surface tailored microstructure of electrode materials through the usage of cheap renewable resources in the manufacture of EDLCs.

In this work, we demonstrate the rapid, simple fabrication of high specific surface area electrode materials via laser irradiation from saccharidic biomass waste, namely poly (furfuryl alcohol). Poly (furfuryl alcohol) is a thermosetting polymer which is synthesized from furfuryl alcohol via acid-catalyzed polycondensation under various conditions. Furfuryl alcohol (FA) is widely studied as a carbon precursor originating from renewable saccharidic biomass waste such as sugar cane and corn husks, through the reduction of furfural[15,37,38]. Carbonization of pFA results in a non-graphitizing carbon structure (**Figure 7**) with randomly oriented aromatic domains interconnected by disordered and curved carbon sheets such as graphene as studied by Foley et al[39]. Unlike polyimide which is a graphitizing carbon structure, pFA is expected to have good electrical

conductivity, mechanical and thermal stability. The main advantage of poly (furfuryl alcohol) is the high content of carbon compared to a polymer with imide groups.

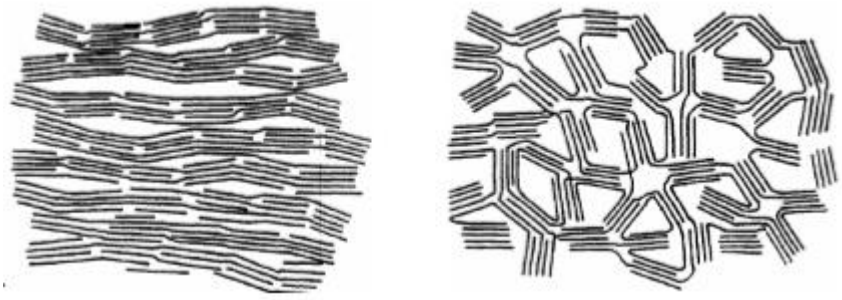

Figure 7. Illustration of graphiting and non-graphiting carbon structures[40]

To investigate electrode performance of renewable resources in a micro-supercapacitor application, poly (furfuryl alcohol) is intensively studied in this work due to its ability to carbonize into a densely packed, conductive structure[15–17,38,41].

2.2.2.1. Poly (furfuryl alcohol) chemistry and synthesis

PFA is synthesized via the poly-condensation of furfuryl alcohol, assisted by an acid catalyst such as hydrochloric, sulfuric, oxalic or p-toluene sulfonic acid. The monomer in the polymerization provides the required hydrophilic identity due the hydroxylic side chain groups and the presence of an oxygen atom in the furan ring. The resulting polymer shows hydrophobic behavior and is not soluble in water[42]. Poly-condensation of furfuryl alcohol is typically highly crosslinked, and appears to be a black resin-like polymer. Although this polymerization mechanism has been studied for more than 50 years, the exact mechanism is still unknown and complex[42]. However, there is no doubt about the formation of two type of products which are connected with methylene or dimethylene oxide bridges, as can be seen in the pFA chemical structure (Figure 8).

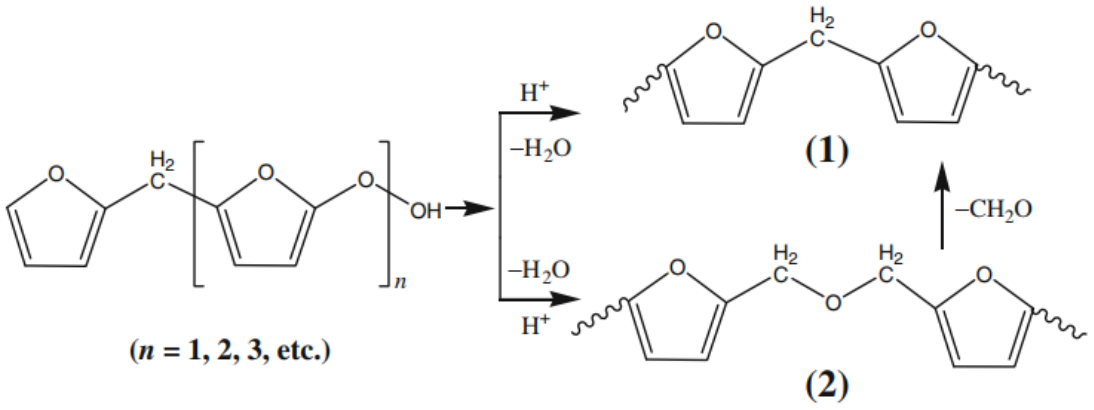

Figure 8. Schematic of polymerization of furfuryl alcohol[43]

Furfuryl alcohol, the monomer of pFA, contains a hydroxyl group in the side chain of its heteroatom furan ring. The formation of two polymer chain structures is related to this hydroxyl group that connects either one side of furan rings or other side of it through a condensation reaction. Therefore, the produced polymer results either in a head-to-tail or head-to-head chain structure as depicted in Figure 8, respectively as 1 and 2. Reported in previous studies, the secondary formation is transferred into head-to-tail chain structure in the presence of strong acid catalyst[43]. This head-to-tail reformation is proposed as the explanation for color formation and polymeric crosslinking in the final product as the interaction of hydrogen atoms in methylene bridges causes a side reaction, eventually forming a dark colored, resin-like polymer product. Crosslinking mechanism can be accelerated by temperature, acid catalyst concentration or reaction time. Although the nature of crosslinking has been intensively in literature, none of the researchers have adequately explained the exact mechanism. However, Gandini et al. suggested that hydrogen atoms in a methylene bridge propagate the polymer chain by removing hydride ions resulting in positive charges on both active units. Neutralization of these positive charged units cause the formation of

conjugations in the resulted polymer (**Figure 9**) [44]. The conjugation in the crosslinked polymer is the likely cause of the dark color present in poly (furfuryl alcohol).

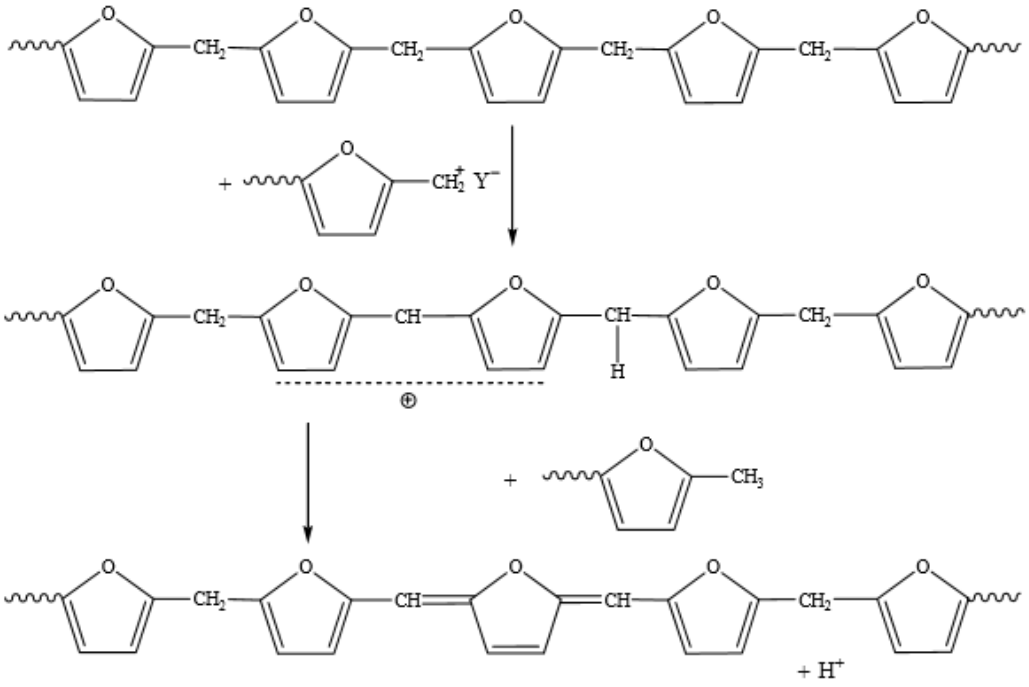

Figure 9. Schematic of conjugation mechanism of poly (furfuryl alcohol)[43]

Pyrolysis of poly (furfuryl alcohol) leads to non-graphitizing carbon structure. Unlike graphitizing carbon structures, the domains in pFA are connected by distorted or twisted aromatic domains which leads to micro-porosity in the material[45]. A thermal treatment enforces the loss of functional groups and cross-linking while producing carbon dioxide, water, methane, carbon monoxide and hydrogen in the presence of an inert atmosphere. The microstructure of carbonized pFA is tailored by varying the temperature during thermal treatment. It has been reported that larger average pores are formed in the low temperature range between 200-500°C, whereas more ordered pore structures are observed at higher temperatures and long thermal treatment times[45]. Foley et al. studied the

role of aromatic microdomains on formation of pores in carbonization of pFA, and based on their study, the microdomains tend to grow under extended pyrolysis time and high temperature, leading to a decrease in average pore size and more ordered porous structures in the bulk material[45].

Furfuryl alcohol polymerizes through polycondensation in the presence of an acid catalyst. There are two main routes that will result in polymerization. The first route is a two-step polymerization (emulsion polymerization and removal of surface reactive groups) while the second second is a bulk resinification polymerization. Emulsion polymerization is capable of synthesizing microsphere particles through emulsion, while the second step serves to crosslink surface reactive groups to prevent agglomeration via high concentration of strong acid catalyst (H_2SO_4). Furfuryl alcohol exhibits a hydrophilic nature whereas polymerized furfuryl alcohol becomes hydrophobic when high crosslinking occurs. This situation indicates a good medium for emulsion; amphiphilic particles such as surfactant creates micellar structures and encapsulates polymerized furfuryl alcohol particles into their cores whereas outside of these micelles is the hydrophilic domain. A systematic study of the emulsion polymerization of poly (furfuryl alcohol) was done by Peer and her co-workers aiming to understand all parameters which affect micellar growth, especially the crosslinking mechanism in the second step and reaction kinetics of acid-catalyzed polycondensation[42]. As a result of this study, they categorized the emulsion mechanism into 3 important parameters; the concentration of surfactant, monomer and solvent. A water and ethanol mixture was selected as the solvent system. Their results are shown in **Figure 10**, where they suggested the choice of solvent is critical for the formation of spherical particles.

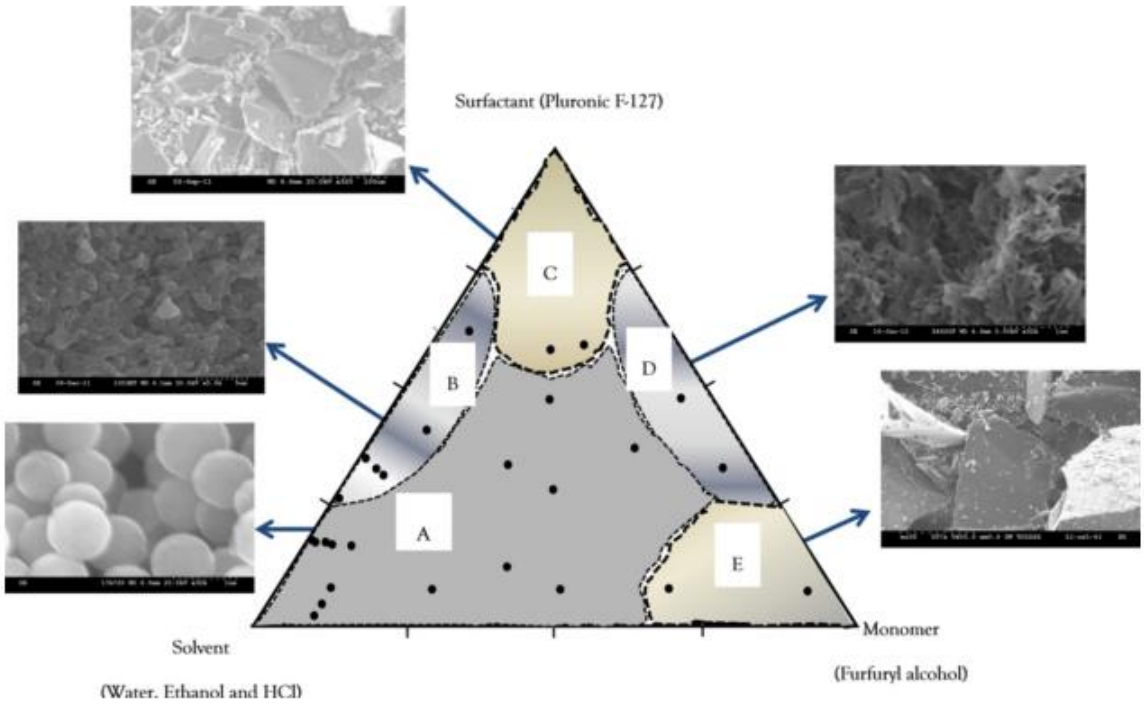

Figure 10. Phase diagram of surfactant monomer and solvent and its effects on morphological formation of carbon for emulsion polymerization of poly(furfuryl alcohol)[42]

2.3. Device Fabrication

2.3.1. Design and Challenges

Typical, large format supercapacitors on the market are built in a sandwich-like structure. The sandwich type of EDLC consists of two high surface area carbon electrodes, physically isolated by a separator and then folded or rolled up into a pouch or cylindrical cell. This type of cell consists of electrodes with thickness ranging from 100 to 300 μm. This is to increase the ratio of active material to inactive material in the device which leads to higher device-level energy densities. Thinner film electrodes typically result in higher power density (due to reduced electrode and electrolyte resistance) but results in a large fraction of inactive mass which limits the energy density achievable[1]. Moreover, the integration of these cells into micro-scaled electronic devices and flexible, lightweight new electronics is challenging due to low volumetric and areal

capacitance. Since the gravimetric and volumetric capacitance of an electrode material does not contain any thickness information, the areal capacitance does and has become an important practical metric for assessing practical device performance. For example, a commercial electrode of 300 μm thick with a bulk density of 0.5 g/cm^3 and a gravimetric capacitance of 120 F/g could achieve an areal capacitance of 1.8 F/cm^2. On the other hand, a 1 μm thick device would be 300× less (6 mF/cm^2).

This thickness effect is particularly important when one considers flexible and micro-patterned supercapacitors which are inherently of the thin film variety. For wearable applications, the capacitance or energy stored per area is critical due to the limited footprint on clothing, etc. One way to increase the thickness without sacrificing flexibility is by moving from a planar/sandwich structured device to an interdigitated one. It also allows for easier fabrication of microscale devices by printing or other direct-write approaches, making it a favourable configuration for integrated technological devices and sensors. These types of supercapacitors are generally called micro-supercapacitors due to their small size and format.

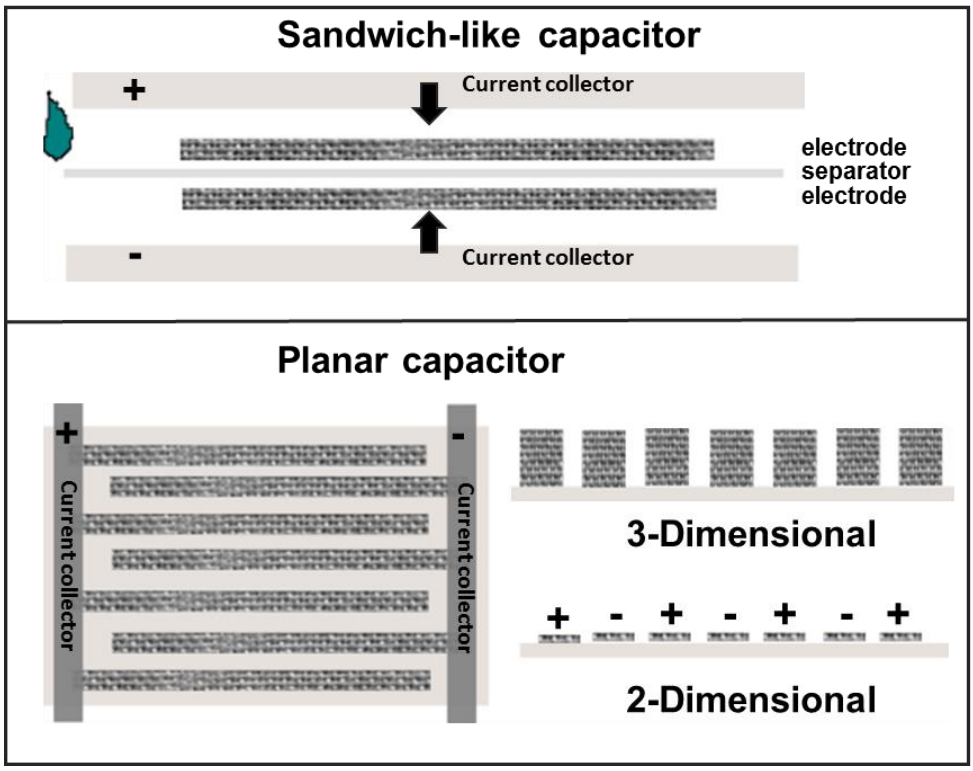

Figure 11. Schematic of different EDLC assemblies

Micro-supercapacitors consist of micro-scaled electrodes typically with hundreds of microns in electrode width and tens to hundreds of microns of separation between electrodes in a planar design as depicted in **Figure 11** and **Figure 12**. Unlike sandwich-like conventional supercapacitors, an in-plane interdigitated micro-supercapacitor has a shortened mean ionic pathway between the negative and positive electrodes. This provides a technical advantage due to a larger interaction surface between both sides of each micro-electrode [1].

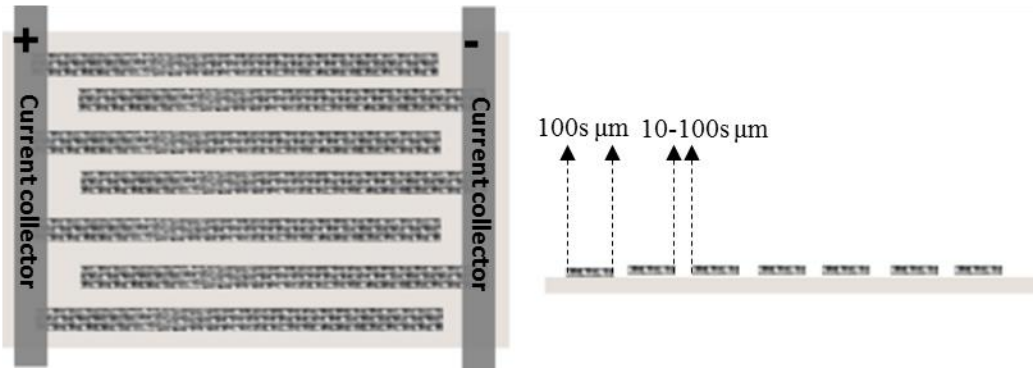

Figure 12. Illustration of in-plane micro-supercapacitors

Consequently, in-plane interdigitated design can typically reach a higher power density compared to conventional supercapacitors and batteries. Moreover, this design makes it easy to integrate micro-supercapacitors into microelectronic devices. However, as discussed, the areal capacitance and energy density of the interdigitated design is typically a small fraction of commercial planar sandwich designs due to the limited thickness of most approaches and sub-optimal electrode properties compared to optimized activated carbons. Fortunately, the advantages of interdigitated architecture can overcome this disadvantage and the general goal of this thesis is to improve the energy density by exploring new materials and methods.

Being integrated into microelectronic devices, a leak-free energy storage solution is desired. Therefore, solid-state and gel electrolytes are a pre-requisite for micro-supercapacitors. However, these often suffer from sub-optimal ionic conductivities. Gel electrolytes are often prepared with non-ionic polymer networks such as poly (vinyl alcohol) (PVA) and poly (methyl methacrylate) (PMMA). Typically, a high viscosity polymer network blends with organic or aqueous based ionic solutions and is cast onto the electrode surface fabricated in the aforementioned interdigitated design. Another advantage of this type of electrolyte is that it also serves as a separator between

oppositely charged electrodes. As a result of these advantages, gel electrolytes are commonly used in micro-supercapacitor applications[4,10,12,27,35].

2.3.2. Fabrication Techniques

A significant portion of studies based on micro-supercapacitors focus on fabrication techniques and their optimization. The fabrication method is expected to achieve certain deliverables; low-cost, simple and fast processing, and accessibility of the technique. Fabrication techniques for in-plane micro-supercapacitors are divided into two main categories; the direct and indirect deposition of electrode material on the surface of a substrate. Photolithography is widely studied as an indirect deposition method for micro-supercapacitor[1,8,47]. The electrode material is fabricated onto the photo-resist material, and the patterned design of electrode is achieved through lifting off the photoresist material from the design. This technique is inexpensive compared to traditional lithography technique and slightly more straightforward. However, it requires an additional step to remove the photo-resist material. Therefore it is not an ideal fabrication method for simple, cost-effective generation of micro-supercapacitors. Another promising method used in micro-supercapacitor research is to fabricate vertically aligned carbon nanotubes through chemical vapour deposition. Hsia and his co-workers reported 0.43 μF/cm^2 with over 1000 cycles of stability[7]. Unfortunately, these micro-supercapacitors specific capacitance is low compared to other micro-supercapacitors based on similar carbon materials which will be described in following part of this section.

Inkjet printing is a direct fabrication method that requires small enough particle size to prevent clogging on the printing nozzle and a specific viscosity to provide consistent ink flow[48]. This technique often requires having an etched current collector to print the ink as the top layer of this

conductive pattern. Hence, it needs to couple with photolithography to create interdigitated architecture on flexible substrates.

2.3.2.1. Laser irradiation technique

Laser irradiation and patterning is a simple, and can be a rapid fabrication technique as an alternative to lithographic fabrication. A laser source has been used as an energy source to remove or ablate polymer material and generate a patterned conductive surface. Recently, laser irradiation has been demonstrated on carbon precursors and in the reduction of graphene oxide on flexible substrates to cause graphitization[4,10,13,14,35,36,49–52]. This simple technique only requires a laser source, and operation in an optical protective chamber due to possible scattering of the laser. It is possible to use different laser types such as femtosecond pulsed laser[53], nano- and picosecond pulsed laser[54], continuous wave laser[13,35,36,50] and the laser irradiation have demonstrated at a various range of wavelength laser, ultraviolet, blue light[55], infrared range[13,35,36,50] and visible range laser sources[4,10,14]. Femto-, nano- and picosecond lasers are a customized type of laser sources; the cost of this equipment is the most prominent disadvantage of the use of this fabrication on an industrial scale as well as the low throughput. As an alternative, CO_2 laser-based etching/cutting machines are inexpensive, widely available and can pattern rapidly due to the larger cross-section of the sample hit by the laser in a single pass due to rapid photothermal heating. Such lasers are widely used in industrial applications for cutting and marking metal, wood, and polymer materials. Therefore, accessibility and scalability of laser irradiation can become possible via this type of laser source.

2.3.2.1.1. Laser Types

Laser systems are distinguished by the type of laser source and the duration of laser emission. Laser sources are divided into five different systems; solid state, gas, excimer, dye and

semiconductor lasers[56]. Depending on the medium used to create the laser beam determines the type of the laser. Solid state lasers were developed in 1960. They use the solid-state host as an active medium, and common active medium are doped with transition metal ions such Neodymium (Nd: YAG). YAG is the most common solid host with a few percentage addition of Nd. These type of lasers are safer due to the absence of compressed gaseous medium in the system. Solid state lasers have an operating wavelength in the range of infrared (IR) to ultraviolet (UV). They are pumped optically by a flash lamp or diode lasers. Flash pumped solid state lasers, unfortunately, are not capable of achieving high efficiency. On the other hand, diode-pumped laser are known for their low power output. These types of lasers suffer due to their short lifetime, inefficiency and low power outage compared to gas lasers[57]. Gas lasers can operate at over 10 kilowatts of power. They are based on a mixture of one or more gases or vapours at an atomic or molecular level. They operate based on electrical discharge rather than optical pumping. Based on these principles, excimer lasers can also be associated with gas lasers. Helium-Neon (He-Ne) and carbon dioxide (CO_2) lasers are two common members of gas lasers' family. Carbon dioxide lasers are made of gas mixtures of CO_2, He, nitrogen (N_2), hydrogen (H_2), water vapours and xenon to cause irradiation at 10.6 μm. CO_2 lasers are the most efficient laser type, and are well known to perform etching of various polymer materials due to their high output power. Most gas lasers irradiate light in the infrared region[58]. Dye lasers are liquid lasers and operate via a liquid medium. Organic dyes inside the solvents can be excited to an energetic state to form a laser beam. These type of lasers emit in the UV to near infrared region, and can be tuned within this spectrum. They are intensively used in astronomy and spectroscopic methods. However, they have a short dye life and complicated maintenance due to the liquid source of the medium. The semiconductor laser is the last in the family of the lasers. They are very compact and simple to build. However, they are

not capable of working at the high power required for applications. Therefore, they are typically used in telecommunications which do not require such high power.

In summary, lasers can be distinguished based on laser sources, where gas lasers are a common type used to cut or etch various type of materials compared to alternatives. The CO_2 laser is well known in etching applications due to its high working efficiency. The majority of recently published research using lasers in material fabrication are using CO_2 gas sources.

As mentioned at the beginning of the section, the duration of laser emission is also another parameter that distinguishes the lasers. Pulsed, varied frequency of the pulse and continuous laser sources each cause different results when applied onto a material. A pulsed laser is good choice to fabricate high resolution and high-quality features due to the relatively lower thermal contribution onto the incident material surface[59]. Femtosecond lasers, a class of pulsed laser, are well known for the majority of micropatterning experiments in academic research laboratories. However, their high cost and operating complexity make them less favourable when scaling towards industrial applications. Consequently, carbon dioxide lasers have been employed as an alternative microfabrication method due their low cost and simple operating conditions.

2.3.2.1.2 Laser Wavelengths

The wavelength of the laser is one of the most critical parameters that has a significant effect on laser emission and final absorption onto the surface of the material. In most cases, the wavelength is a constant parameter from the laser's source. Depending on the laser wavelength, a different type of reaction will result in the crystalline structure. For example, infrared lasers induce a photothermal effect which contributes to carbonization via local heating on the surface[59]. Infrared lasers are well suited to pattern micro-scale features onto a material surface since their penetration depth is in the range of microns. On the other hand, photochemical effects of the laser are more

dominant in the visible range (300-800 nm) by removing chemical bonds and initiating new chemical reactions. Ultraviolet lasers perform well in situations requiring fine penetration in the range of nanometers. In light of this information, the formation of micro-scale conductive arrays from carbon precursors is the most rapidly and efficiently accomplished using infrared laser sources[59].

2.3.2.2 Materials for Laser irradiation Technique

In this research, we focus on laser irradiation as a simple and promising fabrication technique in the manufacture of micro-supercapacitors. As this type of method and application has been attempted in research before, it is useful to generate a comparison of all previous studies; comparing what they used as precursors, their method, design and results in Table 1. Several studies promote polyimide as a promising carbon precursor due to its ability to carbonize via laser irradiation and a high electrochemical performance compared to graphene oxide. Polyimide contains many heterocyclic groups in its polymer structure. Hence, it exhibits the ability to be graphitized by laser irradiation. This behaviour is also observed in polyetherimide (PEI), another imide group polymer[60]. The studies listed below demonstrated the use of different type of electrolytes (aqueous, organic, ionic liquid) in micro-supercapacitors. However, laser irradiated polyimide primarily has been reported with the use of an aqueous-based electrolyte, this indicates the ion accessibility of this carbon structures is limited otherwise large molecule electrolyte compounds such as ionic liquid and organic electrolytes would perform similarly. Aqueous based electrolytes are well known due to their smaller sized ions; however, they have a limited voltage window between 0-1 V due to a water splitting potential around 1.2 V. On the other hand, organic and ionic liquid electrolytes can provide a wider voltage window of 2.5 V and 4 V respectively.

The combination of polyimide via CO_2 laser irradiation patterned into interdigitated architecture, and aqueous-based electrolyte in the gel formed has resulted in the highest reported specific capacitance in recently studied literature[55]. It achieved up to 31.9 mF/cm^2 at a 0.05 mA/cm^2 current density following a plasma treatment which improved the contact between the pores and ions at the interface of the electrolyte and the electrode. Plasma treatment helps to improve the surface hydrophilicity of the polyimide after laser irradiation; polyimide tends to exhibit higher hydrophobicity after laser irradiation. This has been studied and demonstrated in an early study in literature[61].

This research is motivated by several possible improvements to these recently studied micro-supercapacitors. First, investigation of an alternative material which improves the hydrophilicity relative to polyimide, possibly through controlling the micro-structure. Secondly, use of a cheaper and more easily accessible electrode material, best if recyclable and industrially available. Third, a material which can be rapidly and easily graphitized or carbonized with high conductivity, preferentially when exposed to laser irradiation. Fourth, that micro-scale features are well-resolved in order to optimize and maintain the electrode structure. Based on these criteria some potential candidates emerge worth investigating including saccharidic based biomass waste materials.

Table 1. Studies based on micro-supercapacitor fabricated through laser irradiation

Electrode Material	Electrolyte material	Fabrication Technique	Device Configuration	Specific Capacitance	Cycle Life	Ref.
rGO	Hydrated GO	Laser irradiation (CO_2 Laser printer)	In-plane circular design	0.51 mF/cm2	<10,000 cycles	[11]
rGO	PVA/H_3PO_4 H_3PO_4 Organic IL	DVD-writer (732 nm Laser beam)	Sandwich-like cell	3.67 mF/cm^2 4.82 mF/cm^2 5.02 mF/cm^2	>10,000 cycles	[37]
rGO	Ionogel PVA/H_2SO_4	DVD-writer (732 nm Laser beam)	Interdigitated design	2.35 mF/cm^2 3.05 mF/cm^2	>10,000 cycles	[4]
CNT	Ionogel	Laser-assisted dry transfer and lifted off	Interdigitated design	0.43 mF/cm^2	-	[7]
Laser-induced Graphene (Polyimide)	PVA/H_3PO_4	Laser irradiation (532 nm)	Interdigitated design	0.8 mF/cm^2	>3,000 cycles	[12]
Laser induced Graphene (Polyimide)	Aqueous electrolyte	Laser irradiation (CO_2 Laser printer)	Interdigitated design	4 mF/cm^2	9,000 cycles	[27]
Laser-induced Graphene (Polyimide)	PVA/ H_2SO_4	Laser irradiation (CO_2 Laser printer)	Sandwich-like cell	9.11 mF/cm^2	8,000 cycles	[13]
Boron doped graphene (Polyimide)	PVA/ H_2SO_4	Laser irradiation (CO_2 Laser printer)	Sandwich-like cell	16.5 mF/cm^2	12,000 cycles	[38]
Laser-induced Graphene (Polyimide)	PVA/ H_2SO_4	Laser irradiation (405 nm pulsed laser)	Interdigitated design	31.9 mF/cm^2	-	[43]
Laser-induced Graphene (Polyimide)	PVA/ H_2SO_4	Laser irradiation (405 nm pulsed laser)	Interdigitated design	25 mF/cm^2	-	[55]

In this thesis work, different carbon precursors are tailored by an infrared (CO_2) laser source with a 10.6 um wavelength. A CO_2 laser was chosen to perform experimental patterning via thermal effects on localized areas of a crystalline substrate. Furthermore, other significant parameters, namely the laser power, scan rate, and local environment are optimized to control carbonization of the base materials (polyimide, graphene oxide, poly (furfuryl alcohol) and their composites).

Chapter 3. Laser-Induced Graphene using Carbonizable Precursors

3.1. Introduction

As discussed in Chapter 2, laser patterning techniques are promising for the rapid fabrication of graphene-like structures to create conductive patterns for flexible electronic and electrochemical devices. Laser irradiation has only recently been adopted as a technique to modify the morphology and chemical structure of polymers and graphene oxide. This technique has several advantages such as its accessibility, scalability, cost and time efficiency compared to chemical, thermal and other photo-thermal techniques such as photolithography. The first study to use light to create patterned graphene films was published in 2009 by Cote et al. They demonstrated the ability to pattern freestanding GO films using a high power xenon lamp under an inert atmosphere. This study proved that photo-thermal energy could initiate reduction of GO to create rGO into conductive arrays for chemical sensing[62]. However, one of the disadvantages of this method was the need for an external mask to create the desired pattern on the material surface. This study inspired many others by proving the concept of fast and straightforward fabrication of conductive arrays from an initially non-conductive substrate.

Around the same time, Abdelsayed et al. reported the photo-thermal reduction of GO under ambient conditions through the water dispersion of GO. This study demonstrates the laser-assisted reduction process on individual GO sheets rather than the previous study that carried out the reduction on thick films of restacked GO. They focused on different laser wavelengths to aid in distinguishing the reduction behaviour of graphene oxide. They found that two-photon absorption has contribution to reducing GO dispersion in water[63]. Their study consists of using two different wavelengths of laser beam to reduce GO into rGO; 355 and 532 nm respectively. Moreover, they provide information to shed light on the mechanism of removal of functional groups. Based on the

X-ray diffraction (XRD) pattern of exfoliated and reduced GO, they observed an increased d-spacing in exfoliated water dispersed graphene oxide sheet up to 8.14 Å due to the presence of hydroxyl and epoxy groups between sheets through oxidation of graphite flakes[63]. By the time of exposure to the irradiation, the intensity of 2θ peak decreases and eventually disappears which indicates the restoration of sp^2 hybridization in the lattice structure. They have found similar behaviour for both 355 and 532 nm laser exposure. However the time required for conversion varied between two different laser beams. They have also noted that there is no deoxygenation of graphene oxide observed after the exposure of a 1064 nm, YAG based laser beam. Moreover, their investigation demonstrated the presence of carbon-oxygen double bond disappears after laser exposure at 355 and 532 nm and the absorption shift during characterization through UV-viscometer indicates the transition of π to π^* due to aromatic carbon-carbon bonds. Similar results are also observed in chemical reduction of graphene oxide. Increased time and the volume of the solution for the laser exposure resulted in higher degree of deoxygenation in GO solution and the color of dispersion changed into black from light brown as indication of the presence of rGO[35]. The volume and exposure time were also investigated in several later studies[14,52], and their results are supported with various types of laser exposure including femtosecond laser, DVD-writer, CO_2 laser, KrF excimer pulsed laser. As a consequence of these findings, it has been demonstrated several times that an amorphous carbon structure can be patterned rapidly without using any harmful chemicals or high-temperature furnaces. The laser or photo-assisted reduction process can be a substitute for chemical or thermal annealing and exfoliation procedures.

In recent years, Kaner and his coworkers took laser irradiation of graphene oxide a couple of steps further by performing deoxygenation via rapid and inexpensive laser source. They demonstrated that a simple commercial LightScribe technology, which is a DVD-writing software that uses the

738 nm laser of a DVD writer, to activate dye particles on DVD labels, could create over 100 small supercapacitors on a DVD surface in 20 mins[49]. This technique was a breakthrough for supercapacitor fabrication regarding accessibility of the method and the low-cost production. However, they were only able to reach areal capacitances of up to 9 mF/cm^2 with these miniaturized supercapacitors. Expanding on this work, Tour and his research group in 2014, demonstrated the use of a low-cost CO_2 laser cutting/etching system to pattern a graphene-like material into a commercial polyimide (Kapton™) film[35]. This study showed that the commonly used CO_2 laser is very capable of fabricating conductive arrays from several types of commercially available polymers such as polyimide and polyetherimide. Unfortunately, the use of polymer chains is limited to a small group of polymers which contains imide groups in their backbone to carbonize through laser irradiation based on this study. Later studies by the same group have focused on creating custom polyimide films which can be doped, for example, with boron[64] or loaded with nanoparticles[65]. They demonstrated improved double-layer charging compared to previous work on rGO. However, they have only been able to achieve a maximum areal capacitance of 19 mF/cm^2 using the boron-doped graphene[64] which is still far from the areal capacitance of a large format EDLC (~1 F/cm^2) as discussed above.

In the following chapter, a newly procured commercial CO_2 laser system is investigated for laser-induced carbonization studies on polymer and polymer nanocomposites. Here we focus on developing protocols for and finding optimum laser processing parameters using this system by employing both Kapton™ films and homemade GO films supported on polyethylene terephthalate (PET) substrates.

3.2. Material and methods

3.2.1. Materials

For GO synthesis, phosphoric acid (97%, Sigma-Aldrich), sulfuric acid (98%, Sigma-Aldrich), graphite flakes (Natural, 99.9%, -10 mesh, metal basis, Alfa-Aesar), potassium permanganate (EMD Millipore), hydrogen peroxide (30% solution contains inhibitor, Sigma-Aldrich), hydrochloric acid (ACS Reagent 37%, Sigma-Aldrich) and Reagent alcohol (90% ethanol, 5% isopropyl alcohol, 5% methyl alcohol, Sigma-Aldrich) were used as received. Commercial Kapton™ polyimide films and tapes (25HN tape, 15HN tape and 0.005" thick film, semi-clear amber) were obtained from McMaster-Carr and phosphoric acid and sulfuric acid has been blended with dissolve poly (vinyl alcohol) (165 kDa molecular weight, hydrolyzed, 98%, Fischer Scientific) for gel electrolyte and they used as received without any purification.

3.2.2. Methods

3.2.2.1. Laser irradiation of carbon precursors

Carbon precursors were irradiated via a CO_2 laser (BossLaser 1416XL) in order to fabricate patterned electrodes for EDLCs. Polyimide and GO were used to gain a better understanding of and to optimize laser patterning protocols such as operating mode, power and scan rate. All experiments are designed for micro-supercapacitors application. Moreover, the effect of the electrode and the electrode design on EDLC performance are discussed in this part of the study as preliminary experiments for the further study of poly (furfuryl alcohol)/graphene oxide composite (Chapter 4).

3.2.2.2. Characterization of patterned electrodes

The performance of laser patterned electrodes were characterized electrochemically using cyclic voltammetry, galvanostatic charge/discharge and electrochemical impedance spectroscopy (EIS). Raman spectroscopy (Horiba Raman Division, Olympus BX41, 532.06 nm) and scanning electron microscopy (Zeiss FESEM Leo 1530, at 5 kV) are used for further characterization of carbon structure and the electrode morphology, respectively.

Raman spectroscopy was carried out on a dense film prepared the same way as the electrode films. The spectra were fit using Lorentzian fit for both D and G peak. The Lorentzian fit is described by Equation 20:

$$y = y_0 + \frac{2A}{\pi} \frac{w}{4(x - x_c)^2 + w^2} \qquad (20)$$

Where x is the frequency, w describes the full width of half maximum (FWHM), x_c is the centre point of the peak, and A indicates the area of the peak.

Using Raman spectroscopic data, the crystalline size (L_a) in the a-axis direction of the lattice is calculated using Equation 21 below:

$$L_a = \frac{560}{E_1^4} \frac{I_G}{I_D} \qquad (21)$$

Where E_1 is the excitation laser energy used in Raman spectroscopy in eV units, and the ratio of intensities between G and D peak is represented by I_G / I_D in the equation[66].

3.3. Results and Discussion

3.3.1. Power and Scan Rate

Laser power and scan rate are the two crucial factors in the amount of energy transferred into the material upon exposure by the laser. The power of the laser can be tailored between 1-100% of its maximum power; altering the depth of penetration and amount of energy transferred into localized heat. The scan rate defines the amount of energy that is transferred over time into a specified area. Hence, the first step of this study was to determine the optimum power and scan rate to carbonize the material effectively. This was gauged by measuring the resistance of the traces.

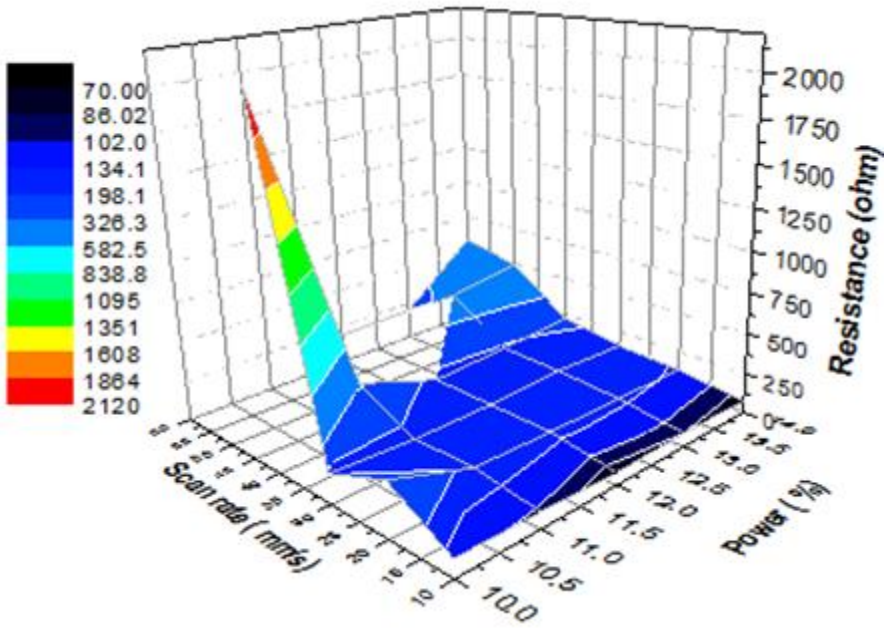

Figure 13. Electrode resistance as a function of the laser power and scan rate using electrodes 1 mm in length and 350 µm in width. The precursor material was Kapton and the system was operated in scan mode.

Figure 13 is a 3D plot to find the in which varied laser power and scan rates resulted in a change in resistance, where a low resistance indicates higher carbonization. For this specific CO_2 laser, the recommended range for scan rate is between 1 to 375 mm/s, while the power range varies between 0-100% of the total power of 50W. A series of sample polyimide films were irradiated between 10-16 % of maximum power (5-8 W) at scan rate between 10 and 60 mm/s as shown in **Figure 14**. The test was limited to the specific ranges such that it will carbonize the polyimide rather than cutting through or ablating the polymer substrate. At low scan rates (10, 20 mm/s), the resistance values tend to be low (70 to 100 Ohms) in the wide range of laser power (between 10% to 14% of 50 W). From this series of experiments, the optimum scan rate is determined as 30 mm/s in the range of 10 to 14 % of the total power since it provides low resistance and provides the best resolution in controlling the electrode width (~350 µm). These results lead us to consider the effect of laser exposure towards local heating and thermal exposure rather than photonic exposure of the laser. This optimization study is repeated every time for each type of base material including GO, Kapton™ with different thicknesses, and the polymeric nanocomposites (discussed in Chapter 4) that have been studied in this thesis work. The resistance and consistency of the electrode design (i.e., no breaks in the conductive trace) after laser exposure were the two main criteria to determine the optimum point for laser power and scan rate. Fluctuations in laser power due to misalignment over time or sample to sample variation led us to make small changes within the ranges specified (**Table 2**) during the course of day-to-day electrode fabrication.

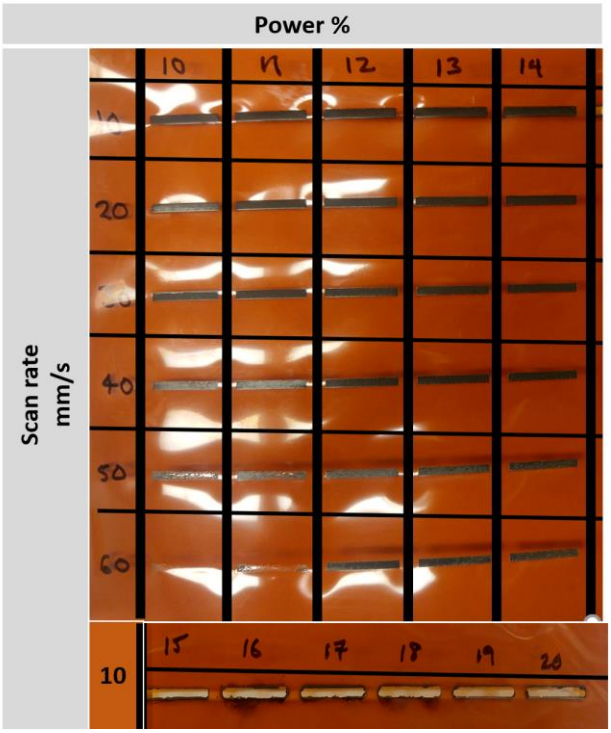

Figure 14. Photograph of scans at various powers and rates illustrating the optimization results for polyimide-based laser-induced graphene in the scan operating mode.

Table 2. Approximate power required to cause carbonization of the base material at 30 mm/s scan rate through laser irradiation

Material	Power range at 30 mm/s
GO	8 to 9.5 %
pFAGO	8.5 to 9.5 %
PI (125 µm)	10 to 12 %

3.3.2. Patterning Parameters

Lasers have been broadly applied as an intense photo-thermal source to cut through or ablate specific materials in the fabrication of various electronic devices. The excitation energy of the laser is transferred and absorbed into the incident material to remove or partially degrade the structure.

The amount of energy can be tailored to remove a specific degree of functional groups in the base material. Most CO_2 lasers are operated by two different modes; either vector cut or scan (engraving) mode. In this study, two different operating modes of the CO_2 laser are used to pattern electrodes on a polymer composite surface: scan mode and cutting mode. Either mode is used to create conductive electrodes array in interdigitated micro-supercapacitors. In **Figure 15**, the electrodes are created through carbonization of polyimide in both scan and cutting mode of the laser. In order to operate a cut mode, the line is drawn using the laser design software (RdWork 8.0) and the laser is automatically operated to cut the line on polyimide surfaces. There is no width assigned to the electrodes. These two methods differ by the operating function of the laser beam. The operating principle of cutting mode relies on a single linear path, designed to penetrate deep and ablate/carbonize with a narrow width. To target a specific electrode width requires either multiple passes in cut mode that are offset by the beam-width or a specified width pass of the scan mode beam. In scan mode, the beam closely follows a square wave path. As demonstrated in Figure 15, as the cut mode progresses, due to the deposits of ablated material and other beam effects there is an inconsistent edge profile of the electrode. On the other hand, the square wave of the scan mode can be repeated reliably in order to achieve the desired exposure while providing a consistent electrode shape. Scan mode is an excellent operating technique to engrave images onto the material since light waves will hit every small pixel on the computer-aided design (CAD) file and is expected to result in more continuous features. For the remainder of test results, all samples were prepared using scan mode settings at various widths.

A comparison of these two modes leads to very obvious differences as shown in Figure 15. The same schematic pattern (**Figure 16**) was used, and the only difference was the type of mode selected in the fabrication of electrodes from pFA/GO thin films assembled into micro-

supercapacitors. Cutting mode demonstrates observably thinner line widths, and will obviously have less material to hold point charges. These micro-supercapacitors are tested via cyclic voltammetry technique, and their results are shown in **Figure 17**. Based on the electrochemical performance, the scan mode specific areal capacitance reaches a three times (3x) higher value compared to the micro-supercapacitors prepared in cutting mode.

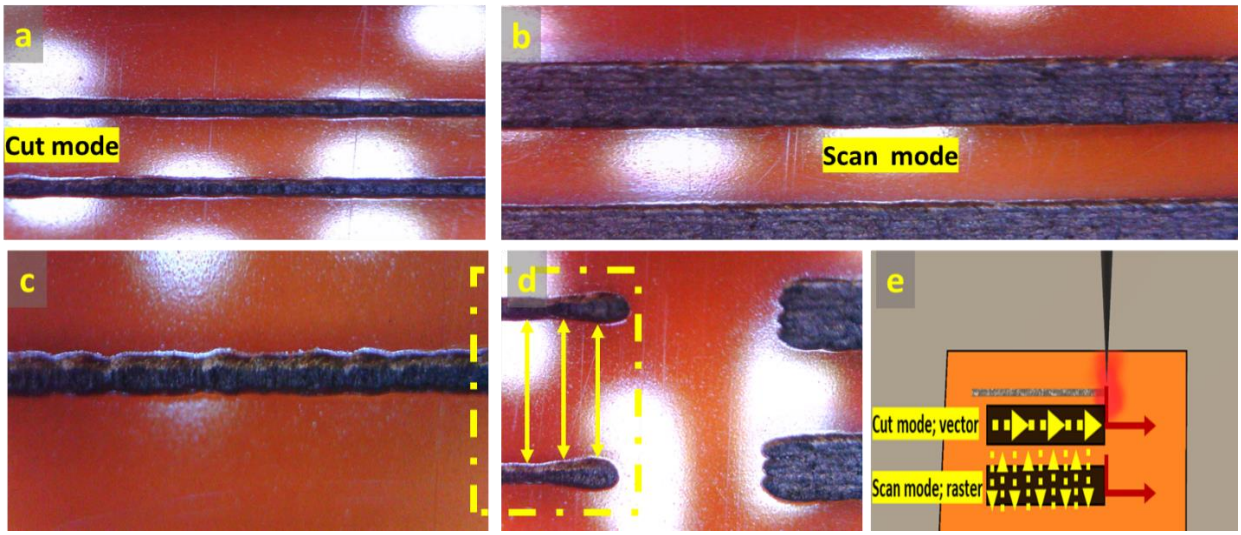

Figure 15. Laser induced graphene electrodes are created through the two operating modes of a CO_2 laser on polyimide surface; cut and scan mode. Electrodes are designed to be 350 µm for scan mode and the line is created in order to carbonize an electrode for cut mode **(a-d)**. Operating principles are animated for cut and scan mode where arrows represent the direction of the laser beam in each operational mode **(e)**.

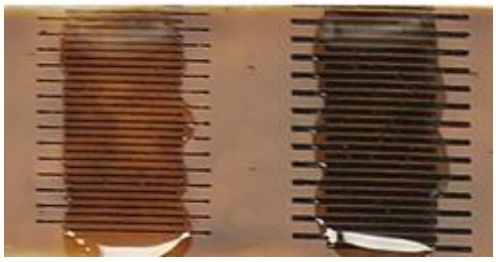

Figure 16. Illustration of pFAGO micro-supercapacitor cells patterned by laser cutting mode (left) and scan mode (right)

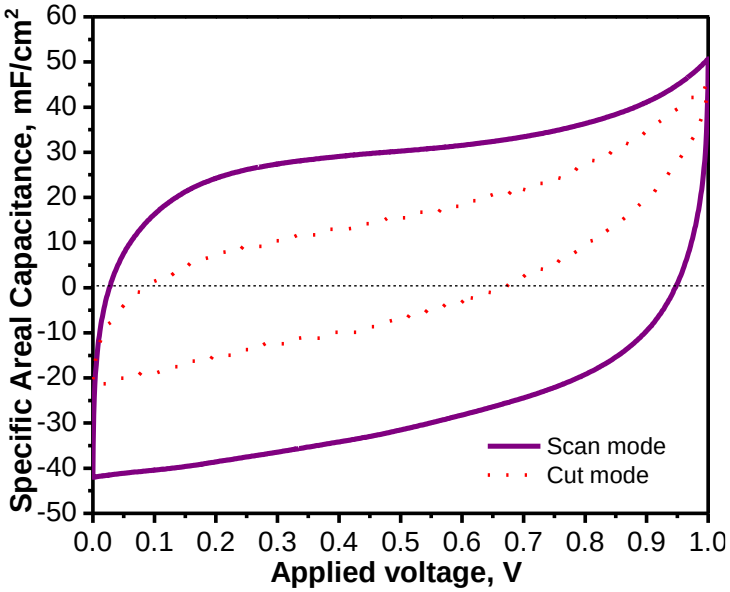

Figure 17. Cyclic voltammograms of two different micro-supercapacitors; the electrodes are carbonized via cut and scan operating mode of the laser on polyimide 125 µm films and results are listed at 5 mV/s, PVA/H_3PO_4 gel electrolyte is used as electrolyte and separator.

The goal of this preliminary study was to obtain higher capacitance by optimizing the laser parameters to maximize the specific capacitance of the device. Based on these results, a scan mode laser was selected to perform the next steps of the work.

3.3.3. Optimization of Exposure Route

The CO_2 laser is an infrared laser source. Therefore it is expected to have a thermal impact on the microstructure and chemistry of the material. Local heating can play a key role in tailoring conductivity, the degree of carbonization and degree of crystallinity or graphitic nature of the lattice structure. Therefore, we tested the effect of multiple laser passes over the conductive traces and its effect on the structure of the material and the performance of the micro-supercapacitors. Results based on this study are tested via electrochemical characterization (cyclic voltammetry) as well as material characterization such as Raman spectrum, optical microscopy. This investigation was carried out by performing laser exposure multiple times on polyimide and graphene oxide films in the pattern of an interdigitated electrode array. Polyimide samples were fabricated into a micro-supercapacitor and tested via cyclic voltammetry. Results in **Figure 18** shows that the number of laser passes affects the electrical double layer capacitances for fabricated micro-supercapacitors. Multiple laser passes led to a higher specific capacitance as indicated by the increasing width of the current response in the cyclic voltammograms. Previously, Cai at al (2017) studied the effect of an increased number of laser exposure on the electrochemical performance of the EDLCs and this group demonstrated a significant increase in the capacitance between 5 and 20 times exposure by LightScribe technology[67]. The increase in the electrochemical performance is assumed to cause an increase in the conductivity of the electrode. However, 125 µm Kapton™ film, when exposed three times with 1-minute breaks between every laser exposure demonstrated capacitance drastically improved compared to multiple continuous or one-time exposure of the laser. This behavior can be explained by the local heating and deposition of oxygen rich-groups back onto the surface of the substrate. From CV curves, samples fabricated by three times laser exposure with 1-minute break demonstrated elongation from the rectangular shape as a sign of

pseudo-capacitance contribution to the specific capacitance. Hence, three times laser exposure is adapted to carry out the rest of the micro-supercapacitor application in the following work.

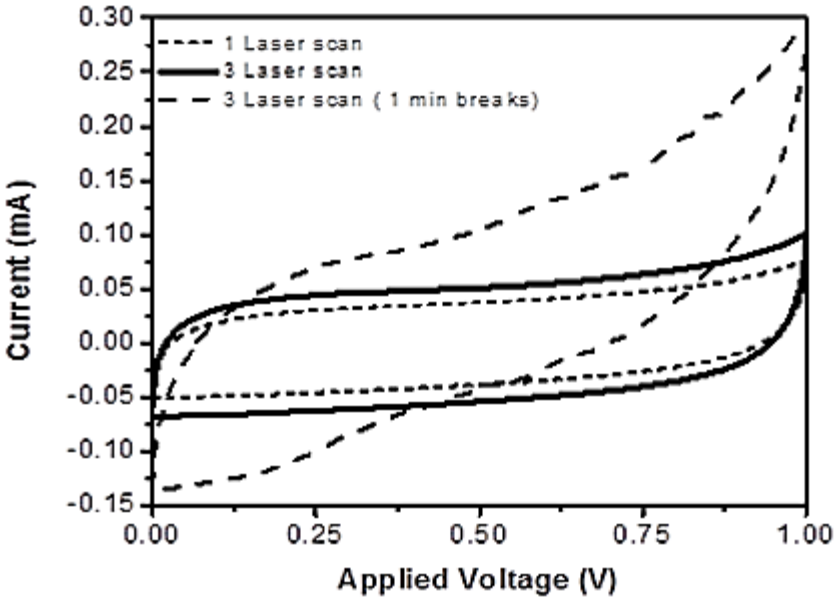

Figure 18. Cyclic voltammograms recorded by testing electrodes fabricated with different number of repetitive scans over the surface and rest time; 125 µm, Kapton™ polyimide films are all irradiated by 6 W power at 30 mm/s speed with scan mode and PVA/H_3PO_4 gel used as a electrolyte and separator.

3.3.3 Raman Spectroscopic Analysis

To further understand how the laser affects the carbonization of graphene oxide and polyimide, different laser exposure times and bulk samples before laser exposure were examined via Raman spectroscopy.

Figure 19 shows the result of Raman spectra of the carbonized polyimide (Kapton™ film, 125 µm thick). The G peak (~1585 cm^{-1}) represents the E2g vibrational mode of the carbon atom, and the

D peak (at around 1350 cm^{-1}) represents the breathing modes for six atom rings and requires a defect for activation. In this spectrum, the D peak decreases in intensity upon repeated laser exposures; however, broadening is observed in G peaks due to the evolution of D' peak in Figure 19. Broadening of G peak is also present in the triple exposure of polyimide. The intensity change between D and G peaks give information about disorder in lattice structures. The ratio of G peak to D peak is calculated as 0.76 after the first laser exposure, increases to 1.09 in the second laser exposure and decreases back approximately to 0.74 in the third laser exposure as shown in Table 3. The Raman spectrum is an important characterization tool in order to measure the characteristic distance between defects; often defined as crystalline size L_a. Approximate crystallite size is calculated using **Equation 22** as expressed in **Section 3.2.2.2**. Based on the calculation, L_a is proportional to the G to D peak ratio and reaches 20 nm in size at the double laser exposure. This study is in agreement with the previous work done by Lin et al in 2014 for laser irradiated polyimide films. In their study, they found the effect of increase laser power leads to increase in crystalline size up to 4.8 W due to contribution of surface temperature and a decrease is observed at higher power value than 4.8 W due to degradation in the quality of graphene[35]. Degradation in the quality of graphene is supported by an increase in the D peak when high laser power is applied. In our case, similar behavior is observed between L_a and D peak intensity. Also, the D' peak at 1675 cm^{-1} appears after the first laser exposure in the Raman spectrum while the intensity of 2D peak increases at 2700 cm^{-1}. However, the peaks are weakened after the second laser exposure on polyimide surface. The two point resistance was measured for electrode lines scribed with one to three laser exposure on polyimide films and results are noted below in **Table 3**. Based on this test, we observed the decrease in resistance with increasing laser exposure. We can combine this

information with the observed changes in the Raman spectra and interpret results in terms of an increase in the lateral crystallite size of the graphene domains.

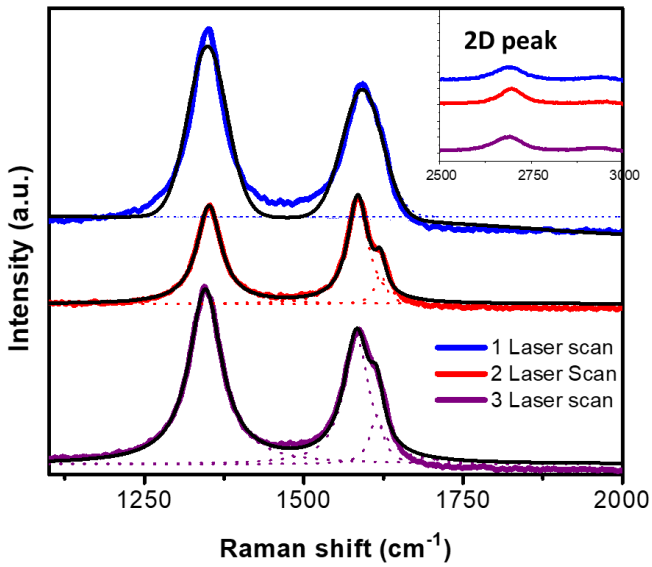

Figure 19. Raman spectrum of different number of exposure on laser irradiated 125 µm polyimide film. Samples were exposed 20 times for 45 seconds at a 533 nm wavelength.

Figure 20a and **20b** show the Raman spectra and peak deconvolution for thermally reduced graphene oxide[68] and laser-reduced graphene oxide. All fitted parameters for the G and D peaks are shown in Table 3. The positions of the peaks may be varied by the excitation energy of the laser; however, the values are reported in this study are based on 532 nm excitation laser. On the other hand, the G peak is located around 1590 cm^{-1} and is associated with sp^2 hybridized carbon pairs and chains. The ratio between G peak and D peak (I_G/I_D) intensities and FWHM provides information about the degree of crystallinity of the material due to changes in sp^2 hybridization in the lattice structure caused by CO_2 laser exposure. Figure 20b shows the structural changes in the graphene oxide lattice using different numbers of laser exposures. As seen in Figure 20 the D peak

is broadened following scanning with an initial 4.7 W laser at 30 mm/s scan rate. On the other hand, the G peak is also observed to broaden. However, compared to the D peak the broadening effect is not as dominant. Broadening in the G peak is usually a sign of defects occurring in the lattice structure. If the laser is removing some functional group from graphene oxide, it will cause defects closer to sp^2 six carbon atom rings. Moreover, the D peak starts to narrow down, and the intensity of the peak is similar to that of the G peak after the second laser exposure. This Raman study was cross checked with the study published in 2015 by Pope et al. which investigated the impact of thermal treatment on the lattice disorder of the resulting graphene oxide. The results are reproduced in Figure 20a and show parallels between the two de-functionalization methods in the Raman spectrum. Specifically, functionalized graphene oxide shows the same behavior as an 1100°C thermally exfoliated sample in the reference study to three times laser exposure.

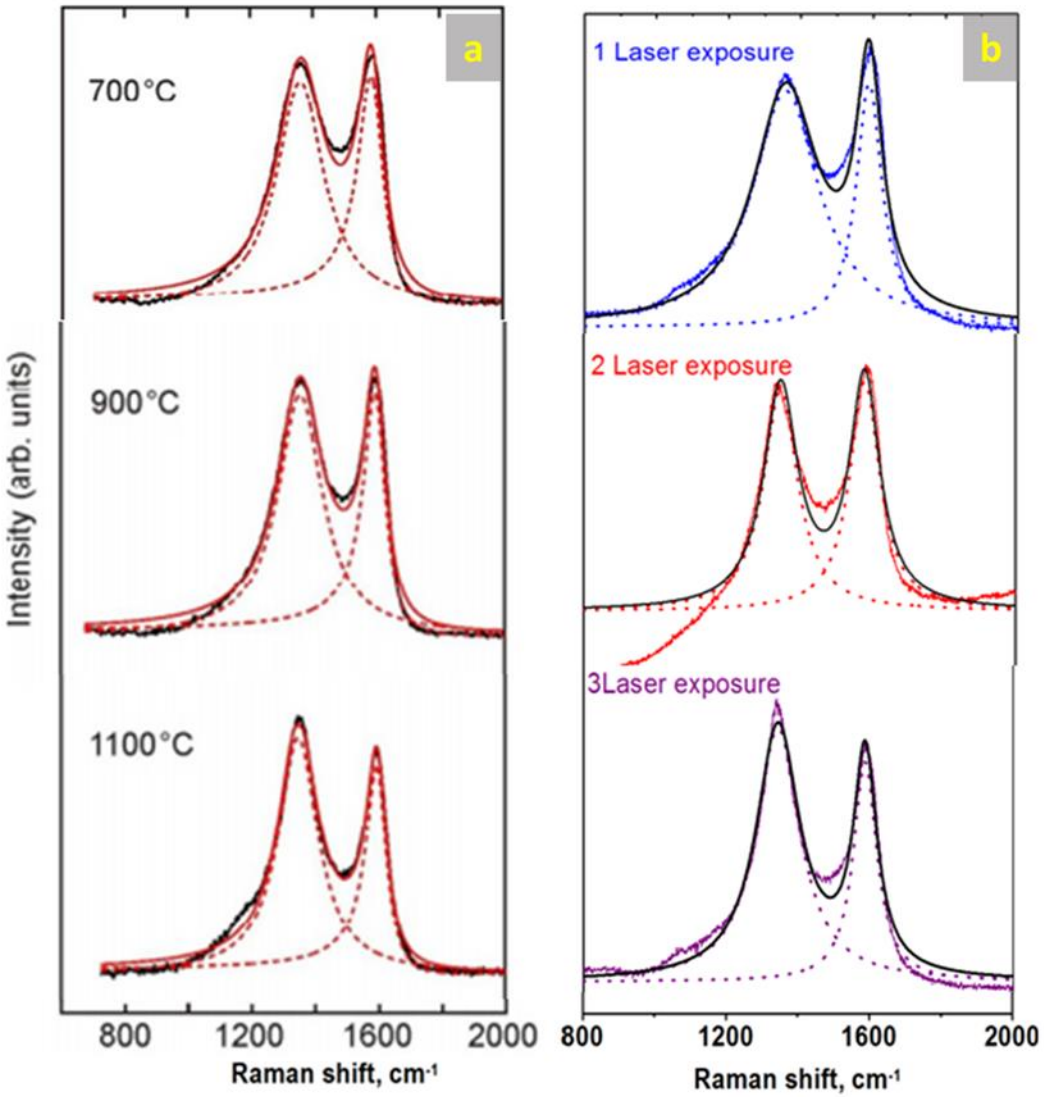

Figure 20. Raman spectrum of thermally exfoliated graphene oxide [68] (left) and laser irradiated graphene oxide (right). Samples were exposed 20 times for 45 second exposures at a 533 nm wavelength.

Table 3. Raman spectroscopy results for D and G peak of laser irradiated graphene oxide and Kapton™ polyimide film

	FWHM		Intensity		Areas		Resistance, ohm	L_a, nm	I_G/I_D
	D peak	G peak	D peak	G peak	D peak	G peak			
GO-1 laser scan	220.68	86.8	439.2	453.29	152,246.06	61,843.98	-	19.22	1.03
GO-2 laser scan	115.34	102.13	563.52	585.89	102,098.97	93,964.17	-	19.99	1.04
GO-3 laser scan	148.44	79.9	346.69	300.02	80,836.55	37,669.89	-	16.72	0.87
PI-1 laser scan	61.34	63.21	157.23	119.5	12,088.95	9,466.25	48.6	14.03	0.73
PI-2 laser scan	46.52	38.59	90.02	97.79	6578.67	5928.3	36.5	20.96	1.09
PI-3 laser scan	62.11	48.96	160.14	115.84	15,625.64	8,909.12	28.2	13.84	0.72

Chapter 4. Laser Patterning of Poly (furfuryl alcohol) and Graphene oxide Nanocomposite

4.1. Introduction

In this Chapter, a CO_2 infrared laser is used to pattern and convert polymer/graphene oxide (GO) composites into high surface area, interdigitated electrodes and their performance investigated as micro-supercapacitors. The polymer used is poly (furfuryl alcohol) (pFA), a thermoset that is easily produced via homo-polymerization of a monomer (furfuryl alcohol) obtained in large-scale from biomass waste such as sugarcane bagasse and corn husk. It is known to carbonize into dense, nanoporous hard carbon (i.e., non-graphitizable) upon heat treatment which we will demonstrate can be induced by the CO_2 laser. In this thesis chapter, we discuss our efforts to optimize the polymerization procedure, casting approach and laser parameters to create a superior micro-supercapacitor technology. We expect this new material to accelerate the development of various technologies such as micro-supercapacitors and micro-batteries in micro-electromechanical systems (MEMs), micro-robots, solar cells and flexible electronics.

4.2. Material and Methods

4.2.1. Materials

Chemical reagents were used as received. These include phosphoric acid (97%, Sigma-Aldrich), sulfuric acid (98%, Sigma-Aldrich), graphite flakes (Natural, 99.9%, -10 mesh, metal basis, Alfa-Aesar), potassium permanganate (EMD Millipore), hydrogen peroxide (30% solution contains inhibitor, Sigma-Aldrich), hydrochloric acid (ACS Reagent 37%, Sigma-Aldrich), reagent alcohol (90% ethanol, 5% isopropyl alcohol, 5% methyl alcohol, Sigma-Aldrich), furfuryl alcohol (98%, Acros Organics, nitrogen flushed), Pluronic F127 (powder, Bioreagent, suitable for cell culture, Sigma-Aldrich), oxalic acid (≥99%, ReagentPlus, Sigma-Aldrich). Phosphoric acid and sulfuric

acid has been blended with dissolve poly (vinyl alcohol) (165 kDa molecular weight, hydrolyzed, 98%, Fischer Scientific) for gel electrolyte and they used as received without any purification.

4.2.2. Synthesis of Poly (furfuryl alcohol)

4.2.2.1. Emulsion polymerization

The synthesis procedure was adapted from the study carried out by Yao et al[69]. The emulsion polymerization of furfuryl alcohol (FA) was carried out under ambient temperature and atmospheric pressure. The amphiphilic triblock copolymers, Pluronic F127 or Pluronic P123 were used to stabilize the oil-in-water emulsion formed during the initial stages of polymerization. In 20 mL of a 7:3 ratio (v/v) ethanol to water mixture, 3 g of surfactant was dissolved. To this solution, 1.4 g of 37% HCl was dissolved as a catalyst for the polycondensation reaction. This solution was stirred for 5 min before adding 3 g of FA drop-wise. The polymerization was carried out for 8 hours, 12 hours, 16 hours and 24 hours to produce different samples.

The second step was to further induce crosslinking within each spherical polymer particle and to prevent irreversible aggregation and crosslinking between particles upon drying as demonstrated by Yao et al[69]. In this step, a strong acid catalyst, 5 M or 9 M H_2SO_4 was used at the half of the volume of polymer solution (~11.9 mL) and added into polymer mixture. The final mixture was left to evaporate at 90°C for one hour. After evaporation of water and ethanol from the polymer solution, the final product was a dark brown, viscous dispersion. This product was diluted with water and vacuum filtered (0.2 μm nitrocellulose membrane) and the filter cake rinsed with 100 mL DI water four times. During this step, unreacted monomer and surfactant were removed. The filter cake of poly (furfuryl alcohol) was left to dry under vacuum oven overnight.

4.2.2.2. Solution polymerization (no surfactant)

In this polymerization technique, the procedure was the same as the emulsion polymerization, except no surfactant was added. Each step of emulsion polymerization was repeated in this procedure.

4.2.2.3. Bulk resinification

The synthesis of a monolithic poly (furfuryl alcohol) resin was carried out by addition of 5 mg of oxalic acid, as a catalyst, per mL of furfuryl alcohol (typically 25 mg oxalic acid/ 5 mL furfuryl alcohol) at 70°C for 21 hours in a oil bath. The mostly polymerized, viscous resin was spin coated at 2500 rpm onto glass slide and left at 70°C for 12 hours more to finalize the polymerization.

For the samples including GO, the polycondensation of pFA resin was carried out by addition of 11.3 mg graphene oxide, as a catalyst, per mL of furfuryl alcohol (typically 22.6 mg GO/ 2 mL furfuryl alcohol) at room temperature for a day and spin coated at 2500 rpm speed onto glass slide and left at 70°C for 6 hours more to finalize the polymerization.

4.2.3. Synthesis of graphene oxide

Graphene oxide was synthesized based on the modified Hummer method[70]. Briefly, 3 g of graphite and 18 g of potassium permanganate ($KMnO_4$) were added under stirring to a 9:1 ratio of sulfuric acid (H_2SO_4, 360 mL) to phosphoric acid (H_3PO_4, 40 mL). The oxidation reaction was carried out at 45°C for 16 hours. The resulting mixture was cooled to room temperature and poured into 400 ml of ice water to offset the heat released by diluting the concentrated acid solution. Approximately 8 ml hydrogen peroxide (H_2O_2) was added to the reaction mixture until the color of suspension turned golden yellow in color from an initial brownish purple. The resulting suspension was washed 6 times through solvent exchanging by centrifugation. Centrifugation was carried out using

a Thermo-IEC Centra-CL2 centrifuge machine at 4000 rpm for 30 min. The first two washes were carried out by resuspending the collected pellet with 37% hydrochloric acid followed by four times washing with ethyl alcohol to remove the HCl.

4.2.4. Preparation of composite for laser irradiation

Graphene oxide and poly (furfuryl alcohol) were each dispersed in ethanol to a final concentration of 12 mg/mL. These two dispersions were then mixed in weight ratios of 1:1, 1:2, 2:3, 3:2, and 2:1. These dispersions were tip ultrasonicated (BioLogic, 150 VT Ultrasonic homogenizer) at 40% amplitude for 15 min to break up aggregates of graphene oxide and the polymer particles. The resulting mixture of polymer and graphene oxide became darker and more viscous when compared to the individual pure dispersions. These dispersions were drop-cast onto cleaned 2.5 x 2.5 cm^2, 100 μm thick poly (ethylene terephthalate) (PET) sheet at 1.61 g/cm^2. The dispersion was spread uniformly on the PET without flowing over the edge, aided by the surface tension of ethanol. A total of 30.6 mg of composite material was deposited on each micro-supercapacitor device based on the determined deposition concentration. Drop-cast films were dried under ambient conditions for at least 12 hours prior to electrode fabrication. In this study, the same deposition method was used for pure graphene oxide films as described above.

4.2.3. Fabrication of Micro-supercapacitor

4.2.3.1. Electrode fabrication

A CO_2 laser cut/etching machine (BossLaser 1416L) was used to selectively carbonize all graphene oxide and graphene oxide/poly (furfuryl alcohol) (GO/PFA) composite films in order to pattern the interdigitated electrode architecture. An electrode vector file was designed using the software used to run the device (RDWorks, Version 8.0). The drop-cast films were placed into the

laser machine's platform and patterned into interdigitated electrode designs as shown below in **Figure 21**. The ruler used for scale is in centimeters.

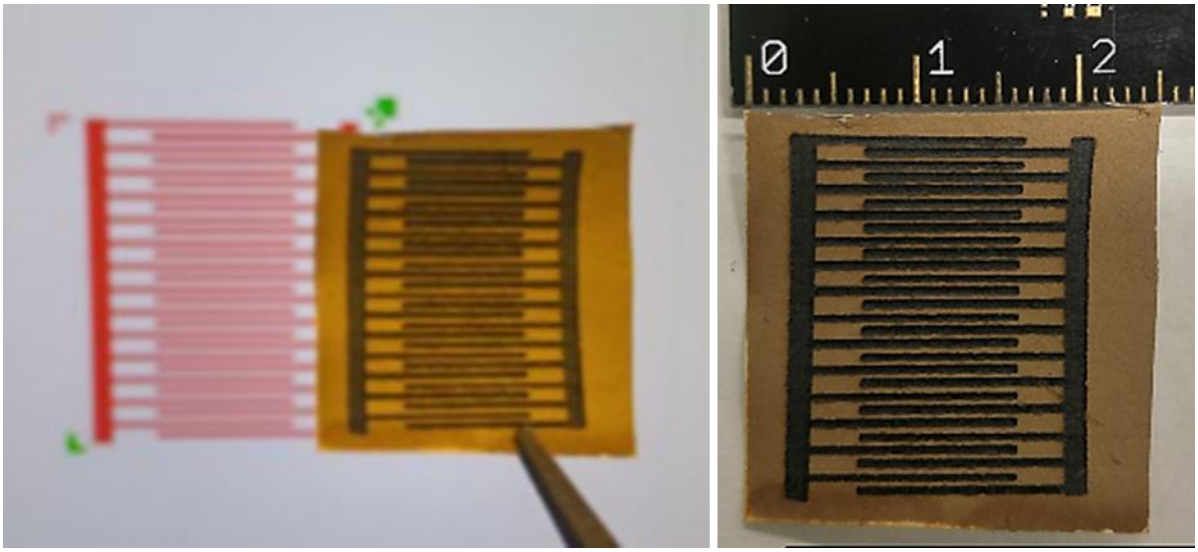

Figure 21. Illustration of electrode fabrication via laser irradiation

The dimensions of fabricated electrodes (i.e., each interdigitated finger) are a rectangle measuring 1.5 cm in length and 350 µm in width. The spacing between each electrode was fabricated as 450 µm, and electrolyte is deposited on a 1 cm width along the center of the entire interdigitated structure to capture the densest interactions of the negative and positive electrodes.

4.2.3.2. Preparation of electrolyte

An aqueous-based gel electrolyte was used in the fabrication of micro-supercapacitors in this study. Poly (vinyl alcohol) (PVA) was chosen as the polymer material to provide high viscosity for the electrolyte solution. 1 g of PVA was dissolved in 9 M phosphoric acid (H_3PO_4) at 85°C for 2 hours, and the resultant viscous solution was cooled to room temperature for deposition onto the electrode surface. 230 mg of the cooled electrolyte solution was spread onto the electrode surface (1 cm width x 2 cm height) using a flat glass slide (1 cm width).

4.2.3.3. Electrochemical testing procedure

Before performing electrochemical testing, the assembled micro-supercapacitor was dried for 24 hr. This ensured that the electrolyte had set as a gel. The micro-supercapacitors were tested with cyclic voltammetry (CV), galvanostatic charge/discharge (GC) and electrochemical impedance spectroscopy (EIS). All the measurements were carried out using a BioLogic SP-300 Potentiostat under ambient conditions using the test cell shown in **Figure 22** which was built from a laser cut poly (methyl methacrylate) (PMMA) sheet to provide stable contacts to the electrode bus bars during measurements.

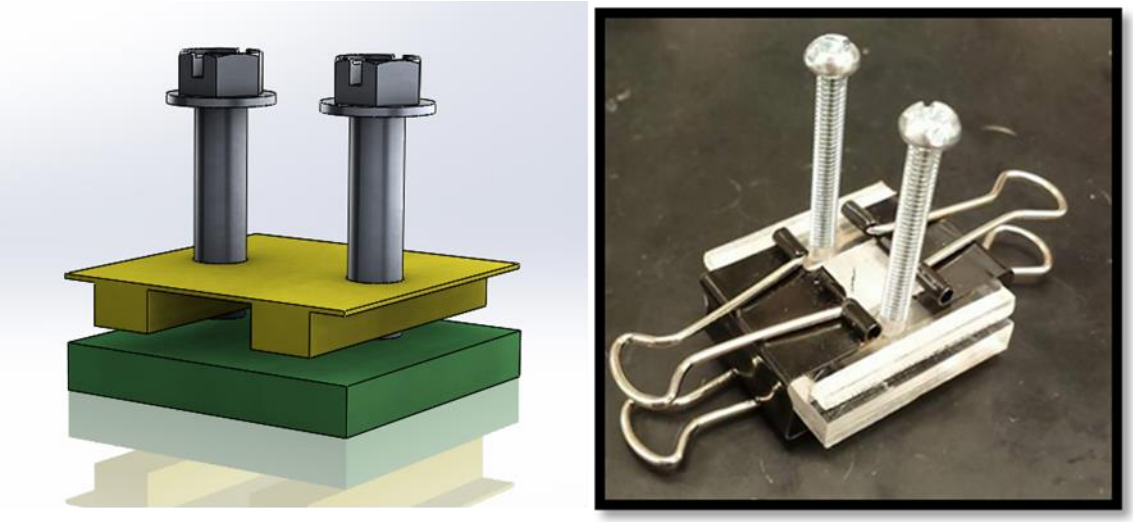

Figure 22: Schematic of testing apparatus in a two-electrode configuration

Cyclic voltammetry is an electrochemical method which probes the double-layer characteristic behavior of the device, providing information about the capacitance. A two-electrode configuration was chosen for cyclic voltammetry testing in this study. The counter electrode and working electrode were connected to one of the current collectors, and a reference electrode was connected to the other current collector. The single electrode capacitance is calculated by using Equation 22 below, where i_{avg} is taken as the average of absolute value for anodic and cathodic current at the midpoint of the total voltage window.

$$C_{specific} = 2 \times \frac{i_{avg}}{\frac{dV}{dt} \cdot A} \qquad (22)$$

$C_{specific}$ is calculated as a function of the scan rate (dV/dt), average current at anodic and cathodic electrodes and the area (*A*) of the total area of electrodes covered by the electrolyte (~0.98 cm^2). Therefore, the results from this measurement are reported in the units of mF/cm^2 at various scan rates in the range from 0.05 to 0.5 V/s. The voltage window for the measurement was 0-1 V. In the case of ionic liquid electrolyte, voltage window was selected as 0-1.5 V in air atmosphere to prevent any redox reaction.

Galvanostatic charge/discharge is a technique that provides a voltage response dependent on the applied current. This technique gives a more realistic view of the performance of the device in applications. In this work, the current input is selected as 0.15 mA for all measurements.

Electrochemical impedance spectroscopy (EIS) is used to understand the frequency dependence of the resistances and capacitances in the device. EIS was carried out between 10^6 Hz to 10^{-2} Hz using sinusoidal perturbation of amplitude 10 mV at a constant 0 V DC potential.

X-ray photoelectron spectroscopy (Thermal Scientific KAlpha XPS spectrometer, 150 eV) was carried out on powders from the electrodes of polyimide and 2:3 pFAGO composite; after laser irradiated powder are scrapped off from the electrode surface. The spectra were fitted using the CasaXPS software.

4.3. Results and Discussion

In the following sections we first discuss the chemistry and morphology of the precursors used for laser-induced carbonization followed by the characterization of the results of drop cast film of

these materials onto flexible PET supports. Robust films are then laser patterned, characterized and tested as micro-supercapacitors. This is followed by a discussion regarding the comparison of laser-induced films created using PI, GO and PFA.

4.3.1. Characterization of PFA

Figure 23 shows representative SEM images of the PFA particles produced via the various suspension and emulsion polymerization recipes used. In the absence of surfactant during the condensation polymerization reaction carried out in a water and ethanol solution, the powder is composed of aggregates of sub-micron-sized primary particles which are non-spherical in shape as shown in **Figure 23a**. This morphology arises as low molecular weight polymers, initially soluble in water, precipitate out from solution as they grow. Since there is no surfactant, there is no stabilization mechanism preventing agglomeration due to van der Waals forces. While this powder morphology is not as uniform or controlled as the others to be discussed, it did have a significant processing advantage in that the lack of surfactant significantly enhanced the filtration rate and expedited washing of the material. Emulsion polymerization, through the use of the triblock copolymer surfactant Pluronic F127, successfully formed very well resolved spherical polymer particles between 200 nm and 3 μm in diameter as shown in **Figure 23b**. These particles were also further cross-linked in the presence of a strong acid at 90°C for 1 hour (9 M H_2SO_4) . Early studies done by Peer et al. in 2012 show the importance of the combined amount of surfactant, solvent and monomer on the formation of specific particles shape as discussed in section 2.2.2.1 and Figure 10. Towards further uniformity in polymer particles, a second surfactant structure, Pluronic P123, was tested and the strength of the acid catalyst reduced. **Figure 23c** and **23d** show the resulting powder obtained after emulsion polymerization with Pluronic F127 and P123, respectively, using the same cross-linking agent of 5 M H_2SO_4 for 1 hour. Pluronic F127

has a molecular weight of 12600 Da and a cloud point at 100°C, while P123 is lower at 5600 Da and a cloud point at 91°C. As the reactions take place at 90°C, phase separation should be avoided in both cases. However, it can be observed that the lower molecular weight and cloud point of P123 resulted in a lesser uniformity of the particulate size and shape, while F127 retained spherical polymer particles between 0.9 and 2 μm. As temperature fluctuations in a vial will vary from the source (hot-plate) and the probe location, it is likely that localized micellar groups experienced temperatures in excess of 90°C, causing the breakdown of the spherical micelle in the case of P123. Thus, the remainder of experimental tests were performed using F127. Several studies[37,42,69] have also reported a suggested concentration of 5 M H_2SO_4. Therefore, two concentrations of acid at 5 M and 9 M following a 12-hour emulsion were chosen to compare their effect on particle aggregation and these results are presented respectively in **Figure 23e** and **23f**. Although slight variances are shown in the particle size, these cannot necessarily be attributed to the change in concentration. Further, the final cross-linking was not visibly different. To maintain the particle integrity, 9 M H_2SO_4 was employed as the cross-linking solution for the bulk polymer synthesis in the preparation of flexible micro-supercapacitors. One additional comparison can be drawn between the 12 and 24-hour reactions presented in Figure 23b and 23f, but which resulted in no observable difference in polymer quality. This two-step synthesis, namely emulsion followed with cross-linking, forms a powder product unlike a resin in a one-step method.

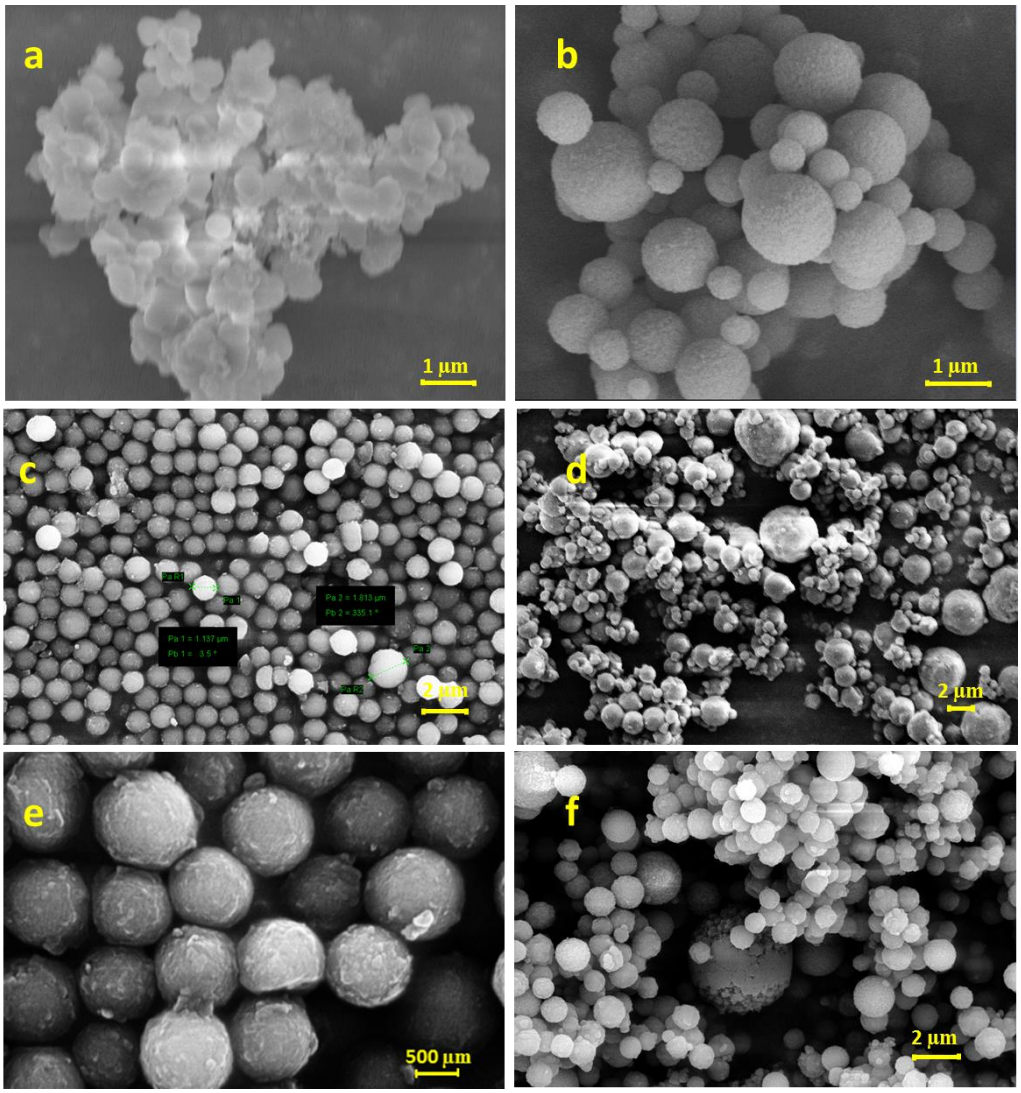

Figure 23. Scanning electron microscopy images PFA particles produced by different recipes. (a) Suspension polymerized pFA without surfactant; (b) Emulsion polymerization using Pluronic F127 , 24 hour first step and crosslinking with 9 M H_2SO_4 for 1 hour; (c) Emulsion polymerization via surfactant Pluronic F127 for 12 hours; crosslinked with 5 M H_2SO_4 for 1 hour (d) Emulsion polymerization using the surfactant Pluronic P123 a 12 hours first step and crosslinked with 5M H_2SO_4 for 1 hour; (e, f) Crosslinking comparison of emulsion polymerized pFA with 5 M (e) and 9 M (f) H_2SO_4 after 12 hours reaction using the surfactant Pluronic F127.

Figure 24 shows the FTIR spectra for the emulsion polymerized using Pluronic F127 as the structure directing agent as a function of reaction time. As the reaction time increased (***24a*** to ***24d***), there are significant changes in the highlighted (dashed) peak intensities related to the structure of pFA. The characteristic peaks of pFA are located at 596 cm^{-1} (C-H out-of-plane), 730 cm^{-1} (furan rings), 788 cm^{-1} (C-H in-of-ring), 1014, 1150, and 1505 cm^{-1} (furan rings), 1559 cm^{-1} (C=C stretching in furanic ring), 1711 cm^{-1} (carbonylic furan ring opening). An increase in peak intensity is observed for the 24 hour reaction for ring formation at 1350 cm^{-1} (aromatic ring), and C-O stretching peak at 1100 cm^{-1} and C=C stretching in the rings at 1559 cm^{-1}. Little to no change was observed between the 8, 12, and 16 hour reactions for pFA, except for a slight decrease in the peak intensity between the 8 and 12 hour reaction at 788 cm^{-1} and 1711 cm^{-1} which are associated with carbonyl groups. These same peaks increased in intensity between the 12 hour and 24 hour reactions.

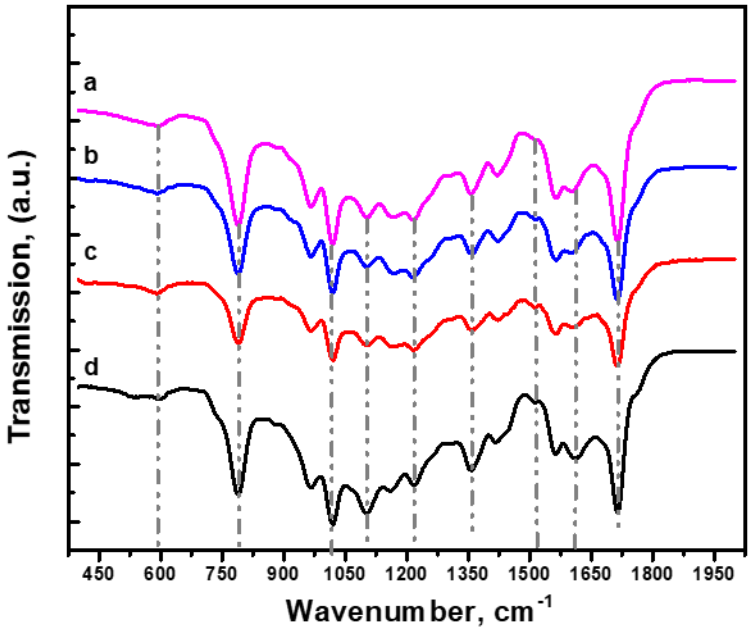

Figure 24. Fourier transform-infrared spectroscopy results for different reaction time 8 hours (a), 12 hours (b), 16 hours (c), and 24 hours (d)

4.3.2. Characterization of graphene oxide

Figure 25 shows AFM images of the graphene oxide (GO) sheets produced after spin coating a film from the ethanol dispersion on an atomically flat muscovite mica. This method results in the identification of GO sheet thickness and size. Based on AFM measurements, the sheets are approximately 1 nm in thickness indicating successful exfoliation of the material into single sheets. A few overlapping double and triple layer sheets apparent in AFM images are likely caused by the spin coating process. The average lateral size of the GO sheets ranged between 1-2 μm, while outliers reached up to 7 μm. This indicates that the GO sheets are only slightly larger in diameter than the PFA spheres discussed above. It is well known that GO contains a significant number of functional groups in the form of epoxy, hydroxyl and carboxylic acid groups with an overall C/O ~ 1.7. Unless the material is thermally or chemically reduced to remove this oxygen and partially reform graphene domains, GO acts as an electrical insulator.

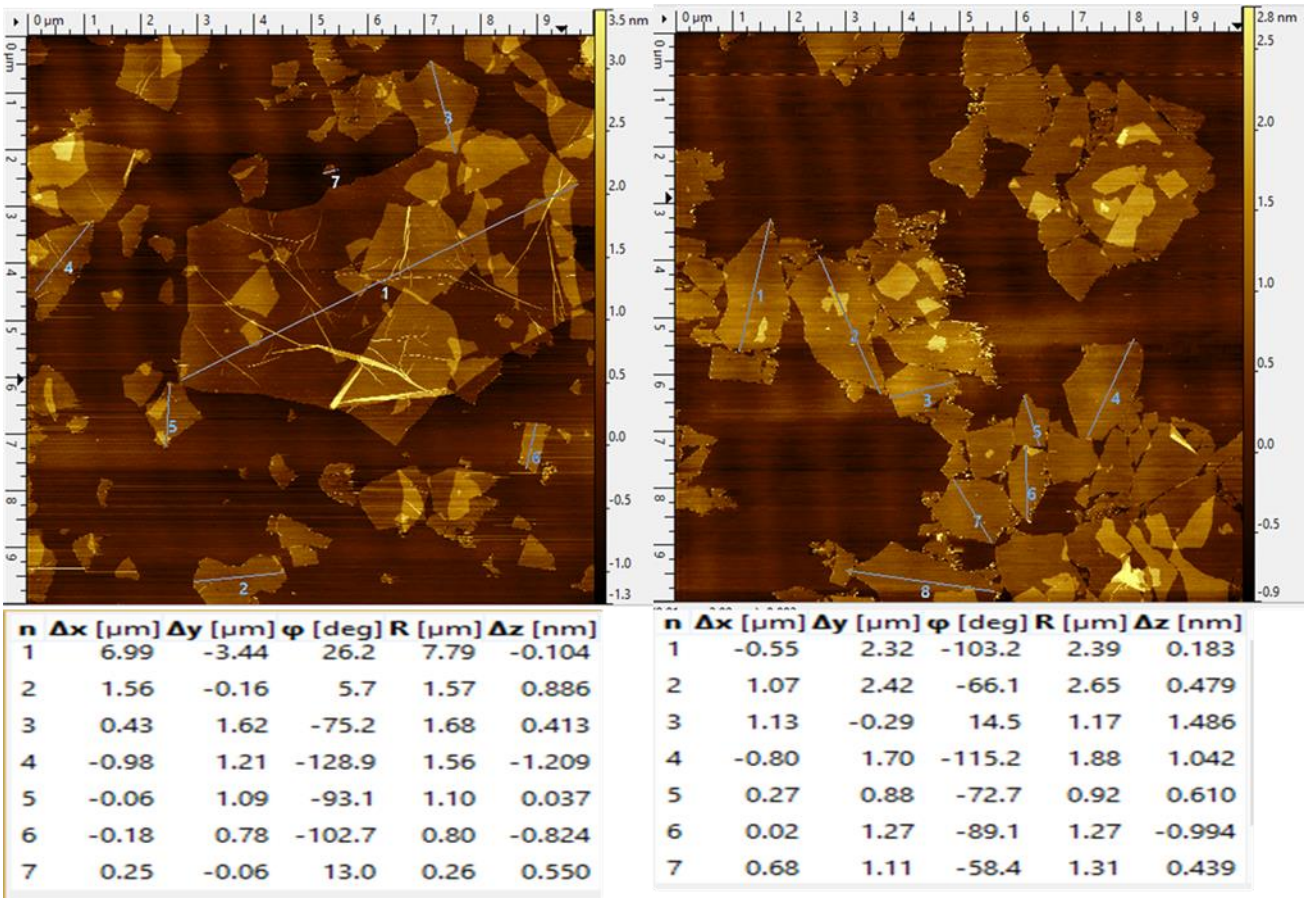

n	Δx [µm]	Δy [µm]	φ [deg]	R [µm]	Δz [nm]
1	6.99	-3.44	26.2	7.79	-0.104
2	1.56	-0.16	5.7	1.57	0.886
3	0.43	1.62	-75.2	1.68	0.413
4	-0.98	1.21	-128.9	1.56	-1.209
5	-0.06	1.09	-93.1	1.10	0.037
6	-0.18	0.78	-102.7	0.80	-0.824
7	0.25	-0.06	13.0	0.26	0.550

n	Δx [µm]	Δy [µm]	φ [deg]	R [µm]	Δz [nm]
1	-0.55	2.32	-103.2	2.39	0.183
2	1.07	2.42	-66.1	2.65	0.479
3	1.13	-0.29	14.5	1.17	1.486
4	-0.80	1.70	-115.2	1.88	1.042
5	0.27	0.88	-72.7	0.92	0.610
6	0.02	1.27	-89.1	1.27	-0.994
7	0.68	1.11	-58.4	1.31	0.439

Figure 25. Atomic force microscopy images of exfoaliated graphene oxide sheet in 0.5 mg/ mL ethanol dispersion and their sheets sizes are listed below AFM images

4.3.3. Film formation

Figure 26 illustrates the two different routes to create PFA films. In one case, a powder resulting from the emulsion polymerized material is cast onto PET while in the other case the FA is polymerized directly on the PET as a dense, monolithic resin. The pFA resin deposited on PET produced a film that was somewhat brittle and dark brown as shown in **Figure 26a**. After testing its flexibility, it was immediately apparent that it was too brittle to be used as a flexible micro-supercapacitor. As will be discussed later, it also did not carbonize effectively under laser irradiation. **Figure 26b** is the polymer powder produced from the two-step synthesis described in

4.3.1. A thin film could be produced from the dispersed powder through casting (solvent evaporation) or via spray coating onto PET. However, without the presence of a binding molecule, the resulting film was also brittle and did not dry evenly using the film casting procedure used. To aid in the film formation, graphene oxide (GO) was added to the PFA dispersion which was found to significantly enhance the uniformity and mechanical integrity of the films. This is likely due to several reasons. It's incorporation modifies the viscosity and drying rate of the cast solution while the flexible sheets can wrap around and bridge adjacent PFA particles. This is demonstrated in the cross-sectional SEM image shown in **Figure 26e**. **Figure 26c** shows several solution ratios of GO in pFA. Upon drop-casting all solution ratios on PET as shown in **Figure 26d**, the film uniformity varied greatly depending on the ratio. Under the conditions tested, the most uniform films of intermediate composition (20 to 80% pFA to GO) were used in subsequent testing.

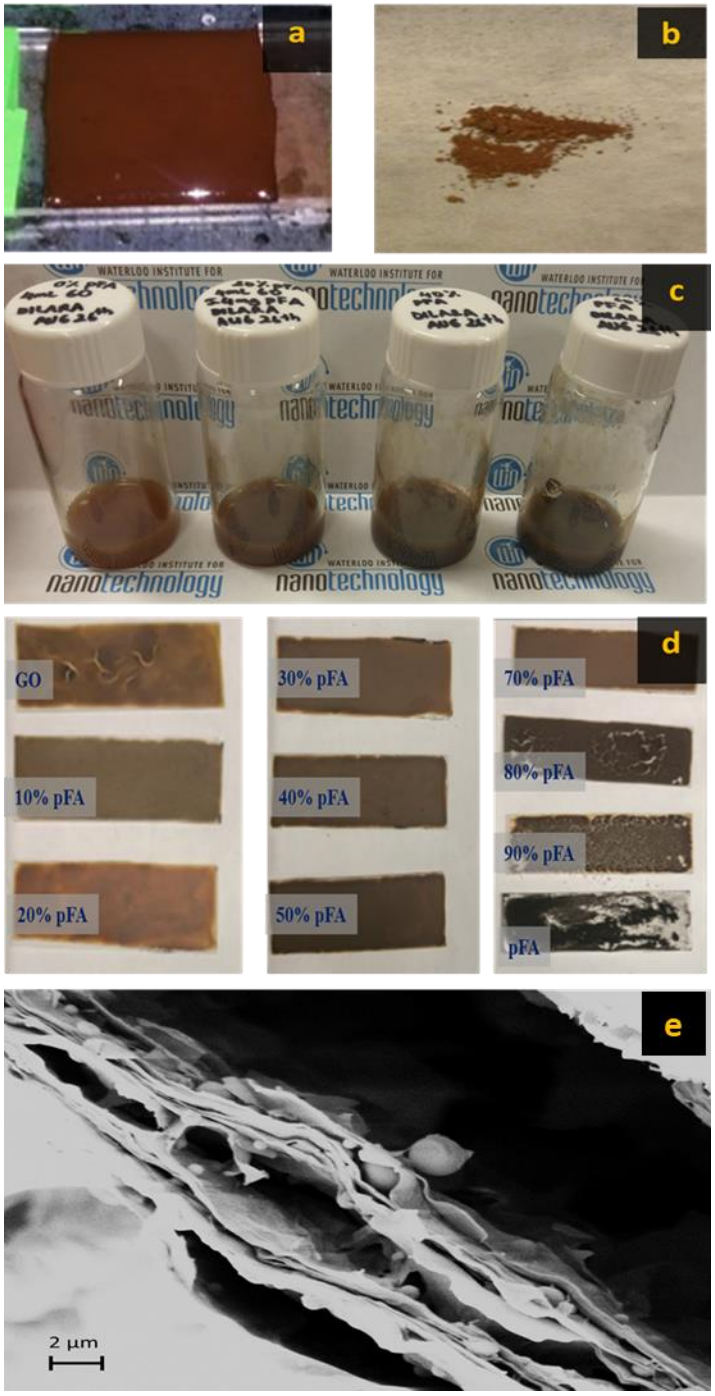

Figure 26. (a) Illustration of resin film after one-step polymerization of pFA (b) Powder product of two-step emulsion polymerization of pFA (c) Different ratio dispersion of pFA and GO (d) Different ratio of pFA and GO films deposited on PET substrates (e) SEM images of pFA and GO dispersed film on PET surface.

4.3.4. Laser-induced carbonization of PFA and GO

Figure 27 demonstrates several attempts to form conductive electrodes on the surface of bulk pFA. Pure films were formed from the two-step emulsion powder and pFA resin. Laser irradiation using a CO_2 laser at varying power (1-15 W) and scan rates (10-50 mm/s was unsuccessful in carbonizing either surface. As demonstrated by PI in Chapter 3, normally a conductive, black line of material forms upon laser exposure. As shown in **Figure 27a**, the films deposited from the emulsion-based PFA were ablated or cut through by the laser, possibly oxidizing further under the atmospheric conditions. However, the edges of the cut areas showed evidence of some carbonization, possibly indicating that multiple passes at a lower power would reproduce this effect without cut through. **Figure 27b** shows the results obtained when laser processing the monolithic films formed by bulk resinification of FA. Instead of forming black, carbonized lines, laser irradiation formed light brown lines. Testing showed this to be non-conducting material suggesting the material formed is a further oxidized product. Since these films were not flexible nor capable of carbonizing, the bulk resin was discontinued as a candidate. On the other hand, the coating originating from the emulsion polymerization route also did not initially carbonize but could be made to do so with several passes of the laser. The laser power resulting in this partial carbonization was between 4 and 5 W which is lower compared to PI to carbonize (5-6W).

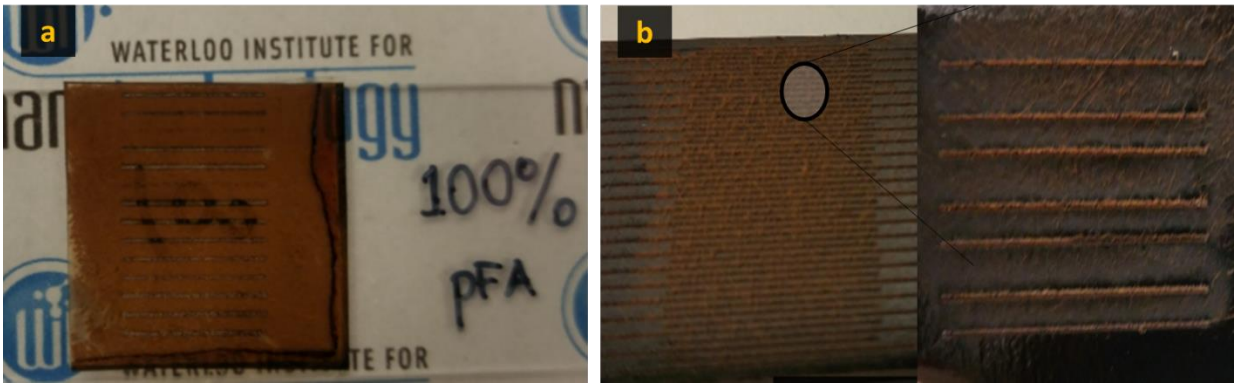

Figure 27. Illustration of laser irradiation of emulsion polymerized pFA **(a)** and pFA through bulk resinification **(b)**

Figure 28 demonstrates laser irradiation of flexible films formed from a mixture of GO and pFA. Unlike the bulk product, uniform and continuous lines of carbonized material were present following a single laser pass. PFA to GO ratios of 1:4, 2:3, 1:1, 3:2, 4:1 and 1:0 of PFA to GO are shown with only one laser pass. The carbonization of poly (furfuryl alcohol) has been achieve by the addition of graphene oxide. Based on the hypothesis in this experiment, graphene oxide serves as a catalyst in the carbonization process. This behavior is recently observed on carbon nanotubes which improves the pyrolysis of carbon precursors. The decrease in the pyrolysis rate and the temperature is observed due to the presence of the carbon nanoparticles in the composite[20]. This claim has been proved by successful carbonization of resinified pFA in the integration of only 1% of graphene oxide shown in **Figure 29**.

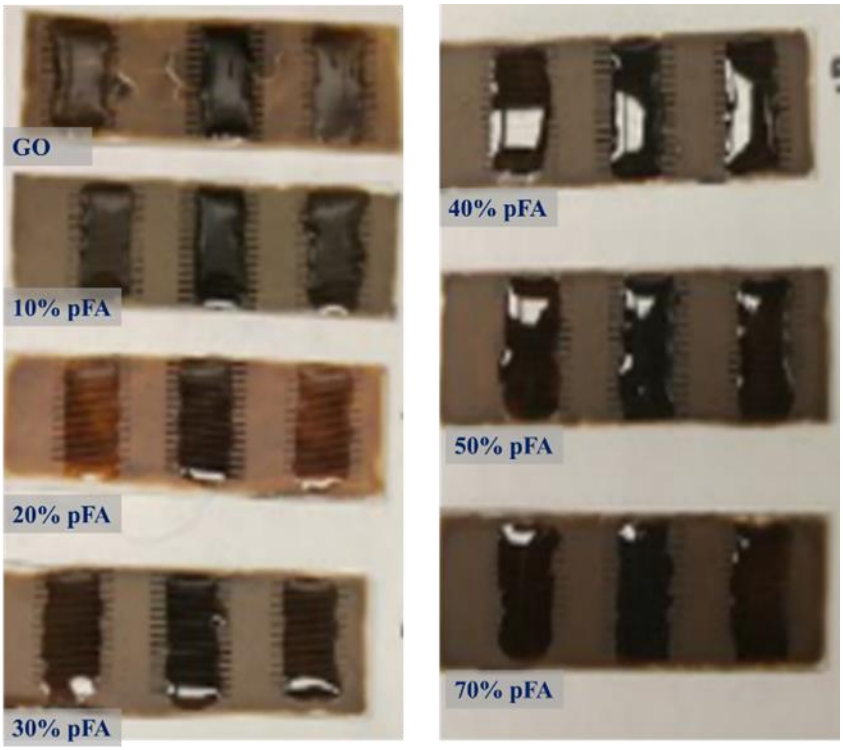

Figure 28. Illustration of laser irradiated graphene oxide and emulsion polymerized pFA samples with electrolyte deposition on electrodes for different the ratio of pFA

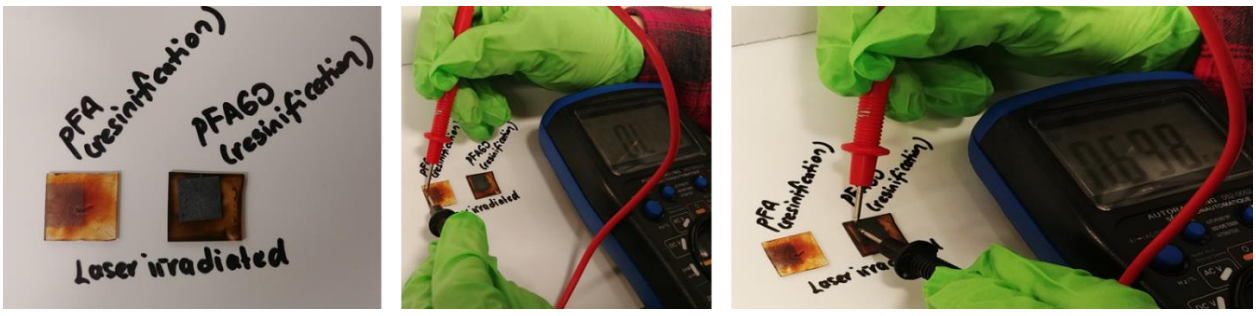

Figure 29. Illustration of laser irradiated polymerized furfuryl alcohol through resinification with and with 1% of graphene oxide addition into polymerization step; 0.81 cm^2 area is laser irradiated with 4.75 W power at 30 mm/s speed using scan mode.

4.3.3.2. The effect of film thickness via drop casting techniques

The typical amount of carbon precursors tested for each electrode surface sample is 1.61 mg/cm^2. To further investigate thickness verses performance, multiple layers of carbon precursors were tested at each ratio. **Figure 30** shows the most negative effect of multiple layers, where successive evaporation and deposition resulted in brittle, cracked or peeling coatings on PET. Each layer of deposition consisted of the same amount of material (1.61 mg/cm^2), and were tested for pFAGO samples at 1:4, 2:3, 3:2 and 4:1 pFAGO respectively. Following each deposition, the current layer was fully dried and then the next layer was deposited via drop casting. The amount of tearing on the film surface depended on the ratio of pFA and GO of the composite. The 1:4 pFAGO sample started to tear after a second deposition of composite on the first layer of the film as shown in Figure 26 (top right). This same behaviour was observed on other ratios of composite at 3 or more depositions, likely due to evaporation of ethanol. Untorn, or successful surface coating of pFAGO composite on PET for 1, 2, and 3 layers were tested by laser irradiation and then electrochemically analyzed (see section 4.3.4). Irrespective of performance, multilayered pFAGO on PET demonstrated a clear loss in flexibility, and higher likelihood to crack following repetitive bend tests. Therefore future optimization experiments were carried out on single-layer depositions of pFAGO composites.

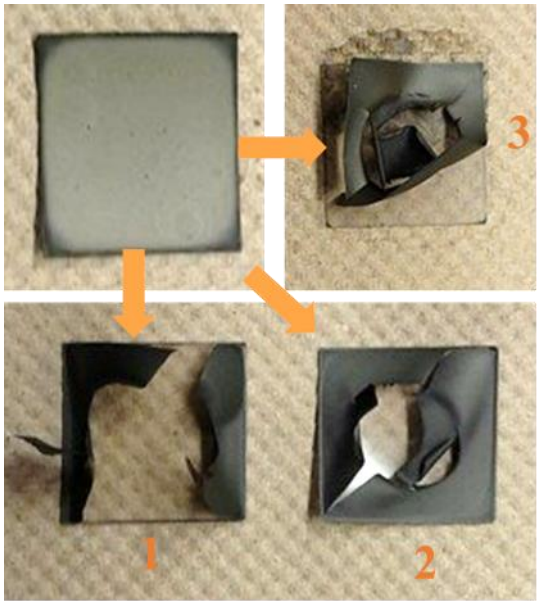

Figure 30. Illustration of film quality as a function of coating number for 2:3 ratio emulsion polymerized (F127, 24 hours, 9M H_2SO_4) pFA and graphene oxide; 1, 2 and 3 times respectively.

4.3.4. Summary and electrochemical characterization of poly (furfuryl alcohol) synthesis

Figure 31 demonstrates a comparison of areal capacitance at 5 mV/s of micro-supercapacitors produced from different batches of emulsion pFA synthesis. PVA/H_3PO_4 was used as a gel electrolyte to test micro-supercapacitors' electrochemical performance at multiple scan rates from 5 mV/s to 500 mV/s in a random order to prevent experimental bias. From this bar chart, micro-supercapacitors reached a maximum capacitance (87.2 mF/cm^2) when emulsion polymerization of pFA was synthesized with a 24 hour reaction time, with Pluronic F127 surfactant assisted emulsion polymerization and crosslinking with 9M H_2SO_4. Other observations were that only small capacitance increases were observed between 8 to 16 hours reaction time while a fourfold (4x) increase was observed between 12 hours and 24 hours reaction time, from 22.28 mFcm^{-2} to 87.2 mFcm^{-2} respectively.

The emulsion polymerization synthesis procedure also allowed us to eliminate washing pFA after synthesis compared to other synthesis procedures tested in this study. Producing the highest specific capacitance, good columbic efficiency and simplistic synthesis conditions make this procedure the most favorable to use for further development of the micro-supercapacitor based pFAGO nanocomposites.

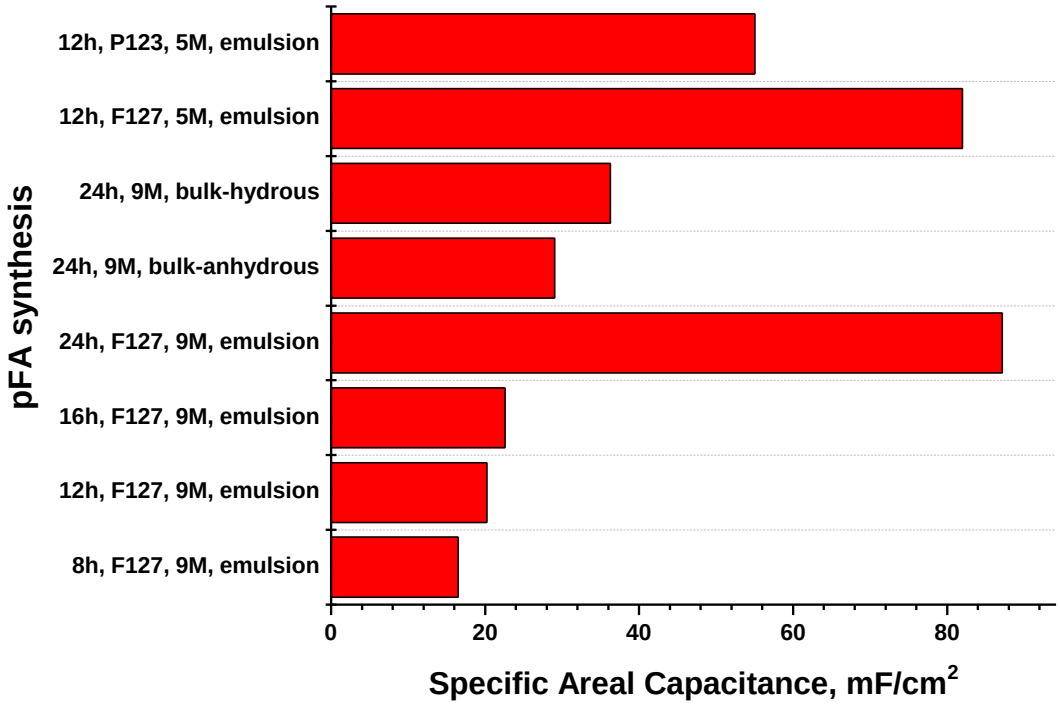

Figure 31. Comparison of specific areal capacitance at 5 mV/s in terms of the synthesis parameters are tested in this study, each sample are fabricated by using PVA/H_3PO_4 as electrolyte and titanium as current collector and tested after 1 day of the preparation

As mentioned earlier in section *4.3.3.2*, multi-layer depositions of the composite material were laser irradiated and carbonized to test their electrochemical performance. **Figure 32** shows a comparison between the double-layer behavior of a combination of single and triple layers and laser scans. The left graph is a cyclic voltammogram (CV) scan while the right compares their electrochemical impedance spectroscopy (EIS). These results show a correlation between a

thickness and increased areal capacitance. On the other hand, increased passes of laser exposure had a negative effect on capacitance and the double-layer behavior of micro-supercapacitors for the lower thickness of the material. This phenomenon can be explained by the effect of laser penetration through base material of pFAGO composite on a flexible substrate surface. The thickness of a single layer of composite material is around 20 μm whereas PI samples used in chapter 3 demonstrate 125 μm thickness, therefore the effect of the laser exposure relative to the thickness of the base material is more pronounced in pFAGO micro-supercapacitors.

The best result for capacitance was found in the 3-layer deposition of the composite utilizing 3 laser scan passes. However, our earlier decision to focus on more flexible, single-layer coatings of pFAGO prevents continuing with this sample due to its inflexible nature. Based on CV and EIS results, the second-best sample was 1 layer at 1 laser scan exposure. It has lower electrolytic resistance (shorter hemi-sphere) and electrical resistance (initial resistance value started at approximately 170 Ohms). Thus, optimization of the flexible micro-supercapacitor synthesis utilized a single layer deposition of pFAGO composite and a single laser pass to perform carbonization.

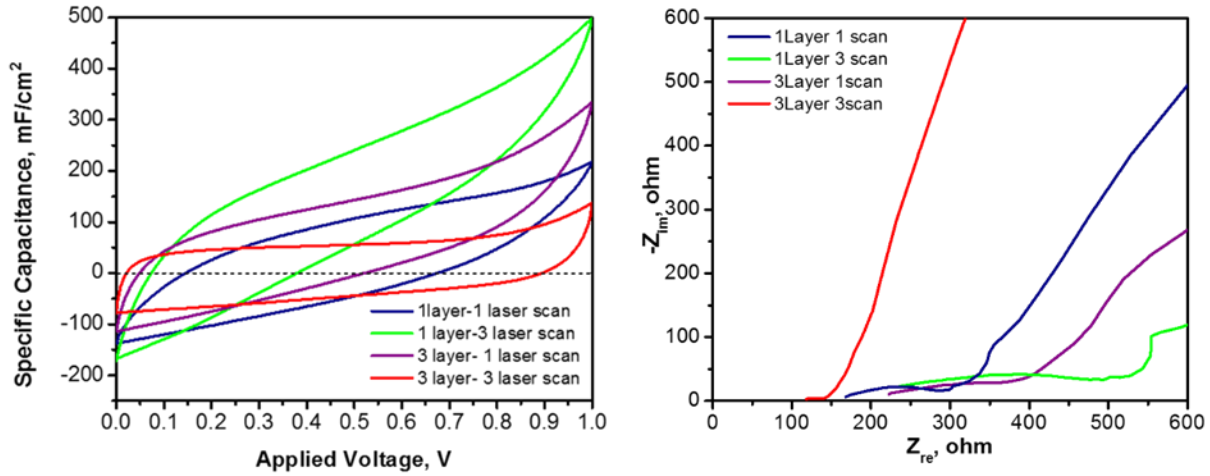

Figure 32. Cyclic voltammogram showing effect of layer number coated on flexible substrate and number of laser exposure **(**right) and EIS for number of layers coated on flexible substrate and number of laser exposure (left) for 24h, F127, 9M emulsion synthesis conditions

One of the biggest challenges during electrochemical testing of micro-supercapacitors for different parameters was result inconsistency due to observed pseudo-capacitive behavior that we believe comes from degradation of the copper current collector as a function of time due to exposure to the H_3PO_4-based electrolyte. Expected CV curves of ideal double-layer is shaped in rectangular form; therefore, any elongation from rectangular shaped in the voltammogram interprets as the contribution of pseudo-capacitance. Oxidation on the copper surface due to the presence of strong acid can cause to the pseudo-capacitance that has been observed in electrochemical testing. To better understand these results, we analyzed the role of current collector and time-dependent degradation of the current collectors. **Figure 33** demonstrates the CV scan results for 3 different types of current collectors over time. The selected current collector alternatives were titanium foil, carbon fiber and copper foil. Copper demonstrated low coulombic efficiency and severe corrosion over the time when in the presence of aqueous acid-based electrolyte, therefore the test focused on

titanium and carbon fiber as possible corrosion resistant alternatives. Ideal double-layer CV plots appear as a perfect rectangle when there is no reaction contributing to the capacitance. The left figure shows the electrochemical behaviour of carbon, titanium and copper current collectors at day 1. Even in day 1, copper provides poor coulombic efficiency due to its asymmetric curve at zero current, while titanium and carbon fiber exhibited more rectangular and symmetric shaped curves. The specific capacitance maximum differed 18 % between titanium, carbon fiber and copper; 61.1, 55.5 and 66.14 mF/cm^2 respectively. On the 3^{rd} day of testing EDLC cell, presented in the graph on the right, the capacitance had roughly doubled which can be explained with further diffusion of ions into pores improving the capacitance in the micro-supercapacitor. Fortunately, both carbon fiber and titanium current collectors retained the characteristic rectangular shape. However, the carbon fiber samples exhibited time-dependent changes while titanium showed a more stable rectangular shape in both the 7^{th} and 3^{rd} day. The specific capacitance reached its maximum value (146. 28 mF/cm^2) on the 7^{th} day with a titanium current collector.

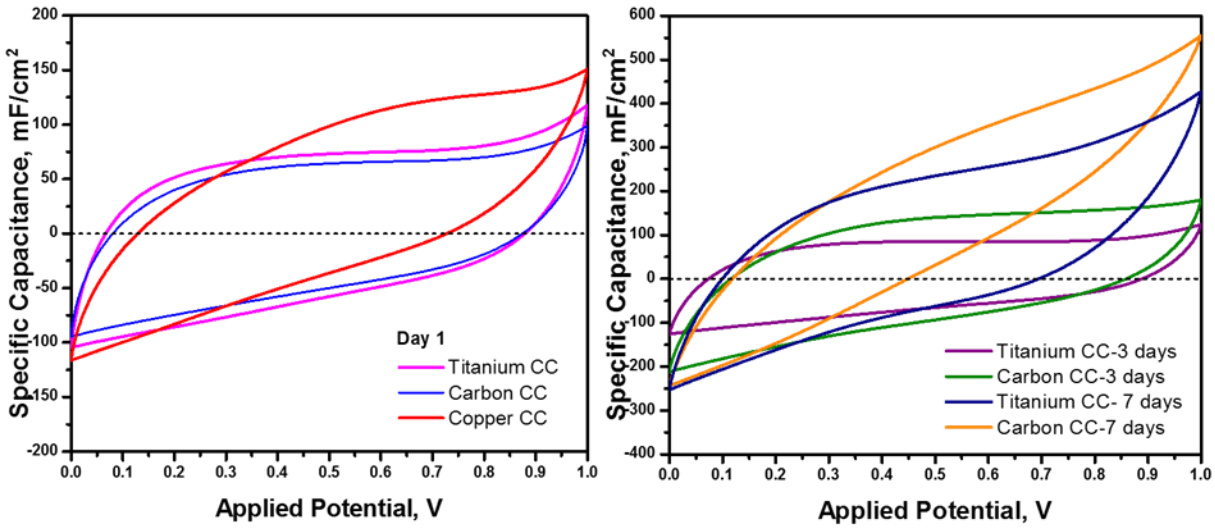

Figure 33. Cyclic voltammogram for microsupercapacitors using different current collectors: titanium, carbon fiber, copper and their electrochemical stability by time at 5 mV/s for 2:3 pFAGO, 1 layer, 1 scan, pFA synthesized by 24 h, F127, 9 M, emulsion synthesis procedure

The next section, we demonstrated the results and the changes with the amount of pFA increased in the composite content.

4.3.5. Optimization of the amount of pFA in composite of pFAGO

Figure 34 shows the electrochemical performance of laser-scribed supercapacitors created using varied ratios of pFA to GO. Ratios varied between 20 to 80%, where each sample was fabricated using the optimized emulsion polymerization with a F127 surfactant for 24 hours, followed by crosslinking with 9M H_2SO_4 for 1 hours at 90°C. A titanium current collector and PVA/H_3PO_4 gel electrolyte were used to fabricate micro-supercapacitors after a single laser irradiation onto a 20 μm single layer of pFAGO film. **Figure 34a** demonstrated a symmetrical rectangular CV plot with twofold increase in capacitance relative to all other ratios. Galvanostatic charge/discharge curves supported the CV analysis, with 2:3 pFAGO providing a voltage drop of 85mV after 100 cycles in

Figure 34b. EIS also proved that the 2:3 pFAGO micro-supercapacitor had the minimum electrical resistance and second-lowest electrolytic resistance in **Figure 34c**. The minimum electrolytic resistance was in the 4:1 pFAGO composition. However, this composition was showed 5 times lower specific capacitance compared to 2:3 pFAGO. The 2:3 pFAGO composition appeared to provide the best electrochemical performance compared to other compositions of pFA content in the composite as shown in **Figure 34d.** **Figure 34e** shows the retention of 2:3 pFAGO micro-supercapacitor that has been irradiated using 4.75 W power, 30 mm/s speed at scan mode. As can be seen from the figure, it has protected the performance over 15,000 cycles; however, the increase in the retention can be addressed to the increase ion diffusion at the interface of the electrode and the electrolyte as mentioned above discussion of the current collector.

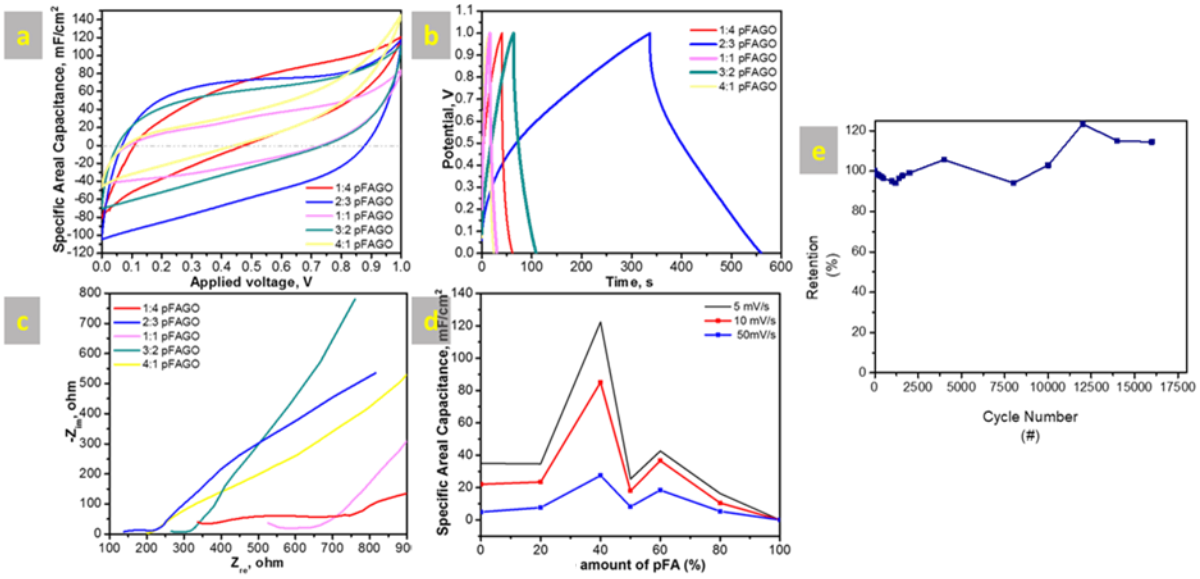

Figure 34. Electrochemical performance of composites. a. Cyclic voltammograms of pFAGO-010 (9M H_2SO_4, 24 hours, F127) for different ratio of pFA and GO; **b.** Galvanostatic charge/discharge curves of pFAGO (9M H_2SO_4, 24 hours, F127) for different ratio of pFA and GO after 100 cycles; **c.** Electrochemical impedance spectrum of pFAGO (9M H_2SO_4, 24 hours, F127) for different ratio of pFA and GO; **d.** Comparison of the specific areal capacitance of

pFAGO (9M H_2SO_4, 24 hours, F127) for different ratio of pFA and GO; **e.** The cycling retention of laser irradiated 2:3 pFAGO micro-supercapacitor at 0.6 mA/cm^2 current density (9M H_2SO_4, 24 hours, F127 at 4.75 W power, 30 mm/s speed san mode laser irradiation).

4.3.6. Comparison of other carbon precursors

Figure 35 provides information about laser exposure effects on 2:3 and 3:2 pFAGO electrodes and their differences from laser irradiated polyimide electrodes. The optimized pFAGO sample is selected in order to examine and compare with other carbon precursors; polyimide and graphene oxide. The spectrum of polyimide and graphene oxide is analyzed in more detail in **section 3.3.3.** In the spectrum of 2:3 pFAGO composite, there is significant decrease in D and G peak due to increase number of the laser exposure onto film surface. FWHM of D peak shows decreases as well as the intensity of the peak with increase number of exposure. However, there is no increase observed in the FWHM of G peak. Similar behavior observed in the spectrum of 3:2 pFAGO films at various laser exposures as shown in **Figure 35c**. In **Figure 35d,** the I_G/I_D ratio of all carbon precursors shows drastically decrease after triple laser exposures. There is consistent increase in the peak position of D peak with increase number of the exposure; G peak position stayed consistent. Increase in D peak position.

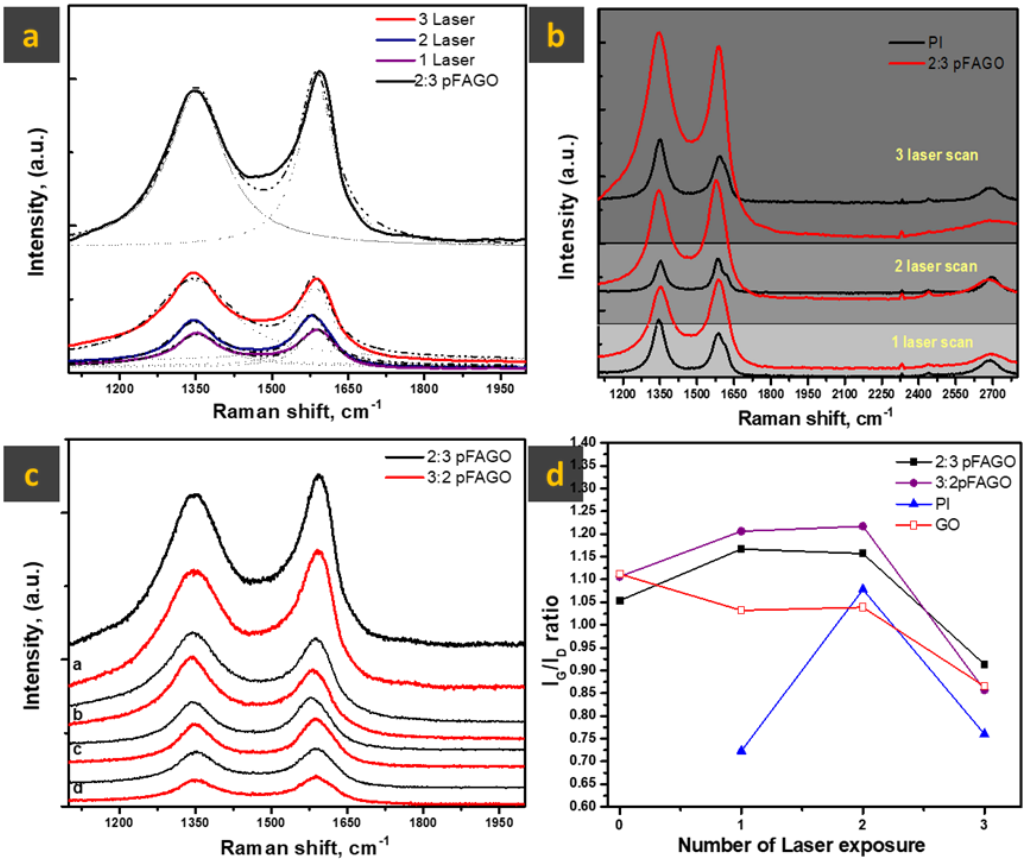

Figure 35. Raman spectra were sampled 15 times for 45 seconds with a 533 nm incident wavelength **a.** Raman spectrum of 2:3 ratio of pFAGO composite for different laser exposures; 0,1,2,3 **b.** Comparison of Raman spectrum of 2:3 ratio of pFAGO composite and PI for different laser exposures;3,2,1 **c.** Comparison of Raman spectrum of 2:3 and 3:2 ratio of pFAGO composite for different laser exposures; no laser (a), 1 laser scan (d), 2 laser scan (c), 3 laser scan (b) **d.** The ratio of G to D peaks (I_G/I_D) for 4 different carbon precursors.

Figure 36 shows the elemental analysis of both laser irradiated polyimide and 2:3 pFAGO composites' electrodes through X-ray photoelectron spectroscopy technique. The C/O ratios in laser irradiated PI and pFAGO composite were found to be ~17 and 11.2 respectively. Both of the ratios of C/O are in the average range of thermally, and chemically reduced graphene oxides, above

10 respectively[68]. Polyimide is observed to be higher carbon ratio than pFAGO composite. The high-resolution spectrums of C1 and O1 of laser irradiated PI and pFAGO composites are carried out after binding energy correction considering the binding energy of C1s as 284.5 eV. During the peak fitting, the minimum full width at half maximum (FWHM) was considered as 1. The high resolution C1s spectra of laser irradiated PI can be deconvoluted into 3 major peaks with the binding energies of 284.6, 285.2, and 288.7 eV corresponding to the sp^2 carbon (C=C) (40%), carbon atoms to oxygen cyclization (C-O) (37%), and C atoms directly bonded to nitrogen configurations (C-N) (23%), respectively. These assignments are in agreement with the literature[35]. The deconvolution of the C1S of the laser irradiated pFAGO showed three different binding energy peaks at 284.6, 288, and 285.3 eV, corresponding to the sp^2 carbon (C=C) (40%), carbonyl groups (C=O) (23 %) and carbon atoms to oxygen cyclization (C-O) (37%), respectively. The high resolution C1 spectra of these two carbon materials demonstrated very similar results based on the ratios of specific functional groups.

The high resolution O1 spectra of laser irradiated polyimide can be deconvoluted into two peaks with binding energies of 532.2 and 533.3 eV corresponding to the carbonyl groups (50%) and carbon atoms to oxygen cyclization (50%), respectively. On the other hand, the high resolution spectra O1 of laser irradiated pFAGO demonstrated two major peaks with binding energies at 532.8 and 533.7 eV, corresponding to ether bond (C-O-C) (90%) and ester (O=C-O) (10%), respectively. The clear difference in the oxygen rich functional groups of these two laser irradiated polymer materials is expected. The nature of poly (furfuryl alcohol) has repeated furan ring domains that are connected by methyl ether bridges as shown in **Figure 8** in **Section 2.2.2.1.**

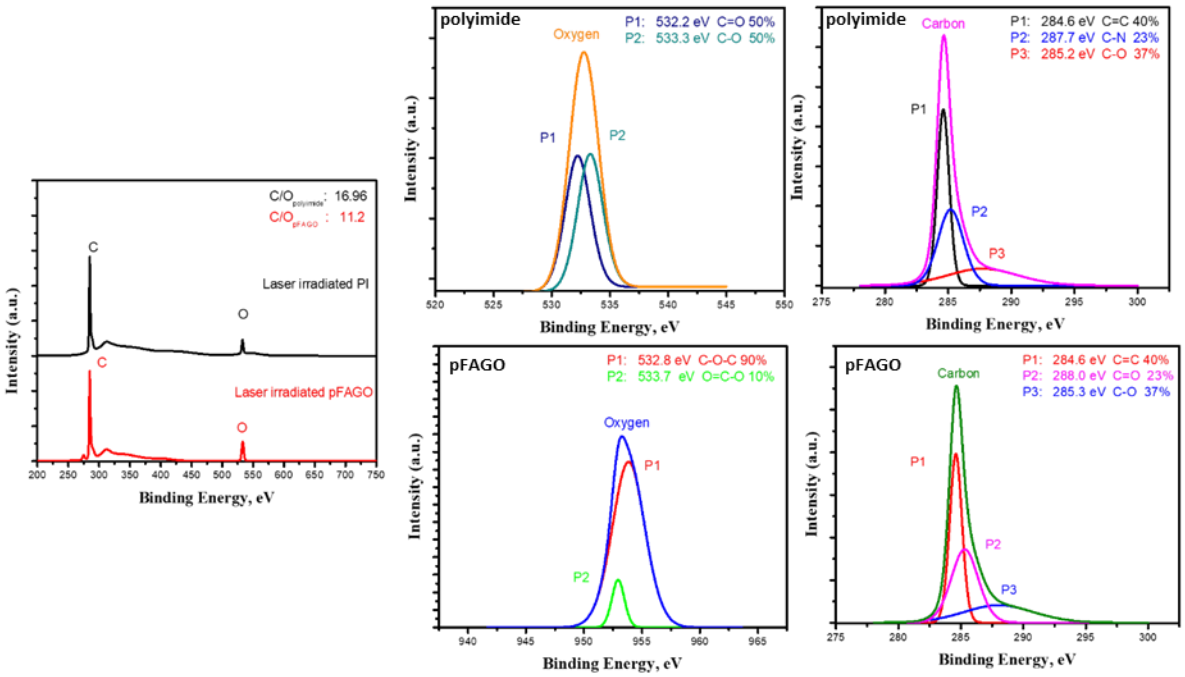

Figure 36. X-ray photoelectron spectroscopy (XPS) results for laser irradiated 125 µm thick Kapton™ polyimide film,3 times laser exposures at 5.5 W power with 30 mm/s scan rate, and laser irradiated 2:3 pFAGO film, 3 times laser exposures at 4.8 W power with 30 mm/s scan rate.

Figure 37 summarizes the specific areal capacitance of micro-supercapacitors that are fabricated through laser irradiation from carbon precursors such as polyimide, graphene oxide and 2:3 pFAGO composites. The results that marked with star (*) represents the micro-supercapacitors fabricated in this study. All the micro-supercapacitor performed in this study shows significantly higher specific areal capacitance compared the ones studied in the literature. The higher specific capacitance can be explained due to differences in the design of electrodes and the type of laser. Moreover, 2:3 pFAGO microsupercapacitors are also shown higher specific areal capacitance than polyimide samples. The progress in the maximization of the specific areal capacitance can be seen between 2:3 pFAGO samples that are marked a, b c and d. Initial samples before optimization of the synthesis procedure shows 50 mF/cm^2 specific capacitance. After increase in the synthesis time

from 12 hours (**2:3 pFAGO a**) to 24 hours (**2:3 pFAGO c**); 75% of increase in the specific capacitance is observed. There is also slight increase in the capacitance and the consistency of the results after switching the copper current collectors with titanium ones. The specific capacitance reaches 87.2 mF/cm^2 at first day (**2:3 pFAGO c)** and the same sample is tested after 7 days of charging and discharging; the specific capacitance improves due to increase diffusion of ions at the interface and reaches up to 147 mF/cm^2. This value is highest reported value for laser irradiated carbon precursors in the literature.

On the other hand, the higher specific capacitance of polyimide based microsupercapacitors are observed in this study compared to the literature studies. In the initial test of polyimide samples, we observed closer value to the literature. These samples are prepared by using cut mode of the CO_2 laser (**PI a and b**). When the operational mode of the laser change from cut mode to scan mode, 50% increase in the specific capacitance observed (**PI c**).

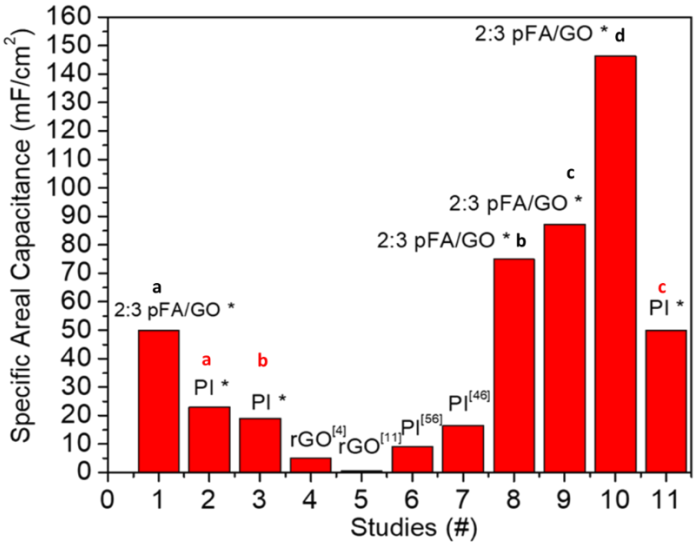

Figure 37. Comparison of specific areal capacitance of the studies published on micro-supercapacitors by laser irradiated carbon precursors and micro-supercapacitors fabricated in this work; **2:3 pFAGO a.** 9M H_2SO_4, 12 hours, F127 synthesis route adopted and the samples are

irradiated at 4.75 W, 30 mm/s with scan mode, and PVA/H_3PO_4 as a gel electrolyte and titanium as a current collector (day 1) **b.** 9M H_2SO_4, 24 hours, F127 synthesis route adopted and the samples are irradiated at 4.75 W, 30 mm/s with scan mode, and PVA/H_3PO_4 as a gel electrolyte and copper as a current collector (day 1) **c.** 9M H_2SO_4, 24 hours, F127 synthesis route adopted and the samples are irradiated at 4.75 W, 30 mm/s with scan mode, and PVA/H_3PO_4 as a gel electrolyte and titanium as a current collector (day 1) **d.** 9M H_2SO_4, 24 hours, F127 synthesis route adopted and the samples are irradiated at 4.75 W, 30 mm/s with scan mode, and PVA/H_3PO_4 as a gel electrolyte and titanium as a current collector (day 7) **polyimide a.** laser irradiated at 6W power, 30 mm/s speed at cut mode and PVA/H_2SO_4 as a gel electrolyte and titanium as a current collector **b.** laser irradiated at 6W power, 30 mm/s speed at cut mode and PVA/H_3PO_4 as a gel electrolyte and titanium as a current collector **c.** laser irradiated at 6W power, 30 mm/s speed at scan mode and PVA/H_2SO_4 as a gel electrolyte and titanium as a current collector

4.4. Conclusion

The carbonization of insulated polymeric nanocomposite through laser irradiation is demonstrated and the capabilities of the fabricated microsupercapacitor based on this polymeric nanocomposite is shown in the study. Poly (furfuryl alcohol) is an alternative carbon precursor that can be converted into conductive arrays and exhibits remarkable electrochemical performance as a miniaturized energy storage device. To the best of our knowledge, this is the highest specific areal capacitance reported in the literature using a carbon precursor without the contribution of pseudo-capacitance. The device fabricated during the study is showed over 15,000 cycles with full retention. This study shows a promising opportunity for the recycling of a bio-waste material into a source of a storage device with a simple, inexpensive fabrication route.

Chapter 5. Conclusion

5.1. Summary

This thesis presents new findings in the field of renewable energy and material science and chemical engineering. Beginning with the literature review on fabrication techniques and possible carbon sources to develop a miniaturized energy storage device, a micro-supercapacitor and the parameters that are effective on the electrochemical performance of the device were established. With this knowledge, a novel polymer material, pFA and its composites (pFAGO) were developed as a micro-supercapacitor using laser irradiation technique. The device fabricated based on new composite material showed high specific capacitance compared to other carbon precursor materials studied in this study and the literature studies. Thus, this thesis provides promising results for micro-supercapacitor and for their commercialization and integration into miniaturized electronic technologies.

5.2. Conclusion

The creation of the perfect micro-supercapacitor would be worthless if the cost of raw material and device fabrication is prohibitive. The first part of the thesis work was to identify and optimize a suitable fabrication technique for micro-supercapacitors. Based on literature work, laser irradiation was selected as the most suitable method. Commercial and well-studied carbon samples, respectively Kapton™ polyimide and a synthesized graphene oxide, were irradiated under various environmental and parametric conditions. At this stage, the goal was to identify the effect of changed parameters on the base material so that changes in new materials can be tuned similarly. From this work, the laser was operated at 10% power or less, aiming for high conductivity at a 30 mm/s scan rate. The mode was chosen to be scan mode to improve electrode trace consistency and conductivity. A Raman spectrum closely identified specific laser exposures

on GO with thermally exfoliated GO spectra, indicating that the laser irradiation is inducing thermal carbonization. Finally, micro-supercapacitors tested with the optimized settings on polyimide films resulted in higher specific areal capacitance (49 mF/cm^2) than literature on the same material (31 mF/cm^2). Optimized laser irradiation is demonstrated as a quick, effective and cheap methodology in the fabrication of micro-supercapacitors.

Moving away from expensive polyimide as a carbon pre-cursor would drive down the fabrication cost further. To improve the energy density requires higher density of energy storing material, namely conductive carbon. Poly (furfuryl alcohol) (pFA) is chosen due to several key characteristics; cheap and available, renewable, carbon heavy and able to be thermally induced to form dense nano-porous carbon. Multiple variations of pFA synthesis were employed in order to ensure micro-supercapacitor performance. SEM and FTIR characterization ensured that the synthesis parameters chosen would provide consistent spherical pFA particles. However, pure pFA cast into a film was lacking an ability to effectively carbonize and was both brittle and un-evenly agglomerated as a thin layer (1.6 mg/cm^2). The integration of GO sheets (2 mm and larger) into pFA acted as a thermal catalyst and binding agent for pFA particles, greatly improving uniformity and flexibility of a pFAGO composite film. Single-film single-pass carbonization proved to be the most effective in supercapacitor performance, providing a record areal capacitance of (87.2 mF/cm^2).

Having selected a cheap and high performing material, some more experiments were performed to improve long-term usability. It was noted that the common current collector, a copper trace, was degrading due to the presence of the electrolytic solution. Copper is well known to oxidize over time as well. Carbon and Titanium were investigated as replacement materials as they are chemically resistant, biologically inert and highly conductive. A pFAGO film supported by PET

and using titanium current collectors demonstrated reliable and increasing power storage at more than 100 mF/cm^2. After more than 15,000 cycles of charge and discharge, the film was providing 147 mF/cm^2. This represents greater than four times (4x) an improvement in specific areal capacitance versus the highest reported carbon precursor for micro-supercapacitors.

Integrated and self-sufficient electronics will require reliable power sources, more critical when evaluating or measuring health or remote system variables. Micro-supercapacitors are poised as the most effective long-term solution in providing that power. Overcoming energy density requirements and ensuring stable and safe performance is no easy feat. The research demonstrated here is a massive improvement in energy density while simultaneously reducing cost and complexity. Further advances in micro-supercapacitors will ensure their integration into every modern device. Choosing materials that are ecologically responsible and achieves power requirements is the golden rule in tomorrow's portable power market.

5.3. Recommendation for Future Work

Based on the results of this research, the following avenues are recommended for future work;

1. Test and investigation on operational mode of the laser to further improvement for the electrochemical performance and to gain better understanding on the mechanism of the carbonization. In general, the mechanism of the laser irradiation is not well understood. It is recommended to test the effect of x and y swing settings in scan mode and to proceed the complete study on understanding the relation between depth and the material thickness for polyimide, graphene oxide as carbon precursors.
2. The investigation and improvement of the electrochemical performance of micro-supercapacitors can be expanded by exploring different electrode's dimension and patterns.

This would provide broader understanding on the mechanism of double-layer charging and design parameters of a micro-supercapacitor.

3. The effect of graphene oxide in this study is briefly demonstrated mainly in the samples synthesized through emulsion polymerization. However, the exploration the effect of graphene oxide is recommended in order to increase flexibility and simplicity of the fabrication method for pFA based microsupercapacitors.
4. Extended cycle life test and flexibility test is recommended to prove the use of this devices in commercial application for miniaturized technologies.

References

(1) Majid Beidaghi, Y. G. Capacitive Energy Storage in Micro-Scale Devices: Recent Advances in Design and Fabrication of Micro- Supercapacitors. *Energy Environ. Sci.* **2014**, *7*, 867–884.

(2) Tyagi, A.; Tripathi, K. M.; Gupta, R. K. Devices and Future Aspects. *J. Mater. Chem. A Mater. energy Sustain.* **2015**, *3*, 22507–22541.

(3) Halper, M.; Ellenbogen, J. Supercapacitors: A Brief Overview. *Rep. No. MP 05W0000272, …* **2006**, No. March, Report No. MP 05W0000272, 1-29.

(4) El-Kady, M. F.; Kaner, R. B. Scalable Fabrication of High-Power Graphene Micro-Supercapacitors for Flexible and on-Chip Energy Storage. *Nat. Commun.* **2013**, *4*, 1475.

(5) Lin, J.; Zhang, C.; Yan, Z.; Zhu, Y.; Peng, Z.; Hauge, R. H.; Natelson, D.; Tour, J. M. 3 - Dimensional Graphene Carbon Nanotube Carpet-Based Microsupercapacitors with High Electrochemical Performance. **2013**.

(6) Ahn, Y.; Lee, H.; Lee, D.; Lee, Y. Highly Conductive and Flexible Silver Nanowire-Based Microelectrodes on Biocompatible Hydrogel. **2014**.

(7) Hsia, B.; Marschewski, J.; Wang, S.; In, J. Bin; Carraro, C.; Poulikakos, D.; Grigoropoulos, C. P.; Maboudian, R. Highly Flexible, All Solid-State Micro-Supercapacitors from Vertically Aligned Carbon Nanotubes. *Nanotechnology* **2014**, *25* (5), 55401.

(8) Wu, Z. S.; Parvez, K.; Winter, A.; Vieker, H.; Liu, X.; Han, S.; Turchanin, A.; Feng, X.; M??llen, K. Layer-by-Layer Assembled Heteroatom-Doped Graphene Films with Ultrahigh Volumetric Capacitance and Rate Capability for Micro-Supercapacitors. *Adv. Mater.* **2014**, *26* (26), 4552–4558.

(9) Li, J.; Mishukova, V.; Östling, M. All-Solid-State Micro-Supercapacitors Based on Inkjet Printed Graphene Electrodes. *Appl. Phys. Lett.* **2016**, *109* (12).

(10) El-kady, M. F.; Kaner, R. B.; Angeles, L.; States, U.; Science, M.; Angeles, L.; States, U. Direct Laser Writing of Graphene. **2014**, No. 9, 8725–8729.

(11) Gao, W.; Singh, N.; Song, L.; Liu, Z.; Leela, A.; Reddy, M.; Ci, L.; Vajtai, R.; Zhang, Q.; Wei, B.; et al. Direct Laser Writing of Micro-Supercapacitors on Hydrated Graphite Oxide Films. **2011**, *6* (July), 6–10.

(12) Bin, J.; Hsia, B.; Yoo, J.; Hyun, S.; Carraro, C.; Maboudian, R.; Grigoropoulos, C. P. Facile Fabrication of Flexible All Solid-State Micro-Supercapacitor by Direct Laser Writing of Porous Carbon in Polyimide. *Carbon N. Y.* **2014**, *83*, 144–151.

(13) Peng, Z.; Lin, J.; Ye, R.; Samuel, E. L. G.; Tour, J. M. Flexible and Stackable Laser-Induced Graphene Supercapacitors. *ACS Appl. Mater. Interfaces* **2015**, *7* (5), 3414–3419.

(14) Strong, V.; Dubin, S.; El-Kady, M. F.; Lech, A.; Wang, Y.; Weiller, B. H.; Kaner, R. B. Patterning and Electronic Tuning of Laser Scribed Graphene for Flexible All-Carbon Devices. *ACS Nano* **2012**, *6* (2), 1395–1403.

(15) Kherroub, D. E.; Belbachir, M.; Lamouri, S. Synthesis of Poly (Furfuryl Alcohol)/

Montmorillonite Nanocomposites by Direct in-Situ Polymerization. **2015**, *38* (1), 57–63.

(16) Wang, H.; Yao, J. Use of Poly(furfuryl Alcohol) in the Fabrication of Nanostructured Carbons and Nanocomposites. *Ind. Eng. Chem. Res.* **2006**, *45* (19), 6393–6404.

(17) Liu, J.; Wang, H.; Zhang, L. Highly Dispersible Molecular Sieve Carbon Nanoparticles. *Chem. Mater.* **2004**, *16* (22), 4205–4207.

(18) Bard, A. J.; Faulkner, L. R.; York, N.; @bullet, C.; Brisbane, W.; Toronto, S. E. *ELECTROCHEMICAL METHODS Fundamentals and Applications*; 1944.

(19) Kang, J. H. Fabrication and Characterization of Nano Carbon- Based Electrochemical Double-Layer Capacitors. **2015**.

(20) Zuliani, J. E.; Jia, C. Q.; Kirk, D. W. Elucidating the Importance of Pore Structure in Determining the Double-Layer Capacitance of Nanoporous Carbon Materials. *J. Phys. Chem. C* **2017**, *121* (38), 20555–20566.

(21) Simon, P.; Gogotsi, Y. Materials for Electrochemical Capacitors. 845–854.

(22) Gamby, J.; Taberna, P. .; Simon, P.; Fauvarque, J. .; Chesneau, M. Studies and Characterisations of Various Activated Carbons Used for Carbon/carbon Supercapacitors. *J. Power Sources* **2001**, *101* (1), 109–116.

(23) Frackowiak, E.; Béguin, F. Carbon Materials for the Electrochemical Storage of Energy in Capacitors. *Carbon N. Y.* **2001**, *39* (6), 937–950.

(24) Goubard-bretesché, N.; Crosnier, O.; Favier, F.; Brousse, T. Electrochimica Acta Improving the Volumetric Energy Density of Supercapacitors. *Electrochim. Acta* **2016**, No. 2015.

(25) Ajayan, P. M.; Zhou, O. Z. Applications of Carbon Nanotubes. *Most* **2001**, *425*, 391–425.

(26) Ruoff, R. S. R.; Tersoff, J.; Lorents, D. C.; Subramoney, S.; Chan, B. Radial Deformation of Carbon Nanotubes by van Der Waals Forces. *Nature* **1993**, *364* (6437), 514–516.

(27) Peigney, A.; Laurent, C.; Flahaut, E.; Bacsa, R. R.; Rousset, A. Specific Surface Area of Carbon Nanotubes and Bundles of Carbon Nanotubes. *Carbon N. Y.* **2001**, *39* (4), 507–514.

(28) See, C. H.; Harris, A. T. A Review of Carbon Nanotube Synthesis via Fluidized-Bed Chemical Vapor Deposition. *Ind. Eng. Chem. Res.* **2007**, *46* (4), 997–1012.

(29) Ruan, W.; Wang, Z.; Li, J.; Jiang, K.; Liu, L. Synthesis of Carbon Nanotubes on Suspending Microstructures by Rapid Local Laser Heating. *IEEE Sens. J.* **2011**, *11* (12), 3424–3425.

(30) Geim, A. K.; Novoselov, K. S. The Rise of Graphene. *Nat. Mater.* **2007**, *6* (3), 183–191.

(31) Marcano, D. C.; Kosynkin, D. V; Berlin, J. M.; Sinitskii, a; Sun, Z. Z.; Slesarev, a; Alemany, L. B.; Lu, W.; Tour, J. M. Improved Synthesis of Graphene Oxide. *ACS Nano* **2010**, *4* (8), 4806–4814.

(32) Zhang, C.; Dabbs, D. M.; Liu, L.; Aksay, I. A.; Car, R.; Selloni, A. Combined Effects of Functional Groups, Lattice Defects, and Edges in the Infrared Spectra of Graphene Oxide. **2015**.

(33) Oh, Y. J.; Yoo, J. J.; Kim, Y. Il; Yoon, J. K.; Yoon, H. N.; Kim, J. H.; Park, S. Bin. Oxygen Functional Groups and Electrochemical Capacitive Behavior of Incompletely Reduced Graphene Oxides as a Thin-Film Electrode of Supercapacitor. *Electrochim. Acta* **2014**, *116*, 118–128.

(34) Kumar, R.; Singh, R. K.; Singh, D. P. Natural and Waste Hydrocarbon Precursors for the Synthesis of Carbon Based Nanomaterials: Graphene and CNTs. *Renew. Sustain. Energy Rev.* **2016**, *58*, 976–1006.

(35) Lin, J.; Peng, Z.; Liu, Y.; Ruiz-zepeda, F.; Ye, R.; Samuel, E. L. G.; Yacaman, M. J.; Yakobson, B. I.; Tour, J. M. Commercial Polymers. *Nat. Commun.* **2014**, *5*, 1–8.

(36) Ruquan Ye, Yieu Chyan, Jibo Zhang, Yilun Li, Xiao Han, C. K.; and James M.Tour. Laser-Induced Graphene Formation on Wood. *Adv. Mater.* **2017**, *170211*, 1–6.

(37) He, L.; Li, D.; Dong, D.; Yao, J.; Huang, Y.; Wang, H. Effects of Polymerization Conditions on the Properties of Poly(furfuryl Alcohol) Composite Membranes. *J. Appl. Polym. Sci.* **2012**, *124* (4), 3383–3391.

(38) Oishi, S. S.; Rezende, M. C.; Origo, F. D.; Damião, A. J.; Botelho, E. C. Viscosity, pH, and Moisture Effect in the Porosity of Poly(furfuryl Alcohol). *J. Appl. Polym. Sci.* **2013**, *128* (3), 1680–1686.

(39) Smith, M. A.; Foley, H. C.; Lobo, R. F. A Simple Model Describes the PDF of a Non-Graphitizing Carbon. *Carbon N. Y.* **2004**, *42* (10), 2041–2048.

(40) Harris, P. J. F. New Perspectives on the Structure of Graphitic Carbons. *Crit. Rev. Solid State Mater. Sci.* **2005**, *30* (4), 235–253.

(41) Ozaki, J.-I.; Mitsui, M.; Nishiyama, Y.; Cashion, J. D.; Brown, L. J. Effects of Ferrocene on Production of High Performance Carbon Electrodes from Poly(furfuryl Alcohol). *Chem. Mater.* **1998**, *10* (11), 3386–3392.

(42) Peer, M.; Qajar, A.; Rajagopalan, R.; Foley, H. C. On the Effects of Emulsion Polymerization of Furfuryl Alcohol on the Formation of Carbon Spheres and Other Structures Derived by Pyrolysis of Polyfurfuryl Alcohol. *Carbon N. Y.* **2012**, *51*, 85–93.

(43) Choura, M.; Belgacem, N. M.; Gandini, A. Acid-Catalyzed Polycondensation of Furfuryl Alcohol: Mechanisms of Chromophore Formation and Cross-Linking. *Macromolecules* **1996**, *29* (11), 3839–3850.

(44) Burket, C. L.; Burket, C. L. The Pennsylvania State University The Graduate School Department of Chemical Engineering GENESIS AND EVOLUTION OF POROSITY AND MICROSTRUCTURE IN NANOPOROUS CARBON DERIVED FROM POLYFURFURYL ALCOHOL A Thesis in Chemical Engineering by Submitted in Partial F. **2007**, No. December.

(45) Mariwalat, R. K.; Foley, H. C. Evolution of Ultramicroporous Adsorptive Structure in Poly (furfury1 Alcohol) -Derived Carbogenic Molecular Sieves. *Ind. Eng. Chem. Res.* **1994**, *33*, 607–615.

(46) Peng, Z.; Ye, R.; Mann, J. A.; Zakhidov, D.; Li, Y.; Smalley, P. R.; Lin, J.; Tour, J. M.;

Preston, R.; Lin, J.; et al. Flexible Boron-Doped Laser Induced Graphene Microsupercapacitors. *ACS Nano* **2015**, No. Cc, 1–17.

(47) Lin, J.; Zhang, C.; Yan, Z.; Zhu, Y.; Peng, Z.; Hauge, R. H.; Natelson, D.; Tour, J. M. 3-Dimensional Graphene Carbon Nanotube Carpet-Based Microsupercapacitors With High Electrochemical Performance. *Nano Lett.* **2013**, *13* (1), 72–78.

(48) Qi, D.; Liu, Y.; Liu, Z.; Zhang, L.; Chen, X. Design of Architectures and Materials in In-Plane Micro-Supercapacitors: Current Status and Future Challenges. *Adv. Mater.* **2017**, *29* (5), 1–19.

(49) El-Kady, M. F.; Strong, V.; Dubin, S.; Kaner, R. B. Laser Scribing of High-Performance and Flexible Graphene-Based Electrochemical Capacitors. *Science (80-.).* **2012**, *335* (6074), 1326–1330.

(50) Peng, Z.; Ye, R.; Mann, J. A.; Zakhidov, D.; Li, Y.; Smalley, P. R.; Lin, J.; Tour, J. M. Flexible Boron-Doped Laser-Induced Graphene Microsupercapacitors. **2015**, No. Xx.

(51) Joseph, G.; Kirubaraj, A. A.; Satheesh, U.; Devaprakasam, D. Fabrication of Flexible Super Capacitor Using Laser Lightscribe Technique. **2014**.

(52) Petridis, C.; Lin, Y. H.; Savva, K.; Eda, G.; Kymakis, E.; Anthopoulos, T. D.; Stratakis, E. Post-Fabrication, in Situ Laser Reduction of Graphene Oxide Devices. *Appl. Phys. Lett.* **2013**, *102* (9).

(53) Zhang, Y.; Guo, L.; Wei, S.; He, Y.; Xia, H.; Chen, Q.; Sun, H. B.; Xiao, F. S. Direct Imprinting of Microcircuits on Graphene Oxides Film by Femtosecond Laser Reduction. *Nano Today* **2010**, *5* (1), 15–20.

(54) Trusovas, R.; Ratautas, K.; Račiukaitis, G.; Barkauskas, J.; Stankevičiene, I.; Niaura, G.; Mažeikiene, R. Reduction of Graphite Oxide to Graphene with Laser Irradiation. *Carbon N. Y.* **2013**, *52*, 574–582.

(55) Cai, J.; Lv, C.; Watanabe, A. Cost-Effective Fabrication of High-Performance Flexible All-Solid-State Carbon Micro-Supercapacitors by Blue-Violet Laser Direct Writing and Further Surface Treatment. *J. Mater. Chem. A* **2016**, *4* (5), 1671–1679.

(56) Types of lasers - Solid state laser, Gas laser, Liquid laser & Semiconductor laser www.physics-and-radio-electronics.com/physics/laser/differenttypesoflasers.html (accessed Nov 28, 2017).

(57) Arieli, R. Rami Arieli: "The Laser Adventure" Chapter 6.2 Solid State Lasers https://perg.phys.ksu.edu/vqm/laserweb/Ch-6/F6s2p1.htm (accessed Nov 14, 2017).

(58) Arieli, R. Rami Arieli: "The Laser Adventure" Chapter 6, Carbon Dioxide Lasers https://perg.phys.ksu.edu/vqm/laserweb/Ch-6/F6s1t6p1.htm (accessed Nov 14, 2017).

(59) Kumar, R.; Singh, R. K.; Singh, D. P.; Joanni, E.; Yadav, R. M.; Moshkalev, S. A. Laser-Assisted Synthesis, Reduction and Micro-Patterning of Graphene: Recent Progress and Applications. *Coord. Chem. Rev.* **2017**, *342*, 34–79.

(60) Cossio, M. L. T.; Giesen, L. F.; Araya, G.; Pérez-Cotapos, M. L. S.; VERGARA, R. L.;

Manca, M.; Tohme, R. A.; Holmberg, S. D.; Bressmann, T.; Lirio, D. R.; et al. Supplementary Figures Supplementary - Laser-Induced Porous Graphene Films from Commercial Polymers. *Nat. Commun.* **2012**, *XXXIII* (2), 81–87.

(61) Li, Y.; Luong, D. X.; Zhang, J.; Tarkunde, Y. R.; Kittrell, C.; Sargunaraj, F.; Ji, Y.; Arnusch, C. J.; Tour, J. M. Laser-Induced Graphene in Controlled Atmospheres: From Superhydrophilic to Superhydrophobic Surfaces. *Adv. Mater.* **2017**, *1700496*, 1700496.

(62) Cote, L. J.; Cruz-Silva, R.; Huang, J. Flash Reduction and Patterning of Graphite Oxide and Its Polymer Composite. *J. Am. Chem. Soc.* **2009**, *131* (31), 11027–11032.

(63) Abdelsayed, V.; Moussa, S.; Hassan, H. M.; Aluri, H. S.; Collinson, M. M.; El-Shall, M. S. Photothermal Deoxygenation of Graphite Oxide with Laser Excitation in Solution and Graphene-Aided Increase in Water Temperature. *J. Phys. Chem. Lett.* **2010**, *1* (19), 2804–2809.

(64) Peng, Z.; Ye, R.; Mann, J. A.; Zakhidov, D.; Li, Y.; Smalley, P. R.; Lin, J.; Tour, J. M. Flexible Boron-Doped Laser Induced Graphene Microsupercapacitors. *ACS Nano* **2015**, No. Cc, 1–17.

(65) Yang, Y.; Ruan, G.; Xiang, C.; Wang, G.; Tour, J. M. Flexible Three-Dimensional Nanoporous Metal-Based Energy Devices. **2014**, 1–4.

(66) Caṇado, L. G.; Takai, K.; Enoki, T.; Endo, M.; Kim, Y. A.; Mizusaki, H.; Jorio, A.; Coelho, L. N.; Magalhães-Paniago, R.; Pimenta, M. A. General Equation for the Determination of the Crystallite Size La of Nanographite by Raman Spectroscopy. *Appl. Phys. Lett.* **2006**, *88* (16), 1998–2001.

(67) Cai, F.; Tao, C. A.; Li, Y.; Yin, W.; Wang, X.; Wang, J. Effects of Amount of Graphene Oxide and the Times of LightScribe on the Performance of All-Solid-State Flexible Graphene-Based Micro-Supercapacitors. *Mater. Res. Express* **2017**, *4* (3).

(68) Pope, M. A. Electrochemical Double-Layer Capacitors Based of Functionalized Graphene. **2013**.

(69) Yao, J. Preparation of Colloidal Microporous Carbon Spheres from Furfuryl Alcohol. **2006**, *43* (2005), 1709–1715.

(70) Marcano, D. C.; Kosynkin, D. V; Berlin, J. M.; Sinitskii, A.; Sun, Z. Z.; Slesarev, A.; Alemany, L. B.; Lu, W.; Tour, J. M. Improved Synthesis of Graphene Oxide. *ACS Nano* **2010**, *4* (8), 4806–4814.